NONLINEAR DYNAMIC MODELING AND ANALYSIS OF SPINDLE-TOOL ASSEMBLIES IN MACHINING CENTERS

A THESIS SUBMITTED TO
THE GRADUATE SCHOOL OF NATURAL AND APPLIED SCIENCES
OF
MIDDLE EAST TECHNICAL UNIVERSITY

BY

ZEKAİ MURAT KILIÇ

IN PARTIAL FULFILLMENT OF THE REQUIREMENTS
FOR
THE DEGREE OF MASTER OF SCIENCE
IN
MECHANICAL ENGINEERING

AUGUST 2009

Approval of the Thesis:

NONLINEAR DYNAMIC MODELING AND ANALYSIS OF SPINDLE-TOOL ASSEMBLIES IN MACHINING CENTERS

submitted by **ZEKAİ MURAT KILIÇ** in partial fulfillment of the requirements for the degree of **Master of Science in Mechanical Engineering Department, Middle East Technical University** by,

Prof. Dr. Canan Özgen _____
Dean, Graduate School of **Natural and Applied Sciences**

Prof. Dr. Suha Oral _____
Head of Department, **Mechanical Engineering**

Prof. Dr. H. Nevzat Özgüven _____
Supervisor, **Mechanical Engineering Dept., METU**

Prof. Dr. Yusuf Altıntaş _____
Co-Supervisor, **Mechanical Engineering Dept., The Univ. of British Columbia**

Examining Committee Members :

Prof. Dr. Y. Samim Ünlüsoy _____
Mechanical Engineering Dept., METU

Prof. Dr. H. Nevzat Özgüven _____
Mechanical Engineering Dept., METU

Prof. Dr. Metin Akkök _____
Mechanical Engineering Dept., METU

Prof. Dr. Yavuz Yaman _____
Aerospace Engineering Dept., METU

Asst. Prof. Dr. Ender Ciğeroğlu _____
Mechanical Engineering Dept., METU

Date : 31.08.2009

I hereby declare that all information in this document has been obtained and presented in accordance with academic rules and ethical conduct. I also declare that, as required by these rules and conduct, I have fully cited and referenced all material and results that are not original to this work.

Name, Last Name : Zekai Murat Kılıç

Signature :

ABSTRACT

NONLINEAR DYNAMIC MODELING AND ANALYSIS OF
SPINDLE-TOOL ASSEMBLIES IN MACHINING CENTERS

Kılıç, Zekai Murat
M.S., Department of Mechanical Engineering
Supervisor : Prof. Dr. H. Nevzat Özgüven
Co-Supervisor : Prof. Dr. Yusuf Altıntaş

August 2009, 100 pages

Chatter is unwanted since it causes deteriorating effects on the milling process. Stability lobe diagrams are developed in order to determine the stable cutting conditions at which chatter-free machining can be made. The need of cutting away more chips to make milling operations quicker has brought the concept of high-speed milling. This increased the importance of estimating stability lobe diagrams of the milling process more accurately. The state-of-art chatter and spindle-toolholder-tool models predict the stability lobe diagram for milling process quite effectively. However, sometimes chatter might occur even at cutting conditions selected using theoretically obtained stability lobe diagrams. One of the reasons for that may be nonlinearities in the system. This being the motivation, in this work, nonlinearities at the bearings of spindle-toolholder-tool system are investigated. In this thesis, cubic nonlinearity is assumed to represent stiffness of a bearing in a spindle-toolholder-tool system. Effects of nonlinearity on stability lobe diagram of a milling process are studied by using the mathematical model developed for

such a system. Frequency response function of spindle-toolholder-tool system without bearings is obtained using Timoshenko beam model. Then, bearings are modeled by using describing function theory and coupled to the dynamics of spindle-toolholder-tool modeled. Solution of the equations of motion of the system in frequency domain is obtained via Newton's method with ALC. It is an effective frequency domain method in which turning points on frequency response function are traced. This is important for the system studied, as bearing nonlinearity may introduce turn backs in the response of the system. Case studies are carried out to study the effects of bearing nonlinearity on stability lobe diagram. The effects of the following factors are studied: Magnitude of cutting force, degree of nonlinearity and number of teeth on cutter. Displacement amplitude dependent stiffness of bearings affects the dynamic response due to rigid body modes of the system. It is observed that an increase in cutting force magnitude or in coefficient of bearing nonlinearity results in increase of natural frequencies, thus showing hardening behavior. Shifting of frequencies in the response curve shifts stability lobes related to the affected modes, to the right. For increased number of flutes on cutter, effect of nonlinearity at bearings on stability of the milling process becomes lower. Experimental studies to determine the changes in dynamics of a system during cutting are also carried out in this thesis. Inverse chatter analysis is conducted to obtain modal parameters of a single-degree-of-freedom system using the experiment data. Decrease in natural frequency is observed at high cutting speeds for the particular spindle used. This shift may be due to speed-dependent bearing dynamics and real time adjustment of preload on bearings.

Keywords : Chatter Stability, End Milling, Bearing Nonlinearity, Inverse Chatter Analysis, Chatter in Nonlinear Systems

ÖZ

İŞLEME MERKEZLERİNDE MİL-TAKIM SİSTEMLERİNİN
İNCELENMESİ VE DOĞRUSAL OLMAYAN DİNAMİK MODELLEMESİ

Kılıç, Zekai Murat
Yüksek Lisans, Makina Mühendisliği Bölümü
Tez Yöneticisi : Prof. Dr. H. Nevzat Özgüven
Ortak Tez Yöneticisi : Prof. Dr. Yusuf Altıntaş

Ağustos 2009, 100 sayfa

İşleme sırasında yarattığı kötü etkilerinden dolayı tırlama frezede istenmeyen bir olgudur. Hangi durumlarda tırlama olmadan işleme yapılacağını tahmin edebilmek için, sürecin kararlılık diyagramı hesaplanır. Frezede süreci hızlandırmak için gereken fazla talaş kaldırma ihtiyacı yüksek hız frezeleri gündeme getirmiştir. Böylece, hesaplanan kararlılık diyagramlarının hassasiyetinin önemi daha da artmıştır. Günümüzde kararlılık diyagramlarını bulmakta kullanılan tırlama ve iş mili-takım tutucu-takım sistemi modelleri oldukça iyi sonuçlar vermektedir. Ancak bazen kesme koşulları teorik olarak bulunan kararlılık diyagramına göre kararlı bölgede bile sistemde tırlama gözlemlenebilmektedir. Bu olgunun sebeplerinden biri, sistemdeki doğrusal olmayan etkiler olarak açıklanabilir. Buradan yola çıkarak, bu tezde, iş mili-takım tutucu-takım sisteminin rulmanlarındaki doğrusal olmayan parametrelerin etkileri incelenmiştir. Bu çalışmada, iş mili üzerindeki rulmanın, kuvvet-yer değiştirme ilişkisinin kübik davranış gösterdiği kabul edilmiştir. Geliştirilen matematiksel model kullanılarak, doğrusal olmayan özellikteki sistemlerde

freze işleminin kararlılık diyagramına etkisi incelenmiştir. Rulmanlar hariç iş mili-takım tutucu-takım sisteminin doğrusal modellemesi Timoshenko çubuk teorisi kullanılarak yapılmış, ardından doğrusal olmayan rulmanlar tanımlama fonksiyonu teorisi kullanılarak modellenerek, önceden frekans tepki fonksiyonu bulunan rulmansız iş mili-takım tutucu-takım sisteminin dinamiği ile birleştirilmiştir. Sistemin elde edilen hareket denklemi, Newton'un metodu yay uzunluğu sürekliliği kullanılarak frekans bölgesinde çözülmüştür. Uygulanan etkili frekans bölgesi metodu sayesinde sistemin frekans tepki fonksiyonundaki geri kıvrılma olan bölgelerde de çözüm elde edilebilmiştir. Bu çözüm, üzerinde çalışılan sistem için, rulmanlardaki doğrusal olmayan etkilerden dolayı sistemin frekans tepki fonksiyonunda geri kıvrılmalara yol açabileceğinden büyük önem taşımaktadır. Rulmanlardaki doğrusal olmayan dinamik özelliklerin kararlılık diyagramına etkisini incelemek için vaka analiz çalışmaları yapılmıştır. Çalışmalarda şu parametrelerin etkileri incelenmiştir: Kesme kuvveti büyüklüğü, doğrusal olmayan parametrelerin derecesi ve kalem üzerindeki kesici sayısı. Rulmanların yer değiştirme miktarına bağlı direngenliği, sistemin rijit cisim modlarına bağlı dinamik tepkisini etkilemektedir. Kesme kuvveti büyüklüğü ya da rulmanın doğrusal olmayan parametresinin katsayısı arttırıldığında doğal frekansların arttığı gözlemlenmiştir. Modların tepki eğrisinde sağa kayması kararlılık loblarını da sağa kaydırmıştır. Kalem üzerindeki kesici sayısı arttırıldığında rulmanlardaki doğrusal olmayan parametrelerin freze kararlılığına etkisi azalmaktadır. Bu çalışmada aynı zamanda, sistem dinamiğinin işleme sırasındaki değişimlerini gözlemlemek için deneysel çalışmalar da yapılmıştır. Tek serbestlik dereceli bir sistemin modal değişkenlerini elde etmek için deney verileri kullanılarak ters tırlama analizi uygulanmıştır. Yüksek hızlarda test yapılan sistemin doğal frekansında azalma gözlemlenmiştir. Bu kaymanın hıza bağlı rulman dinamiği veya işleme sırasında değişen rulman gerginliğine bağlı olabileceği sonucuna varılmıştır.

Anahtar Kelimeler : Tırlama Kararlılığı, Parmak Frezeleme, Doğrusal Olmayan Rulman, Ters Tırlama Analizi, Doğrusal Olmayan Sistemlerde Tırlama

To My Grandmother Neriman Sezgin

ACKNOWLEDGMENTS

I would like to express my deepest appreciation to my advisors, Prof. Dr. H. Nevzat Özgüven and Prof. Dr. Yusuf Altıntaş, for their valuable guidance and instructions, and constant support and interest throughout this study. I would also like to thank to Asst. Prof. Dr. Ender Ciğeroğlu for his comments.

I would like to thank to my dear friends, Dr. Jokin Muñoa for his precious advices during the experiments, Günay Orbay for his support in theoretical study and Zoltán Dombóvári for sharing his experimental data.

My special thanks are for my sister Pelin Kılıç, my father Sadık Engin Kılıç and my mother Nedret Kılıç for their patience and everything they have done throughout my life.

I would also like to thank to my professors for their support, and to my colleagues, Bekir Bediz, Özlem Demirkan, Murat Barışık, Salih Alan, Tuğçe Yüksel, Ali Murat Kayıran, Ural Uluer, Özge Arslan, Ersan Gürkan, Zeynep Erdoğan and to all others in the Department of Mechanical Engineering at METU for their friendship. I would also like to thank to Hakan Mencek for helping me in writing my thesis using Latex.

I also want to thank to all my friends in the Manufacturing Automation Laboratory (MAL) at the University of British Columbia (UBC).

Domestic Master of Science Scholarship provided by the Scientific and Technological Research Council of Turkey (TÜBİTAK) is greatly acknowledged.

TABLE OF CONTENTS

LIST OF FIGURES

Figure

LIST OF TABLES

Table

LIST OF ACRONYMS

2D	two-dimensional
3D	three-dimensional
ALC	arc length continuation
CBM	continuous beam model
DF	describing function
EVP	eigenvalue problem
FEM	finite element model
FRF	frequency response function
HSM	high-speed milling
SHT	spindle-holder-tool
SLD	stability lobe diagram

LIST OF SYMBOLS

$[\alpha]$	Receptance matrix of segment A
$[\beta]$	Receptance matrix of segment B
$[\gamma]$	Receptance matrix of system C
$[\Phi]$	Transfer function matrix in inverse chatter analysis
$[K_l]_b$	Linear part of the bearing stiffness in matrix form
$[Z]$	Dynamic stiffness matrix including linear bearing stiffness
α	Directional cutting coefficients
$\delta(x)$	Dirac delta function
$\eta_r(t)$	r-th modal coordinate
γ	Loss factor
γ_y	Shear distortion angle on x-z plane
γ_z	Shear distortion angle on x-y plane
Λ	Eigenvalues of characteristic equation
ν	Poisson's ratio
ω	Excitation frequency
ω_c	Chatter frequency
ω_n	Natural frequency
ω_r	r-th natural frequency

$\overline{\theta_{zr}}(x)$ r-th mass normalized rotational eigenfunction

$\overline{v_r}(x)$ r-th mass normalized transverse eigenfunction

ρ Density

θ ωt

$\theta_z(x,t)$ Bending rotation of two-dimensional beam

ζ Damping ratio

$\{F\}$ Magnitude of external harmonic force

$\{F_{nl}\}$ Nonlinear bearing force vector

$\{q\}$ Vector of unknowns in arc length continuation

A Cross sectional area of beam

A_r Coefficient for mass normalizing r-th eigenfunction

a_{lim} Limiting depth of cut

A_{rot} Coefficient for mass normalizing rotational rigid body eigenfunction

A_{tr} Coefficient for mass normalizing translational rigid body eigenfunction

E Modulus of elasticity of beam

$F(t)$ Harmonic force in transverse direction

G Modulus of rigidity of beam

H_{mn} Receptance relating translation at point m to unit force at point n

I Moment of inertia of beam

J Polar moment of inertia of beam

k_i Equivalent damping of nonlinear bearing

k_l Coefficient of linear part of bearing stiffness

k_n Coefficient of nonlinear part of bearing stiffness

k_r Equivalent stiffness of nonlinear bearing

k_s Shear coefficient

L Length

L_{mn} Receptance relating translation at point m to unit moment at point n

m Modal mass

$M(t)$ Harmonic moment on x-y plane

m_y Distributed moment on the beam on x-z plane

m_z Distributed moment on the beam on x-y plane

N_{mn} Receptance relating rotation at point m to unit force at point n

P_{mn} Receptance relating rotation at point m to unit moment at point n

q_x Distributed load on the beam in axial x direction

q_y Distributed load on the beam in transverse y direction

q_z Distributed load on the beam in transverse z direction

R, g Residual functions

T Kinetic energy of Timoshenko beam

V Potential energy of Timoshenko beam

$v(x,t)$ Transverse displacement of two-dimensional beam

W_e Work done by external forces

CHAPTER 1

INTRODUCTION

1.1 General

The demand of cutting away more chips to make milling operations quicker has brought the concept of high-speed milling. By the introduction of high-speed milling (HSM) it is possible to have larger depths of cut and higher cutting speeds. But, HSM arouse the importance of an already existing problem, self-excited chatter vibration. The spindle-holder-tool (SHT) system vibrates under the cutting load applied. The vibrations in the system causes variation in the chip-thickness. Under special conditions, the variation of the chip thickness becomes unstable and chip thickness starts to increase. This condition is named as chatter vibration; it is the special condition in which self-excited vibration of the SHT system occurs. Self-excited increase of chip thickness results in cutting forces which are much larger than the normal values. Higher cutting forces cause higher forces at supports of the structure and higher deflection of tool-tip of SHT system. Chatter has deteriorating effect on milling process such as premature tool failure, shortened bearing life, poor surface quality, and dimensional inaccuracy. To avoid chatter, the operation parameters should be selected properly. In other words, conditions of chatter must be understood.

There are different models proposed in the literature to predict conditions of chatter for milling. The models generally predict the stability lobe diagrams (SLDs) of the milling process. SLD is a tool to select the stable cutting

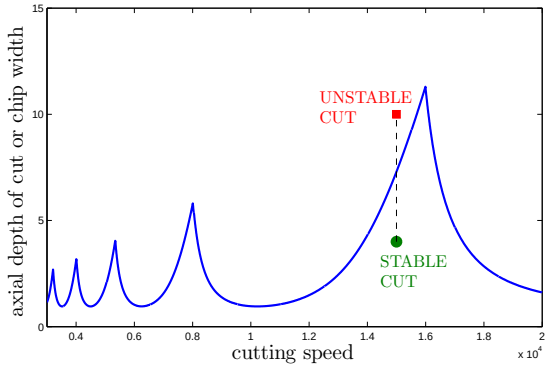

Figure 1.1. A typical stability lobe diagram to determine stable cutting conditions

conditions at which no chatter occurs. A typical example of SLD is shown in Figure 1.1.

During machining the very first tooth of the milling cutter takes away a layer from the workpiece. Since dynamic cutting forces excite the structure during machining, the surface left on the workpiece is wavy. "The wavy surface finish left by the previous tooth is removed during the succeeding tooth period, which also leaves a wavy surface owing to structural vibrations. Depending on the phase shift between two successive waves, the maximum chip thickness may exponentially grow while oscillating at a chatter frequency close to but not equal to a dominant structural mode in the system" [1]. If the wavy surface left by previous cutter and the wavy surface generated by the next cutter are in-phase, chip thickness does not change during the process. Such a condition is called forced vibration, and it is stable. If the left and generated surfaces are out-of-phase the process excites itself, and the waves generated become deeper. The latter condition involves unstable increase of chip thickness, and it is called chatter. Thus, the model of the process and the dynamics of the structure need to be known in order to predict the chatter.

The mechanism of the milling process has been under research for more than 50 years. However, more than a century ago Taylor [2] was the first one reporting chatter. Arnold [3] explained chatter by negative damping effect.

Tlusty and Polacek [4] and Tobias and Fishwick[5, 6] stated the reasons of chatter as regeneration of chip thickness and mode coupling. Merritt [7] came up with a similar solution using feedback control theory. But, the methods proposed were only suitable for orthogonal cutting processes which involve constant cutting force and direction.

Milling is a complicated process to model. During milling, direction and magnitude of cutting forces change. Milling can be considered as interrupted turning with cutter having entry and exit angles. Hence, directional cutting coefficients are not constant. Additionally, in milling process multiple number of teeth might be cutting at the same time. After understanding the mechanism of chatter researchers focused more on modeling milling process. Koenigsberger and Tlusty [8] considered an average direction, and average number of teeth during modeling. In other words, an analogy was made to turning operations in which cutting coefficients are constant. Opitz and Bernardi [9] introduced a similar but an improved model giving more accurate results. Sridhar et al. [10] carried out a more comprehensive study in which numerical integration of dynamic milling equations is done for one revolution of the cutter. In later studies, the milling process is analyzed in time domain [11, 12, 13]. Carrying out computations in time-domain made it possible to include the nonlinearities of milling process in chatter models. Tlusty and Ismail [11] included the effect of tool jump in their time domain study. They stated that loss of contact between tool and workpiece might occur during milling. When the contact is lost the chip thickness and cutting force become zero instantaneously. So, their study was more accurate than the previous ones. For low speed milling another nonlinearity is process damping [14, 15], which still waits to be resolved [16]. Minis and Yanushevsky [17] used Floquet's theorem and Fourier series for the formulation of milling stability on a two degree-of-freedom cutter model with point contact, and solved it numerically using Nyquist criterion.

Later, Altıntaş and Budak [18] developed a stability method in frequency domain. They determined stability of end milling operations by avoiding time consuming time-domain calculations. It has been very useful for industry

because of being fast and comprehensive as well as being accurate. Then, the same method used in the model was applied to three-dimensional cases to consider face milling operations [19, 20]. The studies mentioned up to this point considered milling operations involving high immersion of cutter into the workpiece. For slotting operation, for example, the cutting force can be well approximated by its zeroth harmonic, and accurate predictions for stability can be made as studied in [18] (zeroth order approximation). However, for low immersion cutting, cutting forces are highly interrupted and this affects accuracy of the prediction made by zeroth order approximation, significantly [21]. Merdol and Altıntaş [22] conducted a study considering the effect of multiple harmonics of the interrupted cutting force in frequency domain. Bayly et al. [23] and Insperger and Stépán [24] introduced different methods to solve the delayed differential equations. Later, Insperger and Stépán [25] developed semi-discretization method. Stability predictions based on zeroth-order approximation, and predictions based on studies considering highly interrupted cutting may give different results due to the effect of higher harmonics of interrupted cutting force.

In this thesis, end milling process with large immersion of cut is considered. So, the method of Altıntaş and Budak [18] is adopted for stability analysis. Also, since the cutting speeds considered in this study are not low, effect of process damping is assumed to be negligible as stated by Altıntaş and Weck [16].

Chatter involves the vibrations of the structure, so, stability is highly dependent on the flexibility of the structure which performs cutting. The frequency of vibration of the structure while chatter occurs is called chatter frequency. It is expected to be close to the natural frequency of the mode of the structure which dominates during chatter. Thus, one of the most important factors affecting chatter stability is the dynamics of the structure.

From all the components of the milling machine, SHT system has the most influence on the dynamic response of the structure. Hence, it is important to make accurate predictions for the dynamics of the SHT system. There

are experimental and analytical methods to predict the dynamics of a SHT system. The most widely used experimental technique is impact hammer test. It is a common method used, especially in industry. In hammer test the tool tip of the structure is excited by an instrumented hammer (input signal is obtained) and the response is recorded by a sensor located at the tool-tip (output signal is obtained). Then, after signal conditioning the input and output signals are correlated and tool tip FRF is obtained. Thus, the frequency response function (FRF) of the tool tip of SHT is measured, and SLD of the process is obtained.

Sometimes chatter occurs even when the cutting conditions are selected in the stable zone of the theoretically obtained SLD by using experimental FRFs [26]. The reasons that cause difference between predicted SLD and actual SLD are due to the factors that arise during machining. Therefore, it may not be possible to see their effect by impact hammer test. To estimate the FRF and SLD of a SHT system during rotation or machining there are different methods proposed in the literature. The FRF of the SHT system during rotation is called rotating FRF. It can be measured by making impact hammer test during rotation of spindle [27, 28]. Non-contact FRF measurement was achieved by Rantatalo et al. [29] by exciting the tool tip with electro-magnets and recording response using inductive sensors. The difference between FRFs measured at static and dynamic conditions were reported by Brecher and Esser [30]. An interesting study was reported by Quintana et al. [31] in which SLD was obtained directly during cutting. However, when SLD or FRF is obtained during cutting, the effect of the process is also included in the results. So, additional effects of the process may be seen other than the effects of the dynamics of the SHT system. Kruth et al. [32] and Suzuki et al. [33] proposed inverse methodology to identify dynamic system parameters directly by making a few experiments during cutting.

Apart from the experimental methods, research has been done on analytical methods to determine the FRF of the SHT system. If the computation involves experiment in addition to analytical model, the method is called semi-analytical. Before continuing with the models introduced in literature, a SHT

system is explained below briefly.

Spindle is the most important element of a SHT system. There are generally two types of spindles used in the modern milling machines: Belt-driven spindles and motorized spindles. In belt-driven spindles the power is transmitted from the motor to the spindle by a belt or gear. Because of the speed limitations coming from the use of belt or gear, belt-driven spindles cannot be used at high-speed machining, i.e. for speeds greater than about 10,000 rpm. In motorized spindles the spindle is directly driven by a motor located on the spindle housing. The axes of the motor and the spindle coincide, and no power transmission element such as belt or gear is used. Thus, motorized spindles are used in high-speed machining.

The spindle shaft is confined in and supported by spindle housing, which joins the spindle assembly to the body of the machine. Generally, during modeling spindle housing is considered to be fixed to the machine tool. However, Cao and Altıntaş [34] considered the housing coupled to the machine tool by spring elements giving an additional mode to the system. This brings the requirement for making a modal test to determine the values of the stiffness and damping at the connections. For motorized spindles, the spring elements connecting spindle housing to the machine tool are taken as very stiff. It is possible to assume housing as fixed to the ground. In other words, the outer rings of the bearings are considered fixed to the ground for motorized spindles.

High-speed milling spindle shafts are supported by angular contact ball bearings. When compared to other types of bearings angular contact ball bearings are very stable at high speeds, and they can also withstand axial cutting forces satisfactorily. Spindle shaft is supported by two sets of bearings: front set and rear set. O-arrangement (as shown in Figure 1.2) is selected for the bearings in order to add more rigidity to the set for resisting tilting moments. The bearings at the front set virtually take all the axial cutting load acting in the positive z-direction, which is because of the arrangement of the bearings.

Preload should be applied to the bearings in order to use them under optimum conditions. Minimum preload that should be applied to the bearings is given

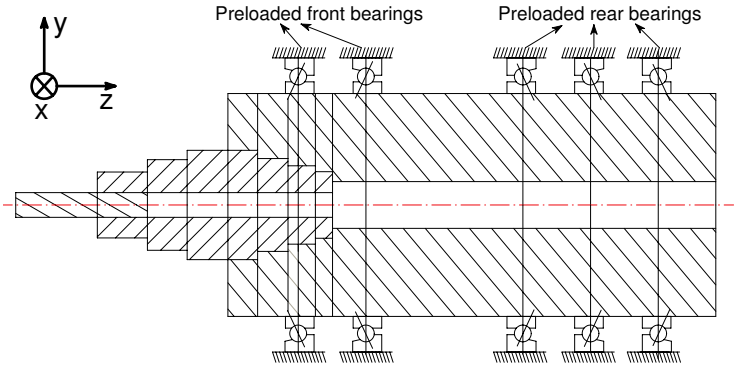

Figure 1.2. A motorized spindle having bearings in O-arrangement with fixed outer rings

by the bearing manufacturer (e.g. as given by [35]). Main reasons for applying preload to the bearings are:

- increasing the rigidity of the bearing, therefore decreasing run-out and deflection of the spindle.
- eliminating the internal clearance.
- preventing skidding of the bearing balls at high accelerations.

There are two ways for applying preload to the bearing on a spindle: Rigid preload and spring preload. Rigid preload is applied using the elements in the structure. The distance between inner and outer rings of the bearing is decreased by putting a spacer or lock-ring. In case of spring preload, a spring is attached to the outer rings of the rear set of the bearings. The spring adjusts the axial force on the outer rings of the bearings of the spindle. The preload force is introduced by displacing the spring (e.g. by using a hydraulic system). The main difference between these two ways of applying preload is that preload on the rigidly preloaded bearings depends on the thermal distortion of the spindle, whereas spring preloaded bearings have almost constant preload during the machining operation. For rigid preloaded bearings the temperature difference between spindle and housing inevitably affects the distance between the inner and outer rings of the bearings. However, for spring

preload the spring is not much affected by the thermal expansion due to the difference in temperatures of spindle and housing. Although it shows higher radial and axial rigidity, rigid preload is not used at high speed applications. Spring preload is preferred for high-speed cutting.

Other than contacts at bearings, there are contacts at toolholder-tool and spindle-toolholder interfaces. According to the toolholder type, the effect of these contacts change. Namazi [36] carried out an extensive study on the effects of different types of toolholders. Both contacts are important for modeling. These contacts are modeled as both single-point (first-generation) or multiple-point (second-generation) contacts. They are modeled using stiffness and damping elements, which are named as contact parameters. Namazi [36], Cao [37] and Schmitz and Duncan [38] used second-generation modeling, whereas Budak et al. [39] and Özşahin et al. [40] used first-generation model. Type of toolholder, length of tool outside holder (tool overhang length), and tool material affect the values of contact parameters. Identification of stiffness and damping parameters to represent the contacts is usually achieved by using nonlinear least-squares best fit method. That is, the analytical FRF is tried to be matched to experimental FRF by changing contact parameter values. Cao [37] used rigid coupling instead of elastic contact, so he took the contact parameter values as infinite. He reported small changes in the accuracy of the FRF prediction by not assuming elastic contact. Namazi [36] and Schmitz and Duncan [38] used nonlinear least-squares fit in order to predict the contact parameters. Cheng [41] correlated contact stiffness with tool overhang length in his study and stated that stiffness decreases linearly with increasing overhang length. Özşahin et al. [42] used a different algorithm for predicting the contact parameters. He made experiments for different tool overhang lengths. Then, using these data he used neural networks to predict contact parameters any tool overhang length. By this way, the number of experiments is minimized.

Spindle, holder and tool are taken as constant cross-section beams coupled to each other. Each component of SHT is assumed axisymmetric, which gives close results to the real case. In reality, all the components of the system except the cutting tool are symmetric. That is why the modal tests are some-

times done by using blank tools (without flutes) to get rid of the effects of the non-axisymmetric cutter. In the model, a constant diameter tool is taken to approximate the fluted tool. Spindle is taken as the main structure and its constant cross-section components are taken as substructures. So, the problem is to model each substructure of the spindle individually. Then, coupling of the substructures gives the whole spindle. Substructures of SHT system are beam elements with constant cross-sections. The boundary condition of each beam is free-free (free at both sides). To investigate a beam element there are four effective beam theories in the literature [43]: Euler-Bernoulli, Rayleigh, Shear and Timoshenko.

Euler-Bernoulli beam theory is also known as classical beam theory. It considers only the bending effect of a beam element. The transverse vibration and rotational vibration of the beam element are coupled, and defining one of the motions, transverse or rotation, is enough for defining the other one. In case of Rayleigh model the area moment of inertia of the beam element is additionally considered in the equation of motion of the beam element. In shear model the shear distortion is considered in addition to the bending effect, but this time it neglects the effect of the rotation of the cross-section. In Rayleigh and shear models the Euler-Bernoulli is modified, but Timoshenko beam theory is a very powerful tool to estimate the response of a beam element. It considers both rotary and shear effects, thus making the analysis more accurate at high speeds for beams having low slenderness ratio, i.e. beams having low "length to radius of gyration ratio". Han et al. [43] discussed these beam theories comprehensively.

Almost all of the recent studies in the literature (e.g. [37, 41, 44]) use Timoshenko beam theory since it is more accurate than the other beam models. There are generally two models used to obtain the response of a constant cross-section Timoshenko beam: Continuous beam model or CBM [39], and finite element model or FEM [34]. CBM considers the actual mode shapes of the beam. It applies eigenfunction expansion to obtain the FRF matrix of a beam. In eigenfunction expansion, the response of the beam is obtained by summing the effects of its infinite number of modes, but considering only the modes

having considerable effect. FEM takes finite number of nodes (cross-sections) on a beam element, and obtains the response of the beam as a function of the displacements of these nodes. It applies Galerkin's method (Meirovitch [45]) to obtain system matrices of the beam element.

To obtain the response of a SHT system, there are two methods to couple beam elements: Receptance coupling (Schmitz and Donaldson [46]) or FRF coupling, and dynamic stiffness coupling (Ewins [47]). The use of the former method keeps only the necessary nodes on the SHT system, whereas use of the latter keeps all the nodes that are involved in the analysis. FRF coupling decreases the calculation time at each step as the matrix size is smaller compared to the dynamic stiffness coupling method. The main objective in many of the recent studies is to model the whole SHT system analytically. However, there is a semi-analytical method, inverse receptance coupling technique. In this method, conducting one experiment at the tip of the spindle, to which holder is connected, is necessary. Then, the response at the tool-tip is predicted by coupling different holder geometries analytically. Namazi [36] used this method.

In their study, Budak et al. [39] and Cao and Altıntaş [34] used Timoshenko beams and determined the FRF of the whole SHT system analytically. Ertürk [44] used 2D model and computed eigenfunctions of the beam element based on the study of Aristizabal-Ochoa [48]. The calculations are made in frequency domain and FRF coupling is used. The bearings at the supports of the spindle are modeled as linear springs. Cao [37] used 3D model to include speed effects and used FEM. System matrices are considered and the response is calculated in time-domain. The bearings at the supports are modeled as nonlinear by using the model of Jones [49].

In addition to the nonlinearities related to process, structural nonlinearities (NL) may have effect on stability of the milling process. The main causes of structural NL are heating-up of the spindle [50, 51] and bearings located at the supports of the SHT system.

It is argued by the researchers that bearing nonlinearity is one of the strongest

which directly alters the spindle dynamics. The bearings are highly nonlinear such that both the changes in speed and cutting force have strong effects on the dynamic characteristics of bearings. The speed dependent characteristics of bearings is not yet fully understood. Shin [52] presented a study on speed effects on chatter stability considering bearing nonlinearity. Rantatalo et al. [29], Schmitz et al. [53] and Jorgensen and Shin [54] investigated the effects of speed on the dynamics of spindles. Rantatalo et al. [29] and Jorgensen and Shin [54] argues that the stiffness of a bearing decreases with increasing speed. The same argument was made by Cao [37], but experimental verification was left for further research. The changes in the magnitude of the cutting force also have nonlinear effect on the bearing dynamics. Hertzian contact theory is taken to define the contact between bearing balls and the inner and outer races. According to the theory, the force and deformation relation is nonlinear. This brings about nonlinear stiffness matrix for the bearing itself [49]. The effect of cutting load was investigated by Jorgensen and Shin [54], but the experimental verification was not made.

Linear component of the angular contact ball bearing comes from the axial preload applied. Nonlinear part depends on its deflection. Its dependance on speed is explained by dependance on load as well. When speed of rotation is increased centrifugal force applied by the balls of the bearing on its outer ring increases. This brings about more deflection at higher speeds with the same force applied on the bearing. In other words, stiffness of the bearing decreases with increasing speed. However, at constant speed radial deflection of an angular contact ball bearing may be assumed to show cubic behavior under increasing load. A study on this subject was conducted by Fleming and Poplawski [55].

Dynamic analysis of systems involving nonlinear elements can be made in frequency domain by using describing function (DF) theory. Such studies were carried out in different application areas by Ferreira [56], Gürkan [57] and Orbay [58]. In DF method the response of a nonlinear element is approximated by Fourier series expansion. For weak nonlinearities taking low number of harmonics or single harmonic may be sufficient to represent the response. In

SHT systems, nonlinearity mainly affects the modes caused by bearings (rigid body modes of the spindle in the housing). If the nonlinearity is high, jumps might be seen in the FRF of the SHT system. The zones at which jumps occur can be investigated clearly by using numerical continuation method ([58, 59]).

1.2 Objective

The aim of this study is to investigate the effect of nonlinearities in spindle bearings on the stability of milling process. The study of the effect of nonlinearities on milling stability is carried out both analytically and experimentally. In the analytical part, whole spindle-toolholder-tool (SHT) system is mathematically modeled, where the bearings of the spindle are taken as nonlinear elements with cubic stiffness behavior. Effects of magnitude of cutting force, degree of nonlinearity at the bearing and number of teeth on cutter on the stability lobe diagram (SLD) of the milling process is studied by using the nonlinear mathematical model developed. The importance of bearing nonlinearity from the stability point of view is investigated with case studies. In the experimental part, an SHT system is modeled as a single-degree-of-freedom (SDOF) system. Changes in the system dynamics during milling are investigated, and a method is proposed to predict SLD during cutting.

1.3 Scope of the Thesis

The thesis is organized as below:

In Chapter 2, theory used in this thesis is given. Frstly equations of motion for a Timoshenko beam element are derived. Then, response of a general spindle-toolholder-tool system is determined. Describing function theory is very briefly summarized, and nonlinearity in a bearing is linearized by using describing function theory. Lastly, numerical solution method used in solving the equations of motion of the system is explained.

In Chapter 3, a motorized SHT system is analyzed to study the effect of the nonlinearities on system response and, more importantly, on chatter stability. Changes in stability lobe diagram of the process are investigated considering effects of magnitude of cutting force, degree of nonlinearity at the bearing, and number of flutes on the cutter.

In Chapter 4, experimental methods used in studying the response and stability of real SHT systems are explained. A method is proposed to estimate SLD for an SHT system which has only one dominating mode in its FRF.

In the last chapter, Chapter 5, conclusions based on studies carried out in Chapter 3 and Chapter 4 are summarized. Also, some recommendations are made for future studies.

CHAPTER 2

MODELING OF SPINDLE-BEARING SYSTEM

In this chapter at first general modeling procedure of a spindle-toolholder-tool (SHT) system is presented. Modeling of SHT is conducted using Timoshenko beam theory. After obtaining linear model of SHT system, nonlinear spring elements representing angular contact ball bearings are linearized using describing function theory. Finally, system of equations obtained by coupling the SHT model and linearized spring elements are solved in frequency domain using a special numerical continuation (path following) method, Newton's method with arc length continuation (ALC).

2.1 Modeling of Spindle-Toolholder-Tool

In this thesis Timoshenko beams are used to model a SHT. The beams forming the SHT are modeled as Timoshenko beams, then these beam models are coupled to obtain the frequency response function (FRF) of the spindle. In this section the equations of motion (governing equations) of the beams are derived. Later, the method for obtaining FRF of the SHT using FRF of beam elements is introduced.

2.1.1 Governing Equations

Lagrangian of the Timoshenko beam element includes the effects of bending moment, lateral displacement, rotary inertia and shear distortion. Nelson and McVaugh [60] and Nelson [61] used Timoshenko beams to investigate dynamics of rotor shafts accurately in their finite element models. In a recent study, Cao and Altıntaş [34] used 3D Timoshenko beam model with 5 degrees-of-freedom as shown in Figure 2.1. For the 2D model, the effects of lateral displacement in y-direction, bending moment in x-y plane, and axial displacement can be considered. For 3D spindle model the effects of lateral displacement in z-direction and bending moment on x-z plane are additionally considered. Thus the 3D model considered in this work includes the speed effect or effect of the gyroscopic moment; but 2D model does not. However, as seen in the study of Movahhedy and Mosaddegh [62], the effects of the speed on the spindle response can be disregarded because of the high slenderness ratio of the spindle. Effects of the speed is considered to be more important for the balls of bearings of a spindle. In this part, the Timoshenko beam theory will be given.

Let us consider an infinitesimal beam element as shown in Figure 2.1. Its freedoms are:

- translation in x-axis (axial freedom)
- translation in y-axis (lateral freedom)
- translation in z-axis (lateral freedom)
- rotation around y-axis (rotational freedom)
- rotation around z-axis (rotational freedom)

The Lagrangian of a Timoshenko beam consists of two parts: Kinetic energy and potential energy. During modeling an infinitesimal disk element of a Timoshenko beam is considered (Figure 2.2). The extended Hamilton's equation

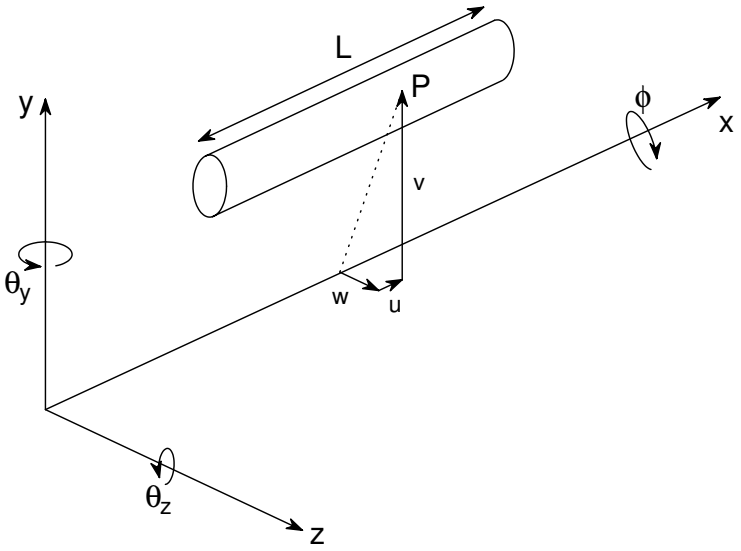

Figure 2.1. 3D Timoshenko beam element

of the system is given as follows [45]:

$$\delta \int_{t_1}^{t_2} (T - V + W_e)\, dt = 0 \tag{2.1}$$

where,

T : kinetic energy of the beam

V : potential energy of the beam

W_e : work done by external forces on the beam

In the following two sections the components of the extended Hamilton's principle is derived.

2.1.1.1 Kinetic Energy of the Beam

Firstly the kinetic energy of an infinitesimal disk element of the beam (see Figure 2.2) is calculated. Yuzhong Cao [34] considered the point P on the infinitesimal disk element shown in Figure 2.2 for finding the kinetic energy of the disk element. Thus, the gyroscopic effects are also included. In this thesis, a 2D model is considered for spindle. However, for the completeness of the derivation calculations are carried out for the 3D model of Cao and Altıntaş [34]. The point P is subjected to rotations around y-axis, θ_y, and around z-axis, θ_z, in addition to translations in x, y and z directions. Coordinate transformation is required to determine the position of point P relative to the x-y-z coordinate system given in the Figure 2.2.

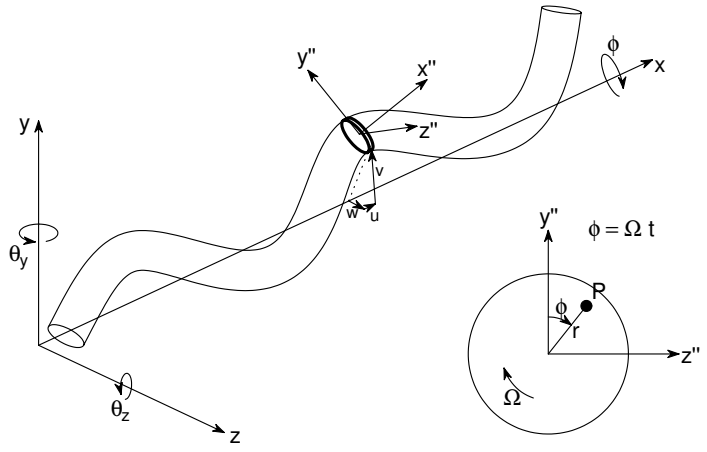

Figure 2.2. Deformed Timoshenko beam

The position of the point P relative to the $x-y-z$ coordinates is:

$$\begin{Bmatrix} x \\ y \\ z \end{Bmatrix} = \begin{Bmatrix} u \\ v \\ w \end{Bmatrix} + \begin{Bmatrix} x_0 \\ 0 \\ 0 \end{Bmatrix} + \Big[T\Big] \begin{Bmatrix} 0 \\ r\sin\phi \\ r\cos\phi \end{Bmatrix} \tag{2.2}$$

where,

x_0 : initial position of the disk element on x-axis (of x-y-z system)

$[T]$: transformation matrix for transforming $x"-y"-z"$ to $x-y-z$ system

ϕ : angular position of point P on the disk element

Translational displacements of the disk element are u, v and w in positive x, y and z directions, respectively (shown in Figure 2.2). $x"-y"-z"$ coordinate system is located on the disk element. Angular deformation of $x"-y"-z"$ by θ_y results in $x'-y'-z'$. Similarly, angular deformation of $x'-y'-z'$ by θ_z results in $x-y-z$. $[T]$ transforms the displacements with respect to $x"-y"-z"$ of the disk element into $x-y-z$ of the Timoshenko beam. Making small angle assumptions and neglecting higher order terms in Equation 2.2 gives,

$$\begin{Bmatrix} x \\ y \\ z \end{Bmatrix} = \begin{Bmatrix} u + x_0 - r\cos\phi\sin\theta_z + r\sin\phi\sin\theta_y \\ v + r\cos\phi\cos\theta_z \\ w + r\sin\phi\cos\theta_y \end{Bmatrix} \tag{2.3}$$

Taking time derivative of Equation 2.3 and applying small rotation assumption give the velocity terms required for computing the kinetic energy of the beam as,

$$\begin{Bmatrix} \dot{x} \\ \dot{y} \\ \dot{z} \end{Bmatrix} = \begin{Bmatrix} \dot{u} + \Omega r\theta_z\sin\phi + \Omega r\theta_y\cos\phi - r\dot{\theta}_z\cos\phi + r\dot{\theta}_y\sin\phi \\ \dot{v} - \Omega r\sin\phi - r\theta_z\dot{\theta}_z\cos\phi \\ \dot{w} + \Omega r\cos\phi - r\theta_y\dot{\theta}_y\sin\phi \end{Bmatrix} \tag{2.4}$$

After finding velocity terms, now the kinetic energy of the beam can be determined. Let point P in Figure 2.2 has an infinitesimal (differential) mass dm.

Kinetic energy of the dm element is,

$$dT = \frac{1}{2} dm(\dot{x}^2 + \dot{y}^2 + \dot{z}^2) \tag{2.5}$$

where,

$$dm = \rho r dr d\phi dx$$
$$dx : \text{thickness of the disk}$$
$$\rho : \text{density of the disk}$$

So, the kinetic energy of the whole beam is determined by integrating Equation 2.5 as,

$$T = \int_0^L \int_a^b \int_0^{2\pi} \frac{1}{2} t\rho r(\dot{x}^2 + \dot{y}^2 + \dot{z}^2) dr d\phi dx \tag{2.6}$$

where,

$$a : \text{inner radius of the disk}$$
$$b : \text{outer radius of the disk}$$

Kinetic energy of the Timoshenko beam element is obtained by substituting Equation 2.4 into Equation 2.6

$$\begin{aligned} T = &\int_0^L \frac{1}{2} J\rho\Omega^2 dx + \int_0^L \frac{1}{2} \rho A(\dot{u}^2 + \dot{v}^2 + \dot{w}^2) dx + \\ &\int_0^L \frac{1}{2} I\rho(\dot{\theta_y}^2 + \dot{\theta_z}^2) + \frac{1}{2} \Omega J\rho(\theta_z \dot{\theta}_y - \dot{\theta}_z \theta_y) dx \end{aligned} \tag{2.7}$$

where,

$$A = \pi(b^2 - a^2) \quad : \quad \text{area of the cross-section of the beam}$$
$$I = \frac{1}{4}\pi(b^4 - a^4) \quad : \quad \text{moment of inertia}$$
$$J = 2I = \frac{1}{2}\pi(b^4 - a^4) \quad : \quad \text{polar moment of inertia}$$

2.1.1.2 Potential Energy of the Beam

For finding the kinetic energy of the Timoshenko beam the disk element on the beam is considered to be rigid. The potential energy of the beam comes from its ability to deform. The deformation occurs on x-y and x-z planes as shear deformation and in x-direction as axial deformation. The point P on the beam can be considered again.

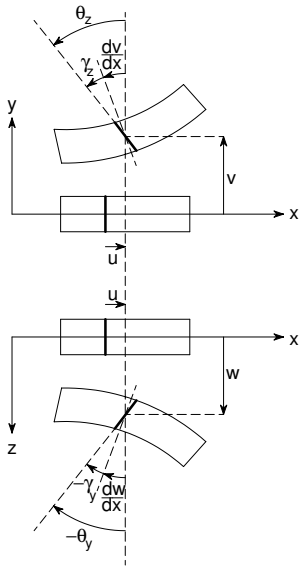

Figure 2.3. Deformation of Timoshenko beam

The deformed beam is shown in Figure 2.3. The coordinates of point P after

deformation are expressed as

$$u(x,y,z,t) = u(x,t) + \theta_y z - \theta_z y \tag{2.8}$$

$$v(x,y,z,t) = v(x,t) \tag{2.9}$$

$$w(x,y,z,t) = w(x,t) \tag{2.10}$$

where the angular deformations on x-y and x-z planes are

$$\theta_z = \gamma_z + \frac{\partial v}{\partial x} \tag{2.11a}$$

$$\theta_y = \gamma_y - \frac{\partial w}{\partial x} \tag{2.11b}$$

The strains at point P are given below (second-order strains are neglected):

$$\gamma_{yx} = \frac{\partial v}{\partial x} + \frac{\partial u}{\partial y} = -\gamma_z \tag{2.12a}$$

$$\gamma_{zx} = \frac{\partial w}{\partial x} + \frac{\partial u}{\partial z} = \gamma_y \tag{2.12b}$$

$$\varepsilon_{xx} = \frac{\partial u}{\partial x} + \frac{\partial \theta_y}{\partial x} z - \frac{\partial \theta_z}{\partial x} y \tag{2.12c}$$

Then, the potential energy of the beam can be written as

$$V = \iiint \frac{1}{2} E \varepsilon_{xx}^2 dx dy dz + \int_0^L \frac{1}{2} k_s A G \gamma_{yx}^2 dx + \int_0^L \frac{1}{2} k_s A G \gamma_{zx}^2 dx \tag{2.13}$$

where $k_s A$ is the effective shear area in which k_s is given by Cowper [63] as shown below

$$k_s = \frac{6(1+\nu)(1+p^2)^2}{(7+6\nu)(1+p^2)^2 + (20+12\nu)p^2} \quad \text{where,} \quad p = \frac{D_i}{D_o}$$

where ν is the Poisson's ratio of the material of the beam element. D_i and D_o are inner and outer diameters of the beam element, respectively.

Substituting Equations 2.11 and 2.12 into Equation 2.13 and rearranging them

give

$$V = \int_0^L \frac{1}{2} EA(\frac{\partial u}{\partial x})^2 dx + \int_0^L \frac{1}{2} EI[(\frac{\partial \theta_y}{\partial x})^2 + (\frac{\partial \theta_z}{\partial x})^2] dx + \int_0^L \frac{1}{2} k_s AG(\theta_z - \frac{\partial v}{\partial x})^2 dx + \int_0^L \frac{1}{2} k_s AG(\theta_y + \frac{\partial w}{\partial x})^2 dx \tag{2.14}$$

2.1.1.3 Work Done by External Forces on the Beam

Last term in extended Hamilton's equation (Equation 2.1) is energy due to external forces applied on the beam. The work done by external forces is:

$$W_e = \int_0^L (q_x u + q_y v + q_z w + m_y \theta_y + m_z \theta_z) dx + \int_0^L \frac{1}{2} \Omega^2 v^2 \rho A dx + \int_0^L \frac{1}{2} \Omega^2 w^2 \rho A dx \tag{2.15}$$

where q_x, q_y and q_z are distributed loads per unit length on the beam in x, y and z directions, respectively, and m_y and m_z are distributed moments per unit length on x-z and x-y planes, respectively. The last two terms in Equation 2.15 are work done by unbalance forces on the beam (when considering speed effects), where the unbalance comes from the translational deformation of the beam.

2.1.1.4 Equations of Motion of Timoshenko Beam

Substituting Equations 2.7, 2.14 and 2.15 into Equation 2.1 and rearranging the integrals give the equations of motion of the Timoshenko beam as below,

$$\rho A\frac{\partial^2 u}{\partial t^2} - EA\frac{\partial^2 u}{\partial x^2} - q_x = 0 \tag{2.16a}$$

$$\rho A\frac{\partial^2 v}{\partial t^2} - \frac{\partial}{\partial x}\left[k_s AG(\frac{\partial v}{\partial x} - \theta_z)\right] - q_y - \Omega^2\rho A v = 0 \tag{2.16b}$$

$$\rho A\frac{\partial^2 w}{\partial t^2} - \frac{\partial}{\partial x}\left[k_s AG(\frac{\partial w}{\partial x} + \theta_y)\right] - q_z - \Omega^2\rho A w = 0 \tag{2.16c}$$

$$\rho I\frac{\partial^2 \theta_y}{\partial t^2} + \Omega J\rho\frac{\partial \theta_z}{\partial t} - EI\frac{\partial^2 \theta_y}{\partial x^2} + k_s AG(\frac{\partial w}{\partial x} + \theta_y) - m_y = 0 \tag{2.16d}$$

$$\rho I\frac{\partial^2 \theta_z}{\partial t^2} - \Omega J\rho\frac{\partial \theta_y}{\partial t} - EI\frac{\partial^2 \theta_z}{\partial x^2} - k_s AG(\frac{\partial v}{\partial x} - \theta_z) - m_z = 0 \tag{2.16e}$$

Boundary conditions for free-free Timoshenko beam are,

$$\left[EA\frac{\partial u}{\partial x}\delta u\right]_{x=0,x=L} = 0 \tag{2.17a}$$

$$\left[EI\frac{\partial \theta_y}{\partial x}\delta\theta_y\right]_{x=0,x=L} = 0 \tag{2.17b}$$

$$\left[EI\frac{\partial \theta_z}{\partial x}\delta\theta_z\right]_{x=0,x=L} = 0 \tag{2.17c}$$

$$\left[(\frac{\partial v}{\partial x} - \theta_z)\delta v\right]_{x=0,x=L} = 0 \tag{2.17d}$$

$$\left[(\frac{\partial w}{\partial x} - \theta_y)\delta w\right]_{x=0,x=L} = 0 \tag{2.17e}$$

If only Equations 2.16a, 2.16b and 2.16e are taken while setting $\Omega = 0$, the analysis would be 2D. Taking all of the governing equations found leads to 3D analysis including speed effects.

2.1.2 Substructure Analysis

In Section 2.1.1 the equations of motion of the Timoshenko beam (Equations 2.16a, 2.16b, 2.16c, 2.16d and 2.16e) are found via Hamilton's principle and considering the kinetic and deformation energies on specified directions and planes. The equations of motion found do not consider large deformations (or large strains) and thermal deformations. Therefore this model is generally called as linear model since it does not include the nonlinear strain and time-dependent thermal effects. In this section the frequency response function (FRF) of the beam is found by solving the equations of motion. Analyzing different beams separately, as substructures and then combining the separate solutions to determine response of the complete system is called substructure coupling. There are two effective models to consider the FRF of substructures: Finite element model (FEM) and continuous beam model (CBM).

2D analysis of the spindle is made by taking $\Omega = 0$ and not considering axial effects. Therefore only Equations 2.16b and 2.16e are taken into consideration in the analysis. The reasons for making these simplifications are:

- Motion on x-y and x-z planes are uncoupled as inferred from the equations of motion (Equations 2.16b to 2.16e).
- Effects of speed are not significant on the motion of the spindle as the slenderness ratio of the whole spindle is large enough, so, it is possible to take $\Omega = 0$
- Effect of the axial deformation is insignificant when compared to other effects, and equation of axial motion (Equation 2.16a) is uncoupled from the other equations. Additionally, the cutting force considered in this study acts only in transverse direction.

Rewriting Equations 2.16b and 2.16e by setting $\Omega = 0$ gives,

$$\rho A \frac{\partial^2 v}{\partial t^2} - k_s AG(\frac{\partial^2 v}{\partial x^2} - \frac{\partial \theta_z}{\partial x}) - q_y(x,t) = 0 \tag{2.18a}$$

$$\rho I \frac{\partial^2 \theta_z}{\partial t^2} - EI \frac{\partial^2 \theta_z}{\partial x^2} - k_s AG(\frac{\partial v}{\partial x} - \theta_z) - m_z(x,t) = 0 \tag{2.18b}$$

Equation 2.18 is solved and FRFs are obtained by using CBM. Using FEM requires discretization of the beam element, and then response of the beam element is determined by using interpolation functions, or trial functions. However, in CBM distributed parameter model is considered (without discretization) and the response is determined by using the exact modeshapes of the structure. That is, partial differential equations in Equation 2.18 are solved analytically.

2.1.2.1 Continuous Beam Model

In FEM the response of the beam is approximated by using special trial functions multiplied by undetermined coefficients. For instance, trial functions of Timoshenko beam can be taken as lowest degree admissible polynomial functions (e.g. cubic polynomials for translation and quadratic polynomials for rotation). FEM discretizes beam element and considers finite number of nodes (cross-sections for this study) on the beam. The problem is to find the undetermined coefficients of the function which relates the nodal displacements with the response on any point on the beam. In CBM, unlike FEM, the beam element is analyzed considering its original mode shapes. So, CBM gives the exact response at any point on the beam.

Eigenfunction expansion is used in CBM analysis. Eigenfunction expansion is a method in which the response of the structure is taken as combination of its eigenfunctions. Contribution of each eigenfunction is taken by multiplying it with a coefficient. The aim is to obtain these coefficients in CBM analysis.

The differential equations are decoupled and following set of equations is obtained.

$$\frac{\partial^4 v}{\partial x^4} - (\frac{\rho}{E} + \frac{\rho}{k_s G})\frac{\partial^4 v}{\partial x^2 \partial t^2} + \frac{\rho A}{EI}\frac{\partial^2 v}{\partial t^2} + \frac{\rho^2 A}{k_s EG}\frac{\partial^4 v}{\partial t^4} = 0 \tag{2.19a}$$

$$\frac{\partial^4 \theta_z}{\partial x^4} - (\frac{\rho}{E} + \frac{\rho}{k_s G})\frac{\partial^4 \theta_z}{\partial x^2 \partial t^2} + \frac{\rho A}{EI}\frac{\partial^2 \theta_z}{\partial t^2} + \frac{\rho^2 A}{k_s EG}\frac{\partial^4 \theta_z}{\partial t^4} = 0 \tag{2.19b}$$

Since harmonic response is assumed, $v(x,t)$ and $\theta_z(x,t)$ can be expressed as

$$\begin{Bmatrix} v(x,t) \\ \theta_z(x,t) \end{Bmatrix} = \begin{Bmatrix} \overline{v}(x) \\ \overline{\theta_z}(x) \end{Bmatrix} e^{i\omega t}$$

So, Equation 2.19 becomes

$$\frac{d^4\overline{v}}{dx^4} + \omega^2(\frac{\rho}{E} + \frac{\rho}{k_s G})\frac{d^2\overline{v}}{dx^2} - \omega^2(\frac{\rho A}{EI} - \omega^2\frac{\rho^2 A}{k_s EG})\overline{v} = 0 \tag{2.20a}$$

$$\frac{d^4\overline{\theta_z}}{dx^4} + \omega^2(\frac{\rho}{E} + \frac{\rho}{k_s G})\frac{d^2\overline{\theta_z}}{dx^2} - \omega^2(\frac{\rho A}{EI} - \omega^2\frac{\rho^2 A}{k_s EG})\overline{\theta_z} = 0 \tag{2.20b}$$

Among the terms in Equation 2.17 the terms including δv and $\delta\theta_z$ give the boundary conditions for the free-free beam used in derivation,

$$EI\frac{\partial\theta_z}{\partial x}\bigg|_{x=0} = 0 \tag{2.21a}$$

$$k_s AG(\frac{\partial v}{\partial x} - \theta_z)\bigg|_{x=0} = 0 \tag{2.21b}$$

$$EI\frac{\partial\theta_z}{\partial x}\bigg|_{x=L} = 0 \tag{2.21c}$$

$$k_s AG(\frac{\partial v}{\partial x} - \theta_z)\bigg|_{x=L} = 0 \tag{2.21d}$$

Eigenvalue problem (EVP) is obtained by substituting the solution of Equation 2.20 in Equation 2.21. The numerical solution of the EVP is obtained by using the method proposed by Aristizabal-Ochoa [48]. The characteristic equation of the EVP can be expressed as

$$\det\begin{bmatrix} D_{11} & D_{12} \\ D_{21} & D_{22} \end{bmatrix} = D_{11}\cdot D_{22} - D_{12}\cdot D_{21} = 0 \tag{2.22}$$

where,

$$
\begin{aligned}
D_{11} &= (\alpha - \lambda)(\cos\alpha - \cosh\beta) \\
D_{12} &= (\lambda - \alpha)\sin\alpha + \frac{\lambda\alpha}{\beta\delta}(\beta - \delta)\sinh\beta \\
D_{21} &= -\lambda\alpha\sin\alpha + \frac{\alpha - \lambda}{\delta - \beta}\delta\beta\sinh\beta \\
D_{22} &= \lambda\alpha(\cosh\beta - \cos\alpha)
\end{aligned}
$$

$$
\begin{aligned}
&\alpha = \sqrt{\Upsilon + \varepsilon} && \beta = \sqrt{-\Upsilon\varepsilon} \\
&\Upsilon = \frac{b^2(s^2 + R^2)}{2} && \varepsilon = b\sqrt{\frac{1}{4}b^2(s^2 + R^2)^2 - (b^2 s^2 R^2 - 1)} \\
&b^2 = \frac{\rho A\omega^2 L^4}{EI} && s^2 = \frac{EI}{k_s AGL^2} \qquad R^2 = \frac{I}{AL^2}
\end{aligned}
$$

The eigenfunctions of the r^{th} elastic mode (excluding rigid body modes) having natural frequency ω_r can be expressed as

$$
\begin{aligned}
\begin{Bmatrix} \overline{v_r(x)} \\ \overline{\theta_{zr}(x)} \end{Bmatrix} = A_r \Bigg[&\begin{Bmatrix} C_1 \\ -\frac{\lambda_r}{L}C_2 \end{Bmatrix} \sin(\frac{\alpha_r}{L}x) + \begin{Bmatrix} C_2 \\ \frac{\lambda_r}{L}C_1 \end{Bmatrix} \cos(\frac{\alpha_r}{L}x) + \\
&\begin{Bmatrix} C_3 \\ \frac{\delta_r}{L}C_4 \end{Bmatrix} \sinh(\frac{\alpha_r}{L}x) + \begin{Bmatrix} C_4 \\ \frac{\delta_r}{L}C_3 \end{Bmatrix} \cosh(\frac{\alpha_r}{L}x) \Bigg]
\end{aligned}
\tag{2.23}
$$

where,

$$
\begin{aligned}
&\lambda_r = \alpha_r - \frac{b^2 s^2}{\alpha_r} \qquad \delta_r = \beta_r + \frac{b^2 s^2}{\beta_r} \\
&C_1 = L \qquad C_2 = \frac{-D_{11}}{D_{12}}C_1 \qquad C_3 = \frac{\alpha_r - \lambda_r}{\delta_r - \beta_r}C_1 \qquad C_4 = -\frac{\lambda_r\alpha_r}{\beta_r\delta_r}\frac{D_{11}}{D_{12}}C_1 \\
&r = 1, 2, 3, \ldots
\end{aligned}
$$

The eigenfunctions expressed by Equation 2.23 are orthogonal with respect to the differential operators of the EVP. The mass normalized eigenfunctions

(modes) satisfy the following orthogonality condition:

$$\int_0^L \begin{Bmatrix} \overline{v_s(x)} \\ \overline{\theta_{zs}}(x) \end{Bmatrix}^T \begin{bmatrix} \rho A & 0 \\ 0 & \rho I \end{bmatrix} \begin{Bmatrix} \overline{v_r(x)} \\ \overline{\theta_{zr}}(x) \end{Bmatrix} dx = \begin{cases} 1, s = r \\ 0, s \neq r \end{cases} \tag{2.24}$$

A_r in Equation 2.23 is obtained by inserting Equation 2.23 into Equation 2.24 (while setting $s = r$) and conducting numerical integration. After finding A_r, mass normalized eigenfunction is obtained for the r^{th} elastic mode. In addition to the elastic modes, Timoshenko beam also has rigid body modes. For the model in this study, there are two rigid body eigenfunctions, translational and rotational. Both Euler-Bernoulli and Timoshenko beams have two rigid body modes: Translational and rotational. However, their mass normalization are different. Since Timoshenko beam model includes rotary inertia of the beam in addition to mass effect, its normalization coefficients are different than those of Euler-Bernoulli beam. To find the rigid body eigenfunctions of Timoshenko beam the eigenvalue is taken as zero ($\omega = 0$) in Equation 2.20a:

$$\frac{d^4\overline{v}}{dx^4} = 0 \tag{2.25}$$

It should be noted that, since the rigid body modes are analyzed, eigenfunction for rotation is the derivative of the eigenfunction for translation. Solving Equation 2.25 considering boundary conditions in Equation 2.21 gives the following eigenfunctions:

$$\overline{v_{tr}}(x) = A_{tr} \tag{2.26a}$$

$$\overline{\theta_{z,tr}}(x) = \frac{d}{dx}\overline{v_{tr}}(x) = 0 \tag{2.26b}$$

$$\overline{v_{rot}}(x) = A_{rot}\left(x - \frac{L}{2}\right) \tag{2.26c}$$

$$\overline{\theta_{z,rot}}(x) = \frac{d}{dx}\overline{v_{rot}}(x) = A_{rot} \tag{2.26d}$$

where the subscript tr stands for translational rigid body mode, and the subscript rot stands for rotational rigid body mode about the centroid of the beam. Coefficients A_{tr} and A_{rot} are determined by mass normalization. For

A_{tr}, eigenfunctions related to translational rigid body mode (given by Equations 2.26a and 2.26b) are inserted into Equation 2.24, which yields

$$\int_0^L \begin{Bmatrix} \overline{v_{tr}}(x) \\ \overline{\theta_{z,tr}}(x) \end{Bmatrix}^T \begin{bmatrix} \rho A & 0 \\ 0 & \rho I \end{bmatrix} \begin{Bmatrix} \overline{v_{tr}}(x) \\ \overline{\theta_{z,tr}}(x) \end{Bmatrix} dx = 1 \tag{2.27a}$$

$$\int_0^L [\rho A \overline{v_{tr}}(x)^2 + \rho I \overline{\theta_{z,tr}}(x)^2] dx = 1 \tag{2.27b}$$

$$\int_0^L (\rho A A_{tr}^2) dx = 1 \tag{2.27c}$$

$$A_{tr} = \frac{1}{\sqrt{\rho A L}} \tag{2.27d}$$

Similarly, for rotational rigid body mode

$$\int_0^L \begin{Bmatrix} \overline{v_{rot}}(x) \\ \overline{\theta_{z,rot}}(x) \end{Bmatrix}^T \begin{bmatrix} \rho A & 0 \\ 0 & \rho I \end{bmatrix} \begin{Bmatrix} \overline{v_{rot}}(x) \\ \overline{\theta_{z,rot}}(x) \end{Bmatrix} dx = 1 \tag{2.28a}$$

$$\int_0^L [\rho A A_{rot}^2 (x - \frac{L}{2})^2 + \rho I A_{rot}^2] dx = 1 \tag{2.28b}$$

$$A_{rot} = \frac{1}{\sqrt{\frac{\rho A L^3}{12} + \rho I L}} \tag{2.28c}$$

After obtaining all mass normalized mode shapes for rigid and elastic modes, the next step is to use eigenfunctions in order to determine the response of the beam. Eigenfunction expansion assumes that solutions of Equation 2.20, $v(x,t)$ and $\theta_z(x,t)$, can be represented as a summation of the eigenfunctions multiplied by functions of time as,

$$\begin{Bmatrix} v(x,t) \\ \theta_z(x,t) \end{Bmatrix} = \sum_{r=0}^{\infty} \begin{Bmatrix} \overline{v_r}(x) \\ \overline{\theta_{zr}}(x) \end{Bmatrix} \eta_r(t) \tag{2.29}$$

To obtain the steady state response to a harmonic force excitation, $q_y(x,t)$ in

Equation 2.18 is written as

$$q_y(x,t) = F(t)\delta(x - x_n) \tag{2.30}$$

where, $F(t)$ is a harmonic force with magnitude F_0, frequency ω, and applied at an arbitrary point $x = x_n$ ($F(t) = F_0 e^{i\omega t}$), and $\delta(x - x_n)$ is Dirac delta function defined as

$$\delta(x - x_n) = \begin{cases} 1 & \text{if } x = x_n, \\ 0 & \text{if } x \neq x_n. \end{cases}$$

Inserting Equations 2.29 and 2.30 into Equation 2.18 and using orthogonality of eigenfunctions with respect to the differential operators and selfadjointness of the differential operators involved, time component of Equation 2.29 is found (for harmonic force applied at $x = x_n$) as,

$$\eta_r(t) = \frac{\overline{v_r}(x_n) F_0 e^{i\omega t}}{(1 + i\gamma)\omega_r^2 - \omega^2} \tag{2.31}$$

where, γ is the loss factor of the material of the beam element. Substituting Equation 2.31 into Equation 2.29 and taking $x = x_m$ gives the response of the beam element at any point $x = x_m$ on the beam element

$$v(x_m,t) = \frac{\overline{v_r}(x_m)\overline{v_r}(x_n)}{(1 + i\gamma)\omega_r^2 - \omega^2} F_0 e^{i\omega t} \tag{2.32}$$

$$\theta_z(x_m,t) = \frac{\overline{\theta_{zr}}(x_m)\overline{v_r}(x_n)}{(1 + i\gamma)\omega_r^2 - \omega^2} F_0 e^{i\omega t} \tag{2.33}$$

Similarly, to obtain the steady state response to a harmonic moment excitation, $m_z(x,t)$ in Equation 2.18 is written as

$$m_z(x,t) = M(t)\delta(x - x_n) \tag{2.34}$$

where, $M(t)$ is a harmonic moment applied at an arbitrary point $x = x_n$ ($M(t) = M_0 e^{i\omega t}$). For harmonic moment applied at $x = x_n$ steady state

response of the beam at any arbitrary point $x = x_m$ is,

$$v(x_m, t) = \frac{\overline{v_r}(x_m)\overline{\theta_{zr}}(x_n)}{(1+i\gamma)\omega_r^2 - \omega^2} M_0 e^{i\omega t} \tag{2.35}$$

$$\theta_z(x_m, t) = \frac{\overline{\theta_{zr}}(x_m)\overline{\theta_{zr}}(x_n)}{(1+i\gamma)\omega_r^2 - \omega^2} M_0 e^{i\omega t} \tag{2.36}$$

The receptance functions of the beam are defined as,

$$H_{mn} = \frac{v_m}{f_n} \qquad N_{mn} = \frac{\theta_{zm}}{f_n}$$
$$L_{mn} = \frac{v_m}{f_n} \qquad P_{mn} = \frac{\theta_{zm}}{m_n}$$

where,

$$f_n = F_0 e^{i\omega t} \quad \text{at} \quad x = x_n$$
$$m_n = M_0 e^{i\omega t} \quad \text{at} \quad x = x_n$$
$$v_m = v(x_m, t) \quad \text{and} \quad \theta_{zm} = \theta_z(x_m, t)$$

Points 1 and 2 on the beam correspond to $x_1 = L$ and $x_2 = 0$, respectively. In order to find the end point receptance functions, m and n are taken as $m = 1, 2$ and $n = 1, 2$. The beam is free-free. So, since there is no shear deformation at the boundaries of the beam at $x = x_1 = L$ and $x = x_2 = 0$,

$$\frac{d\overline{v_r}(x)}{dx} = \overline{v_r}'(x) = \overline{\theta_{zr}}(x) \tag{2.37}$$

End point receptance function at point 1 relating the forcing applied at point 1 and response at point 1, H_{11}, is,

$$\begin{aligned} H_{11} &= \frac{v_m}{f_n} \\ &= \sum_{r=0}^{\infty} \frac{\overline{v_r}(x_1)\overline{v_r}(x_1)}{(1+i\gamma)\omega_r^2 - \omega^2} \\ &= \frac{\overline{v_{tr}}(L)\overline{v_{tr}}(L)}{-\omega^2} + \frac{\overline{v_{rot}}(L)\overline{v_{rot}}(L)}{-\omega^2} + \sum_{r=1}^{\infty} \frac{\overline{v_r}(L)\overline{v_r}(L)}{(1+i\gamma)\omega_r^2 - \omega^2} \end{aligned} \tag{2.38}$$

Substituting Equations 2.26a and 2.26c into Equation 2.38 gives,

$$\begin{aligned} H_{11} &= \frac{A_{tr}A_{tr} + A_{rot}\frac{L}{2}A_{rot}\frac{L}{2}}{-\omega^2} + \sum_{r=1}^{\infty} \frac{\overline{v_r}(L)\overline{v_r}(L)}{(1+i\gamma)\omega_r^2 - \omega^2} \\ &= -\frac{1}{\rho AL\omega^2} - \frac{3L}{(\rho AL^2 + 12\rho I)\omega^2} + \sum_{r=1}^{\infty} \frac{\overline{v_r}(L)\overline{v_r}(L)}{(1+i\gamma)\omega_r^2 - \omega^2} \end{aligned} \tag{2.39}$$

Similar to obtaining Equation 2.39, remaining end point receptance functions can be determined as follows,

$$H_{12} = -\frac{1}{\rho AL\omega^2} + \frac{3L}{(\rho AL^2 + 12\rho I)\omega^2} + \sum_{r=1}^{\infty} \frac{\overline{v_r}(L)\overline{v_r}(0)}{(1+i\gamma)\omega_r^2 - \omega^2} \tag{2.40a}$$

$$H_{22} = -\frac{1}{\rho AL\omega^2} - \frac{3L}{(\rho AL^2 + 12\rho I)\omega^2} + \sum_{r=1}^{\infty} \frac{\overline{v_r}(0)\overline{v_r}(0)}{(1+i\gamma)\omega_r^2 - \omega^2} \tag{2.40b}$$

$$L_{11} = -\frac{6}{(\rho AL^2 + 12\rho I)\omega^2} + \sum_{r=1}^{\infty} \frac{\overline{v_r}(L)\overline{v_r}'(L)}{(1+i\gamma)\omega_r^2 - \omega^2} \tag{2.40c}$$

$$L_{12} = -\frac{6}{(\rho AL^2 + 12\rho I)\omega^2} + \sum_{r=1}^{\infty} \frac{\overline{v_r}(L)\overline{v_r}'(0)}{(1+i\gamma)\omega_r^2 - \omega^2} \tag{2.40d}$$

$$L_{22} = \frac{6}{(\rho AL^2 + 12\rho I)\omega^2} + \sum_{r=1}^{\infty} \frac{\overline{v_r}(0)\overline{v_r}'(0)}{(1+i\gamma)\omega_r^2 - \omega^2} \tag{2.40e}$$

$$P_{11} = -\frac{12}{(\rho AL^3 + 12\rho IL)\omega^2} + \sum_{r=1}^{\infty} \frac{\overline{v_r}(L)\overline{v_r}'(0)}{(1+i\gamma)\omega_r^2 - \omega^2} \tag{2.40f}$$

$$P_{12} = -\frac{12}{(\rho AL^3 + 12\rho IL)\omega^2} + \sum_{r=1}^{\infty} \frac{\overline{v_r}'(L)\overline{v_r}'(0)}{(1+i\gamma)\omega_r^2 - \omega^2} \tag{2.40g}$$

$$P_{22} = -\frac{12}{(\rho AL^3 + 12\rho IL)\omega^2} + \sum_{r=1}^{\infty} \frac{\overline{v_r}'(0)\overline{v_r}'(0)}{(1+i\gamma)\omega_r^2 - \omega^2} \tag{2.40h}$$

$$N_{12} = \frac{6}{(\rho AL^2 + 12\rho I)\omega^2} + \sum_{r=1}^{\infty} \frac{\overline{v_r}'(L)\overline{v_r}(0)}{(1+i\gamma)\omega_r^2 - \omega^2} \tag{2.40i}$$

Using Equation 2.40, end point receptance matrix (or simply FRF matrix) of

the beam, $[A(\omega)]$, is obtained,

$$[\alpha(\omega)] = \begin{bmatrix} H_{11} & L_{11} & H_{12} & L_{12} \\ N_{11} & P_{11} & N_{12} & P_{12} \\ H_{21} & L_{21} & H_{22} & L_{22} \\ N_{21} & P_{21} & N_{22} & P_{22} \end{bmatrix} = \begin{bmatrix} H_{11} & L_{11} & H_{12} & L_{12} \\ & P_{11} & N_{12} & P_{12} \\ & & H_{22} & L_{22} \\ sym & & & P_{22} \end{bmatrix} \tag{2.41}$$

where,

H_{mn} :Harmonic transverse displacement response of the beam at $x = x_m$ for a harmonic forcing excitation at $x = x_n$

L_{mn} :Harmonic transverse displacement response of the beam at $x = x_m$ for a harmonic moment excitation at $x = x_n$

N_{mn} :Harmonic angular rotation response of the beam at $x = x_m$ for a harmonic forcing excitation at $x = x_n$

P_{mn} :Harmonic angular rotation response of the beam at $x = x_m$ for a harmonic moment excitation at $x = x_n$

$x_m = 0, L$ and $x_n = 0, L$

2.1.3 Receptance Coupling of Beam Elements

The SHT system is modeled by using constant cross-section beam elements. In order to obtain the FRF of the whole SHT system by using structural coupling, FRF of each beam element need to be found first. General FRF matrix of a Timoshenko beam element is found in the previous section. Receptance coupling (or FRF coupling) is applied to combine FRF matrices of beam elements to obtain the FRF matrix of the SHT.

FRF coupling of two elements can be applied by taking them rigidly fixed to each other. Then, no relative motion is assumed between two elements, and it is called rigid FRF coupling. Rigid FRF coupling is usually used for coupling beam elements of the same main component of the SHT. Spindle,

toolholder and tool can be considered as main components of the SHT system. For instance, for obtaining FRF of a spindle, beam elements of spindle are coupled rigidly.

However, the main components of the SHT are not rigidly fixed to each other. Instead, they apply high pressures to each other to assure no loss of contact during milling process. For example, for some type of toolholders, toolholder is at first heated up. When the hole of toolholder expands then the tool is put inside of toolholder and thus shrink fit occurs between toolholder and tool. For spindle-toolholder contact, loss of contact is prevented by a force applied on toolholder which pulls it towards the spindle. Therefore, coupling of main components is to be carried out considering the contact zones between them. Equivalent contact parameters (equivalent stiffness and damping) are assigned to define the contact at spindle-toolholder and toolholder-tool contacts. Coupling two elements considering defined contact parameters in between is called flexible FRF coupling.

It should be noted that when two constant cross-section (constant diameter) beam elements (segments) with different diameters are coupled, the resulting beam element has no longer constant-cross section. The procedure of coupling segments with different diameters to each other one after the other is called chain coupling. When Timoshenko beam elements with free-free boundary conditions are coupled, the resulting SHT also has free-free boundary conditions. Spindle of a SHT is supported by angular contact ball bearings. In this study bearings are modeled as nonlinear elements. Stiffness of each bearing depends on its displacement amplitude. Therefore, receptance information for the points on the spindle where bearings are located is necessary for iterative solution of the equations of motion of the system. After performing coupling of beam elements while keeping the receptance information for the bearing connection points on the SHT, bearing dynamics can be coupled to the dynamics of the rest of the system to obtain the whole SHT system model with bearing supports.

2.1.3.1 Rigid FRF Coupling Without Losing FRF Information at Connection Points

When two beam elements are coupled using flexible FRF coupling, displacements of connection points are not identical because of having springs and dampers (equivalent contact parameters) between the connection points of segments. Rigid FRF coupling can be considered as flexible coupling with infinitely large stiffness between connection points. Motion of connection points on the coupled beam elements are identical at rigid FRF coupling. For classical rigid FRF coupling connection points are not kept on the resulting element. However, by applying a modified rigid FRF coupling procedure explained in this section, connection points can be kept for the resulting element. The formulation for applying rigid FRF coupling without losing connection points is based on works of Ferreira [56] and Liu [64].

Generalized FRF coupling without losing connection points is explained by analyzing an intermediate step of a chain coupling. Let us consider two beams, A and B, as shown in Figure 2.4. A is the beam formed by segments coupled by chain coupling. B is the constant diameter beam element to be coupled to A. So, B has only two points on it, and A has k points on it. $k-2$ is the number of connection points kept during chain coupling before coupling with B. FRF matrices of A and B are represented by $[\alpha]$ and $[\beta]$, respectively. FRF matrices of A and B include point and transfer receptance functions of both beams.

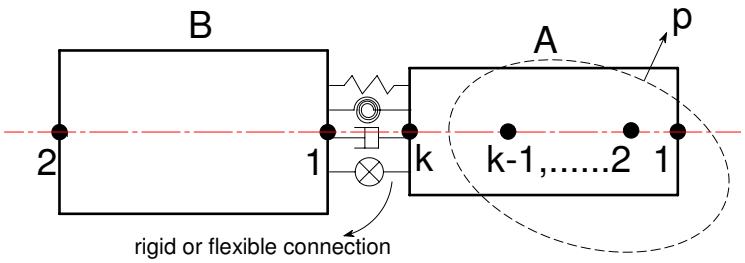

Figure 2.4. Representation of segments A and B to be coupled

$$[\alpha] = \begin{bmatrix} \alpha_{kk} & \alpha_{kp} \\ \alpha_{pk} & \alpha_{pp} \end{bmatrix} \tag{2.42}$$

$$[\beta] = \begin{bmatrix} \beta_{22} & \beta_{21} \\ \beta_{12} & \beta_{11} \end{bmatrix} \tag{2.43}$$

In order to keep the connection points an extended matrix $[\beta']$ is formed by adding duplicate of point 1 (point 1 $\equiv$ point 1$'$) to $[\beta]$ as,

$$[\beta'] = \left[\begin{array}{cc:c} \beta_{22} & \beta_{21} & \beta_{21} \\ \beta_{12} & \beta_{11} & \beta_{11} \\ \hdashline \beta_{12} & \beta_{11} & \beta_{11} \end{array}\right] \tag{2.44}$$

Because of the rigid connection between beams A and B, point k on beam A and point 1 on beam B have equal displacement. Displacement vectors of the beams can be expressed as

$$\{q_A\} = \{q_p\} \tag{2.45}$$

$$\{q_B\} = \begin{Bmatrix} q_2 & q_1 \end{Bmatrix}^T \tag{2.46}$$

Similar to expression for displacement vectors force vectors are formed as

$$\{F_A\} = \{F_p\} \tag{2.47}$$

$$\{F_B\} = \begin{Bmatrix} F_2 & F_1 \end{Bmatrix}^T \tag{2.48}$$

Displacements can be related to forces as follows:

$$\begin{Bmatrix} q_k \\ q_A \end{Bmatrix} = \begin{bmatrix} \alpha_{aa} & \alpha_{ab} \\ \alpha_{ba} & \alpha_{bb} \end{bmatrix} \begin{Bmatrix} F_k \\ F_A \end{Bmatrix} \tag{2.49}$$

$$\begin{Bmatrix} q_B \\ q_{1'} \end{Bmatrix} = \begin{bmatrix} \beta_{aa} & \beta_{ab} \\ \beta_{ba} & \beta_{bb} \end{bmatrix} \begin{Bmatrix} F_B \\ F_{1'} \end{Bmatrix} \tag{2.50}$$

where,

$$\alpha_{aa} = [\alpha_{kk}] \qquad \beta_{aa} = \begin{bmatrix} \beta_{22} & \beta_{21} \\ \beta_{12} & \beta_{11} \end{bmatrix}$$

$$\alpha_{ab} = [\alpha_{kp}] \qquad \beta_{ab} = \begin{bmatrix} \beta_{21} \\ \beta_{11} \end{bmatrix}$$

$$\alpha_{ba} = [\alpha_{pk}] \qquad \beta_{ab} = \begin{bmatrix} \beta_{12} & \beta_{11} \end{bmatrix}$$

$$\alpha_{bb} = [\alpha_{pp}] \qquad \beta_{bb} = [\beta_{11}]$$

Connection between the beams is rigid, so, displacements of point 1 (also, duplicate of point 1) and point k are equal to each other.

$$\{q_{1'}\} = \{q_k\} \tag{2.51}$$

At connection points the forces are equal in magnitude and opposite in direction.

$$\{F_{1'}\} = -\{F_k\} \tag{2.52}$$

From Equations 2.49, 2.50 and 2.51, it is possible to write

$$\begin{bmatrix} \beta_{ba} & \beta_{bb} \end{bmatrix} \begin{bmatrix} F_B \\ F_{1'} \end{bmatrix} = \begin{bmatrix} \alpha_{aa} & \alpha_{ab} \end{bmatrix} \begin{bmatrix} F_k \\ F_A \end{bmatrix} \tag{2.53}$$

Combining Equation 2.52 with Equation 2.53 gives,

$$\beta_{ba}\{F_B\} - \beta_{bb}\{F_k\} = \alpha_{aa}\{F_k\} + \alpha_{ab}\{F_A\}$$

$$\{F_k\} = (\alpha_{aa} + \beta_{bb})^{-1}(\beta_{ba}\{F_B\} - \alpha_{ab}\{F_A\}) \tag{2.54}$$

From Equation 2.52 and Equation 2.54,

$$\{F_{1'}\} = (\alpha_{aa} + \beta_{bb})^{-1}(\alpha_{ab}\{F_A\} - \beta_{ba}\{F_B\}) \tag{2.55}$$

Inserting Equation 2.54 into Equation 2.49 gives

$$\{q_A\} = [\alpha_{bb} - \alpha_{ba}(\alpha_{aa} + \beta_{bb})^{-1}\alpha_{ab}]\{F_A\} + \alpha_{ba}(\alpha_{aa} + \beta_{bb})^{-1}\beta_{ba}\{F_B\} \quad (2.56)$$

Using Equation 2.55 in Equation 2.50 yields

$$\{q_B\} = \beta_{ab}(\alpha_{aa} + \beta_{bb})^{-1}\alpha_{ba}\{F_A\} - [\beta_{aa} - \beta_{ab}(\alpha_{aa} + \beta_{bb})^{-1}\beta_{ba}]\{F_B\} \quad (2.57)$$

$[\gamma]$ the FRF matrix of the resulting multiple-segment beam, C. From Equation 2.56 related components can be written as

$$\gamma_{AA} = \gamma_{pp} = \alpha_{pp} - \alpha_{pk}(\alpha_{kk} + \beta_{11})^{-1}\alpha_{kp} \quad (2.58)$$

$$\gamma_{AB} = \begin{bmatrix}\gamma_{p2} & \gamma_{p1}\end{bmatrix} = \alpha_{pk}(\alpha_{kk} + \beta_{11})^{-1}\begin{bmatrix}\beta_{12} & \beta_{11}\end{bmatrix} \quad (2.59)$$

Similarly, from Equation 2.57,

$$\gamma_{BA} = \begin{bmatrix}\gamma_{2p} \\ \gamma_{1p}\end{bmatrix} = \begin{bmatrix}\beta_{21} \\ \beta_{11}\end{bmatrix}(\alpha_{kk} + \beta_{11})^{-1}\alpha_{kp} \quad (2.60)$$

$$\gamma_{BB} = \begin{bmatrix}\gamma_{22} & \gamma_{21} \\ \gamma_{12} & \gamma_{11}\end{bmatrix} = \begin{bmatrix}\beta_{22} & \beta_{21} \\ \beta_{12} & \beta_{11}\end{bmatrix} - \begin{bmatrix}\beta_{21} \\ \beta_{11}\end{bmatrix}(\alpha_{kk} + \beta_{11})^{-1}\begin{bmatrix}\beta_{12} & \beta_{11}\end{bmatrix} \quad (2.61)$$

So, elements of the FRF matrix of the combined system, C, is

$$\gamma_{22} = \beta_{22} - \beta_{21}(\alpha_{kk} + \beta_{11})^{-1}\beta_{12} \quad (2.62a)$$

$$\gamma_{21} = \beta_{21} - \beta_{21}(\alpha_{kk} + \beta_{11})^{-1}\beta_{11} \quad (2.62b)$$

$$\gamma_{2p} = \beta_{21}(\alpha_{kk} + \beta_{11})^{-1}\alpha_{kp} \quad (2.62c)$$

$$\gamma_{11} = \beta_{11} - \beta_{11}(\alpha_{kk} + \beta_{11})^{-1}\beta_{11} \quad (2.62d)$$

$$\gamma_{1p} = \beta_{11}(\alpha_{kk} + \beta_{11})^{-1}\alpha_{kp} \quad (2.62e)$$

$$\gamma_{pp} = \alpha_{pp} - \alpha_{pk}(\alpha_{kk} + \beta_{11})^{-1}\alpha_{kp} \quad (2.62f)$$

Then, $[\gamma]$ matrix is formed as

$$[\gamma] = \begin{bmatrix} \gamma_{22} & \gamma_{21} & \gamma_{2p} \\ & \gamma_{11} & \gamma_{1p} \\ sym & & \gamma_{pp} \end{bmatrix} \tag{2.63}$$

For the next coupling procedure, elements of the $[\gamma]$ matrix are renamed as shown below:

$$\begin{aligned} \gamma_{22} &\longrightarrow \alpha_{kk} \\ \begin{bmatrix} \gamma_{21} & \gamma_{2p} \end{bmatrix} &\longrightarrow \alpha_{kp} \\ \begin{bmatrix} \gamma_{12} \\ \gamma_{p2} \end{bmatrix} &\longrightarrow \alpha_{pk} \\ \begin{bmatrix} \gamma_{11} & \gamma_{1p} \\ \gamma_{p1} & \gamma_{pp} \end{bmatrix} &\longrightarrow \alpha_{pp} \end{aligned}$$

The procedure explained above can also be used by eliminating the connection point information. The point $1'$ in the above formulation should not be added to FRF matrix of beam element B.

2.1.3.2 Flexible FRF Coupling

If a duplicate connection point is not added to the beams to keep the connection point information, classical coupling procedure is obtained. In this section, classical coupling for flexible connection is given. Then the FRF information for the connection points are lost in the resulting model. For the SHT system it is not necessary to keep the points at the connection of the main components (spindle, toolholder and tool). The connection parameters used in flexible coupling are called contact parameters since they represent contacts between spindle-toolholder, and between toolholder-tool.

The procedure is similar to that given at Section 2.1.3.1. However, FRF

information of duplicate connection points are not added to β in this analysis since connection points are not kept for resulting element.

When there are elastic elements between the connection points, the displacements of these points will not be equal to each other. They are related to each other as shown below:

$$[K_{AB}](\{q_1\} - \{q_k\}) = \{F_1\} \tag{2.64}$$

where,

$$[K_{AB}] = \begin{bmatrix} k_y^{AB} + i\omega c_y^{AB} & 0 \\ 0 & k_\theta^{AB} + i\omega c_\theta^{AB} \end{bmatrix}$$

k_y^{AB} : translational contact stiffness parameter

k_θ^{AB} : rotational contact stiffness parameter

c_y^{AB} : translational contact damping parameter

c_θ^{AB} : rotational contact damping parameter

The force equilibrium yields the relation between the forces at the connection points as

$$\{F_1\} = -\{F_k\} \tag{2.65}$$

Applying a similar procedure as in Section 2.1.3.1 yields the FRF matrix, γ, of the combined system, C:

$$\gamma_{pp} = \alpha_{pp} - \alpha_{pk}(\alpha_{kk} + \beta_{11} + [K_{AB}]^{-1})\alpha_{kp} \tag{2.66a}$$

$$\gamma_{p2} = \alpha_{pk}(\alpha_{kk} + \beta_{11} + [K_{AB}]^{-1})\beta_{12} \tag{2.66b}$$

$$\gamma_{2p} = \beta_{21}(\alpha_{kk} + \beta_{11} + [K_{AB}]^{-1})\alpha_{kp} \tag{2.66c}$$

$$\gamma_{22} = \beta_{22} - \beta_{21}(\alpha_{kk} + \beta_{11} + [K_{AB}]^{-1})\beta_{12} \tag{2.66d}$$

Elements of $[\gamma]$ are renamed for next coupling process as,

$$\gamma_{pp} \longrightarrow \alpha_{pp}$$
$$\gamma_{p2} \longrightarrow \alpha_{pk}$$
$$\gamma_{2p} \longrightarrow \alpha_{kp}$$
$$\gamma_{22} \longrightarrow \alpha_{kk}$$

It should be noted that, if $[K_{AB}]$ is taken very stiff making $[K_{AB}]^{-1} \approx 0$ in $[\gamma]$, results of rigid FRF coupling will be obtained.

2.2 Modeling of Bearings

The receptance coupling (FRF coupling) is used to obtain linear FRF matrix of a SHT system without bearing supports (free-free). The receptance analysis and the coupling procedure described in Section 2.1 are valid for a linear system. However, the spindle of the SHT is supported by angular contact ball bearings, which can be modeled by displacement amplitude dependent stiffness elements. Cubic stiffness element is taken to represent the bearings supporting the SHT system. Nonlinear element representing a bearing in the SHT system has freedom in transverse direction only.

When there is a nonlinear element in the system, harmonic vibration analysis can be achieved by using describing function (DF) theory. It is a common method used for harmonic vibration analysis of a nonlinear system.

2.2.1 Describing Function Theory

Let us consider the SHT system shown in Figure 2.5. Angular contact ball bearings are modeled by cubic stiffness elements in transverse direction. The coefficient of its linear part depends on the magnitude of the preload applied on the bearing [34]. The coefficient of nonlinear part of cubic stiffness element

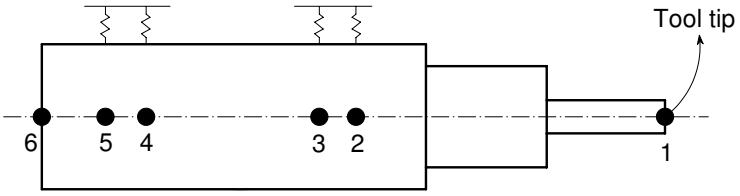

Figure 2.5. SHT system considered

can be predicted using bearing models [55]. Cubic stiffness is assumed for the nonlinear part, and its equivalent stiffness and equivalent damping are determined using describing function theory [65]. Then, equivalent quasi-linear form of the nonlinear bearing force vector is determined using equivalent stiffness of the bearings. The determined quasi-linear force vector is identified only for the considered displacement amplitude, i.e. it is response-dependent. Thus, quasi-linear bearing force vector is determined at each iteration step during solution, when displacement amplitude is modified.

Force on each bearing can be represented as,

$$f_{b,j}(v_j) = k_l v_j + k_n v_j^3 \tag{2.67}$$

where,

k_l : coefficient of linear component of the stiffness

k_n : coefficient of nonlinear component of the stiffness

$f_{b,j}$: reaction force of bearing in transverse direction at point j

v_j : deformation or displacement in transverse direction at point j

$j = 2, 3, 4, 5$ (for Figure 2.5)

In order to make frequency domain analysis using nonlinear bearings, the bearing force vector need to be put into quasi-linear form. With nonlinear bearing forces the equation of motion of the dynamic system may be written as

$$[Z]\{x\} + \{f_b(\{x\})\} = \{F\}\cos(\omega t) \tag{2.68}$$

where,

$[Z]$: dynamic stiffness matrix of the SHT (inverse of receptance of the SHT)

$\{x\}$: response vector

$\{f_b(\{x\})\}$: bearing force vector (expressed as a function of the response vector)

$\{F\}$: magnitude of external harmonic forces

ω : excitation frequency

After obtaining quasi-linear bearing force vector using describing function theory, the equation of motion becomes suitable for the analysis in the frequency domain:

$$[Z]\{x\} + [K_l]_b\{x\} + \{F_{nl}(\{x\})\} = \{F\}\cos(\omega t) \tag{2.69}$$

where,

$[K_l]_b$: linear part of the bearing stiffness in matrix form

$\{F_{nl}(\{x\})\}$: force vector representing nonlinear bearing force

The bearings can be considered as local nonlinearities coupled to the linear SHT system. After finding equivalent stiffness and equivalent damping of the bearings, they can be coupled to dynamics of the SHT. In the following section, quasi-linear form of a single bearing is determined using DF theory.

2.2.2 Quasi-Linearization of Cubic Stiffness Element

A single nonlinear cubic stiffness element, which exerts a force of magnitude proportional to its deformation to the third power, is considered. To make the derivation simple, the linear part of the cubic stiffness element is not considered in the analysis.

If a static load is applied to the cubic stiffness element in Figure 2.6(a), response of the element would be as shown in Figure 2.6(b). If harmonic forcing, $F(\theta) = F(\omega t) = F\cos(\omega t)$, is applied to the element the response of the non-

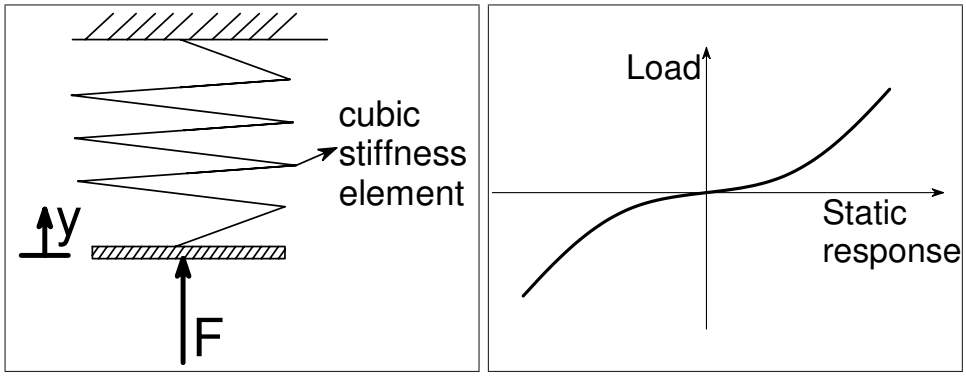

(a) (b)

Figure 2.6. Static load applied to nonlinear element

linear element would also be harmonic. However, generally, the difference of response of a nonlinear element from response of a linear element is that its response would not only include fundamental harmonic (at frequency ω) but also include zeroth and higher harmonics (at frequencies $\omega, 2\omega, 3\omega \ldots$),

$$y(\theta) = Y_0 + \sum_{m=1,2,3,\ldots}^{\infty} [Y_{mc}\cos(m\theta) + Y_{ms}\sin(m\theta)] \tag{2.70}$$

The equation of motion for the cubic stiffness element is

$$F(\theta) = k_n y(\theta)^3 \tag{2.71}$$

Cubic stiffness element is a special element which gives odd and symmetric response. For the symmetric nonlinearity zeroth component (average value) of the response is zero, and for the odd nonlinearity even harmonics of the response are all zero. For cubic stiffness, it is fair enough to approximate the response by using only the first (fundamental) harmonic since the nonlinearity is not heavy. So, representation of the response in Equation 2.70 becomes,

$$y(\theta) = \sum_{m=1,3,\ldots}^{\infty} [Y_{mc}\cos(m\theta) + Y_{ms}\sin(m\theta)] \approx Y_c\cos(\theta) + Y_s\sin(\theta) \tag{2.72}$$

Inserting Equation 2.72 into Equation 2.71 gives,

$$F(\theta) = k_n[Y_c \cos(\theta) + Y_s \sin(\theta)]^3 \tag{2.73}$$

The applied harmonic force may be expressed as

$$F_c \cos(\theta) + F_s \sin(\theta) = Re[(F_c - iF_s)e^{i\theta}] \tag{2.74}$$

where,

F_c : magnitude of cosine component of the forcing

F_s : magnitude of sine component of the forcing

Similarly, the harmonic response is represented as

$$Y_c \cos(\theta) + Y_s \sin(\theta) = Re[(Y_c - iY_s)e^{i\theta}] \tag{2.75}$$

where,

Y_c : magnitude of cosine component of the response

Y_s : magnitude of sine component of the response

The aim in describing function theory is to relate force to response linearly at a specified frequency and for a specific vibration amplitude, for each harmonic term. Only fundamental harmonic of the response is used in this analysis. The value which relates force to displacement response is called equivalent stiffness, and it may be complex if it also has imaginary part representing equivalent damping. This relation can be written as

$$Re[(F_c - iF_s)e^{i\theta}] = Re[\underbrace{(k_r + i \cdot k_i)}_{\text{linearized stiffness}} (Y_c - iY_s)e^{i\theta}]$$

$$F_c - iF_s = (k_r + i \cdot k_i)(Y_c - iY_s) \tag{2.76}$$

where,

k_r : equivalent stiffness [65]

k_i : equivalent damping [65]

Equation 2.76 gives F_c and F_s as follows

$$F_c = k_r Y_c + k_i Y_s \tag{2.77a}$$

$$F_s = k_r Y_s - k_i Y_c \tag{2.77b}$$

When written in matrix form Equation 2.77 becomes

$$\begin{bmatrix} F_c \\ F_s \end{bmatrix} = \begin{bmatrix} k_r & k_i \\ -k_i & k_r \end{bmatrix} \begin{bmatrix} Y_c \\ Y_s \end{bmatrix} \tag{2.78}$$

The matrix multiplied by response vector to obtain force vector in Equation 2.78 is response-dependent and it is called "nonlinearity matrix" in DF theory [66]. Gelb et al. [67] formulated the values of k_r and k_i as,

$$k_r = \frac{1}{\pi Y} \int_0^{2\pi} F(\theta) cos(\theta) d\theta \tag{2.79}$$

$$k_i = -\frac{1}{\pi Y} \int_0^{2\pi} F(\theta) sin(\theta) d\theta \tag{2.80}$$

where, Y is the magnitude (amplitude) of displacement response. Inserting Equation 2.73 into Equations 2.79 and 2.80 and integrating analytically gives

$$k_r = \frac{3}{4} k_n Y^2 = \frac{3}{4} k_n (Y_c^2 + Y_s^2) \tag{2.81}$$

$$k_i = 0 \tag{2.82}$$

Another way of expressing Equation 2.78 is

$$\{F\}^T \left\{cos(\theta)\ sin(\theta)\right\}^T = \left(\begin{bmatrix} k_r & k_i \\ -k_i & k_r \end{bmatrix} \{Y\} \right)^T \left\{cos(\theta)\ sin(\theta)\right\}^T \tag{2.83}$$

In Equation 2.83 it is clear that the cosine and sine components of displacement response and forcing are separated. So, they are no longer complex in the equation of motion. This fact is used in applying numerical path following (continuation) method. For cubic stiffness, knowing that equivalent damping is zero,

$$\{F\} = \begin{bmatrix} k_r & 0 \\ 0 & k_r \end{bmatrix} \{Y\} \tag{2.84}$$

$$\{F\} = \frac{3}{4} k_n \begin{bmatrix} Y_c^3 + Y_c Y_s^2 \\ Y_s^3 + Y_s Y_c^2 \end{bmatrix} \tag{2.85}$$

Jacobian matrix of the nonlinear bearing force vector (or the partial derivative) used in numerical analysis can additionally be obtained,

$$\frac{\partial\{F\}}{\partial\{Y\}} = \left[\left\{ \frac{\partial\{F\}}{\partial Y_c} \right\} \left\{ \frac{\partial\{F\}}{\partial Y_s} \right\} \right] \tag{2.86}$$

$$\frac{\partial\{F\}}{\partial\{Y\}} = \frac{3}{4} k_n \begin{bmatrix} 3Y_c^2 + Y_s^2 & Y_c Y_s \\ Y_c Y_s & 3Y_s^2 + Y_c^2 \end{bmatrix} \tag{2.87}$$

2.2.3 Solution of Equation of Motion

In the previous section, elements of quasi-linear bearing force vector $\{F_{nl}(\{x\})\}$ in Equation 2.69 and its Jacobian are determined. After obtaining equation of motion of the SHT system including dynamics of nonlinear bearings, numerical analysis is used to obtain the FRF of the system. Amplitudes of displacements in the SHT system are small for small external forces applied. Generally, when small external forces are applied effects of displacement amplitude-dependent nonlinearities are considered to be insignificant. In that case, solution of equa-

tion of motion gives linear response of the structure. When applied forces take larger values, displacement amplitudes become considerable so that cubic stiffness nonlinearity affects the response and makes it nonlinear.

Then, the FRF of the system becomes different than linear FRF, and it also becomes a function of response. The FRF may be affected so much that turn-backs may occur in the response. Note that for a nonlinear system it is not possible to talk about FRF, which is basically a transfer function (in control theory). Therefore, it may be appropriate to call these curves pseudo-receptance function or pseudo-FRF. In this study, pseudo-FRFs of the SHT system under different conditions are obtained.

If a numerical method (e.g. Newton's method) is used without path following in the analysis, jumps or discontinuities are observed in FRF at the parts where turn-back occurs. Therefore, a numerical continuation method should be used to follow the solution curve of the FRF and observe turn-back behavior.

Newton's method with arc length continuation (ALC) is a method which yields a solution curve that is continuous. The classical numerical methods involve sweeping of the whole frequency domain with a fixed direction of solution (low-to-high or high-to-low frequency sweeps). In Newton's method with ALC the solution is searched within a sphere centered at the current iteration point. This makes it possible to change the direction of the solution curve (FRF in this study). When Newton's method is used with ALC, instead of observing discontinuities (jumps), turn-backs occur at such points. In this study, adaptive step size between solution points is used. Step size is updated at each solution point according to the error at the end of the iterations carried out to obtain previous solution point.

In Newton's method with ALC, Newton's method is used together with the first order predictors. By using Newton's method, the next solution point at the intersection of the sphere (centered at previous solution point) and solution curve is obtained.

Including the linear part of the stiffness of bearings in $[Z(\omega)]$ the residual

vector is written from Equation 2.69 as

$$\{R(\{X\},\omega)\} = [Z(\omega)]\{X\} + \{F_{nl}(\{X\})\} - \{F\} \tag{2.88}$$

The purpose is to seek solution where residual is zero. So, ALC solves the curve defined by

$$\{R(\{X\},\omega)\} = \{0\} \tag{2.89}$$

Newton-Raphson method is applied to use j^{th} estimate to obtain $(j+1)^{th}$ estimate as,

$$\{X\}_{j+1} = \{X\}_j - \left[\frac{\partial\{R(\{X\},\omega)\}}{\partial\{X\}}\right]^{-1}\Bigg|_{(\{X\}_j,\omega)} \{R(\{X\}_j,\omega)\} \tag{2.90}$$

where, Jacobian of the residual matrix is,

$$\frac{\partial\{R(\{X\},\omega)\}}{\partial\{X\}} = [Z(\omega)] + \frac{\partial\{F_{nl}\}}{\partial\{X\}} \tag{2.91}$$

In this study Jacobian of the residual vector and nonlinear force vector, $\{F_{nl}\}$, are determined analytically. It is also possible to find them numerically. Inverse of the Jacobian of the residual vector is needed in Equation 2.90. Jacobian of the nonlinear force vector contains many zero components, so, it would be time-consuming to take inverse of matrices twice. Instead, method proposed by Özgüven [68] can be used to modify the inverse of the Jacobian of the residual matrix by Jacobian of the force vector.

The next frequency point is searched on the boundary of a sphere (having radius s) centered at the k^{th} solution point.

$$\{\Delta q\}_k^T\{\Delta q\}_k = s^2 \tag{2.92}$$

where,

$$\{q\} = \begin{Bmatrix} \{X\} \\ \omega \end{Bmatrix}$$

s : radius of the sphere

Then, another residual equation may be introduced and its solution is sought:

$$g(\{X\}_k, \omega_k) = \{\Delta q\}_k^T \{\Delta q\}_k - s^2 = 0 \tag{2.93}$$

The corrector can be redefined as,

$$\{q\}_k^{j+1} = \{q\}_k^j - \left[\begin{matrix} \frac{\partial\{R(\{X\},\omega)\}}{\partial\{X\}} & \frac{\partial\{R(\{X\},\omega)\}}{\partial\omega} \\ \frac{\partial\{g(\{X\},\omega)\}}{\partial\{X\}} & \frac{\partial\{g(\{X\},\omega)\}}{\partial\omega} \end{matrix} \right]^{-1} \Bigg|_{(\{X\}_k^j, \omega_k^j)} \begin{Bmatrix} \{R(\{X\}_k^j, \omega_k^j)\} \\ \{g(\{X\}_k^j, \omega_k^j)\} \end{Bmatrix} \tag{2.94}$$

where,

$$\left[\begin{matrix} \frac{\partial\{g(\{X\},\omega)\}}{\partial\{X\}} & \frac{\partial\{g(\{X\},\omega)\}}{\partial\omega} \end{matrix} \right] = \left[2\{\Delta q\}_k^{j^T} \right]$$

$$\{\Delta q\}_k^j = \{q\}_k^j - \{q\}_{k-1}$$

In order to improve convergence at sharp points, step-length is modified at each step as suggested in [69],

$$s_k = s_{k-1} \sqrt{\frac{n_{nom}^{iter}}{n_{k-1}^{iter}}} \tag{2.95}$$

where,

s_k : step length at k^{th} solution point

s_{k-1} : step length at $(k-1)^{th}$ solution point

n_{nom}^{iter} : nominal number of iterations

n_{k-1}^{iter} : number of iterations done at $(k-1)^{th}$ solution point

The Newton's method with ALC is very sensitive to sharp corners. Deter-

mining tolerance level and n_{nom}^{iter} mainly affects convergence of the method. For some cases, solution curve is followed up to a sharp corner (turn-back point), then follows back the same curve that has already been determined. The reason is that there are actually two stable solutions for turning back, the previously determined solution curve and the solution curve that should be followed. In order to force the solution points to follow the solution curve, direction of the solution curve may be set for each solution point. Thus, instead of returning to the initial point, solution path can be followed up to the end point.

Newton's method with ALC is used to solve equation of motion of the SHT system in frequency domain, and determine the FRF of the SHT system. Newton's method with ALC is introduced by Crisfield [69] to carry out nonlinear finite element analysis of statically loaded structures. In a recent study, Orbay [58] used Newton's method with ALC to determine response of nonlinear dynamic structures (bladed-disk assemblies).

CHAPTER 3

APPLICATIONS

3.1 The Spindle-Toolholder-Tool System

A motorized spindle-toolholder-tool (SHT) system is analyzed in this chapter. The model of the SHT is adapted from thesis of Cao [37]. The SHT system used is shown in Figure 3.1. Spindle, toolholder, and tool are considered as rigidly coupled to each other. For this study, contact stiffness values are assumed to be infinitely high. In reality, contact parameters are determined by carrying out an experiment. An experimental FRF is fitted to analytically obtained FRF by setting proper contact parameters. The SHT system is supported by four bearings in the front, and one bearing at the rear. The effect of the rotor mounted on spindle shaft is assumed to have negligible effect, and it is not considered in this analysis.

The SHT shown in Figure 3.1 is first separated into constant cross-section beam elements. Bearing connection points are also kept as the end points of

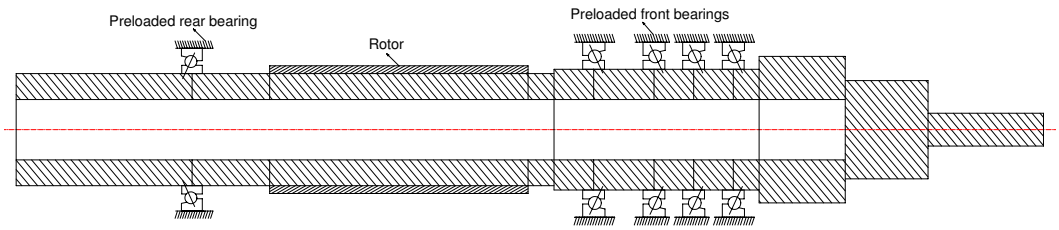

Figure 3.1. Representation of the model of a motorized SHT system

Table 3.1. Dimensions (in mm) of the constant cross-section beam elements in the SHT system (starting from the right hand side)

Beam number	1	2	3	4	5	6	7	8	9	10	11	12
Length	67	48	50	15	23	23	35	23	15	150	45	102
Outer diameter	19.05	57	85	70	70	70	70	70	65	65	65	65
Inner diameter	0	0	0	35	35	35	35	35	35	35	35	35

beam elements by dividing constant cross-section beam elements into multiple pieces. For the SHT system used in this chapter, starting from the right hand side of the system, dimensions of the constant cross-section beam elements are given in Table 3.1.

During end milling process, cutting force is applied at the tool tip of the SHT. In this application chapter, the effect of the following system parameters are studied:

- Magnitude of the cutting force
- Coefficient of nonlinearity of the bearing stiffness
- Number of teeth on the cutter

Type of milling is taken as slotting. In slotting, the cutter is fully immersed (100% immersion) into the workpiece during cutting, where the cutter entry and exit angles are 0 and 180 degrees, respectively. The cutting conditions are given in Table 3.2.

Table 3.2. Cutting conditions of end milling process

Material of the workpiece	Al7075-T6
Cutter diameter	19.05[mm]
Number of flutes on the cutter	1
Type of milling	Slotting

In this chapter, firstly, the linear response of SHT system is presented. Secondly, the effect of magnitude of cutting force on response of SHT and on chatter stability are investigated, while keeping coefficient of cubic stiffness nonlinearity constant. Thirdly, the effect of coefficient of cubic stiffness nonlinearity on response of SHT and on chatter stability are investigated, while keeping magnitude of cutting force constant. Lastly, the effect of number of cutter flutes on chatter stability of milling process is analyzed for a given cutting force magnitude and coefficient of nonlinearity.

3.2 Nonlinear Bearing Properties

The angular contact ball bearings support the SHT system. Each bearing is modeled as a spring acting in transverse direction with cubic stiffness nonlinearity. The coefficient of linear part of the cubic stiffness nonlinearity is determined by the applied preload on a bearing. The linear stiffness of the front bearings are taken $2.1 \cdot 10^8 [N/m]$ each, and of the rear bearing is taken $1.8 \cdot 10^8 [N/m]$. The coefficients of nonlinear components of front bearings are stated in each section, since different values are taken in the analysis.

3.3 Linear Response of the SHT system

Cubic stiffness element which represents bearings in the system has displacement amplitude dependent stiffness. For low forces acting on the SHT system, displacement response of the bearings is low. So, the effect of nonlinearity on the FRF of the system is not considerable for low reaction forces on bearings due to cutting force. For such cases, the system response can be considered as linear. Linear FRF of the tool tip of the SHT can easily be obtained by neglecting nonlinear components of the bearing stiffness, and taking only the linear parts of the bearing stiffnesses. The linear analysis of the system gives the FRF shown in Figure 3.2. The linear FRF of the system can be con-

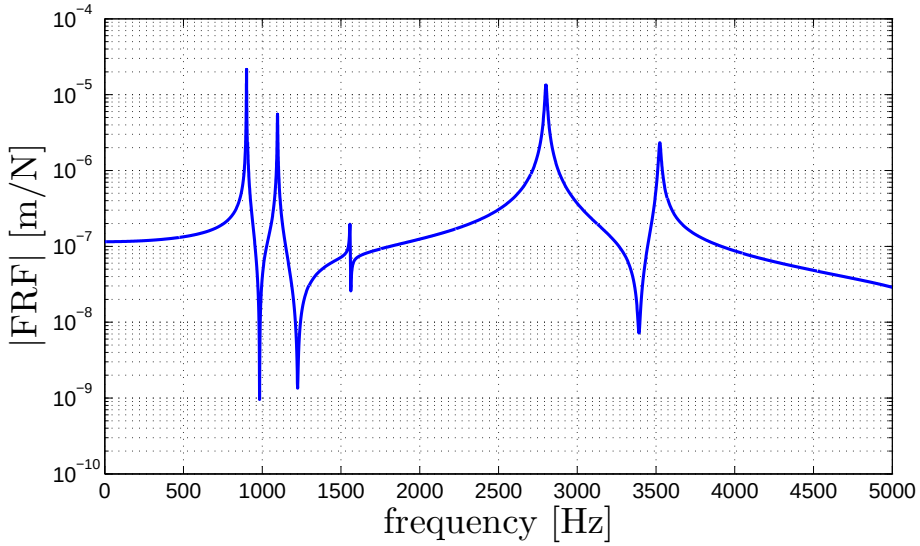

Figure 3.2. Linear tool tip FRF of the SHT system (log vs. linear)

sidered as the frequency response of the system under low force. When the forces acting on the system becomes higher, effect of structural nonlinearities increases.

The first two modes (two peaks) are namely rigid body modes of the SHT. They are due to the almost rigid body motion of the SHT on flexible bearings. The nonlinearities at the bearings mainly affect the rigid body modes of the SHT system. So, the cubic stiffness at the bearings is expected to affect the first two peaks of the FRF curve.

3.4 Effects of Magnitude of Cutting Force

During milling, the cutting forces are applied at the tool tip in one axial and two transverse directions. For the 2D model used in this study, the cutting force is applied at the tool tip in transverse direction only. The cutting force is considered as harmonic force with time invariant magnitude. In this section, the magnitude of the cutting force is increased to observe the effect of the

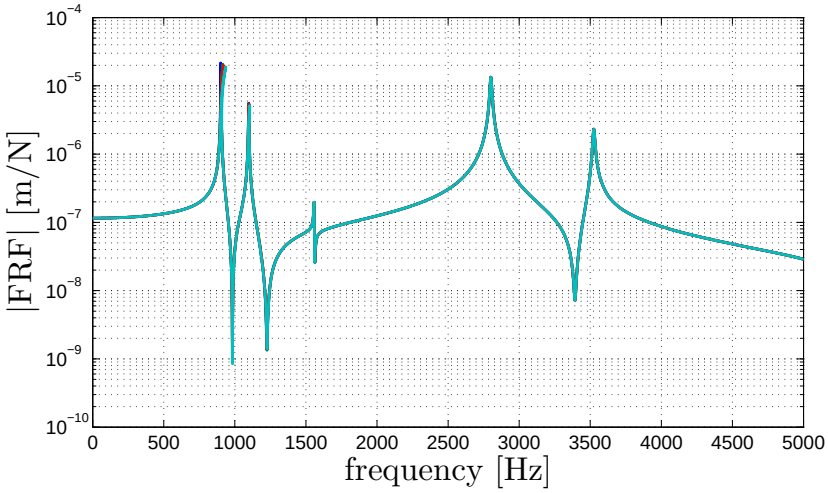

Figure 3.3. Tool tip pseudo-FRFs of the SHT system under high cutting forces (log vs. linear)

nonlinearity at the bearings better.

3.4.1 Effects of Cutting Force Magnitude on Response

The cutting force magnitudes are taken as $F = 70[N]$, $F = 100[N]$ and $F = 150[N]$. The coefficient of nonlinearity is set constant for all cases as $k_n = 1.0 \cdot 10^{14}[N/m^3]$ and $k_n = 0.86 \cdot 10^{14}[N/m^3]$ for front and rear bearings, respectively. Pseudo-FRFs for these two cases are compared in Figure 3.3. As the magnitude of the cutting force increases, the first two modes of the system shift to the right because of the hardening effect of the cubic stiffness. For better view, the first two modes are zoomed in Figure 3.4.

The first mode of the system is more flexible than the second one. This causes the difference in the amount of shift of the peaks. The magnitude of response of the first mode is larger than that of the second one making first mode more sensitive to the stiffness nonlinearity at the bearings. Therefore, the first mode is more sensitive to increase in magnitude of cutting force.

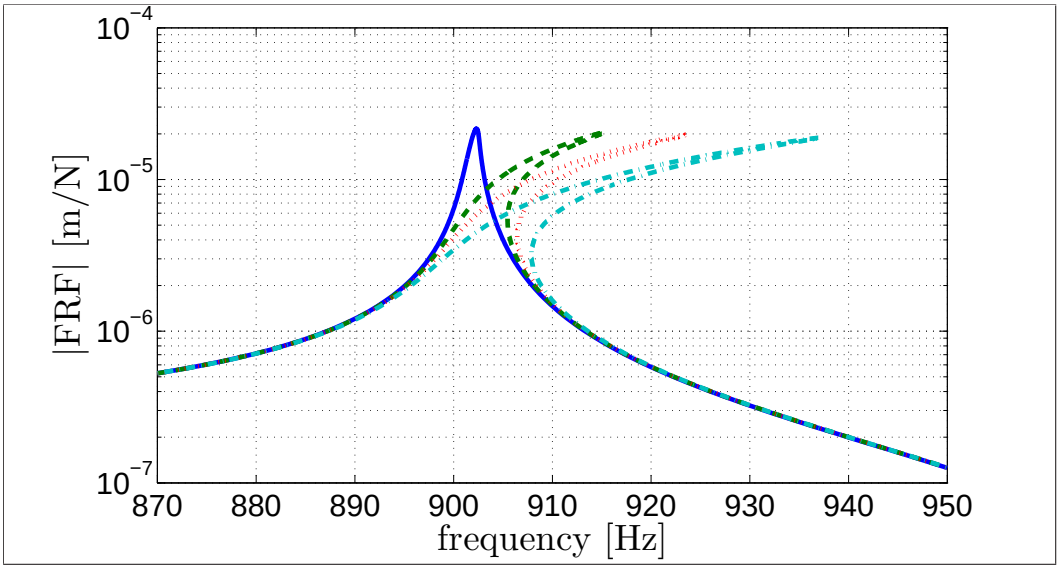

(a) First mode

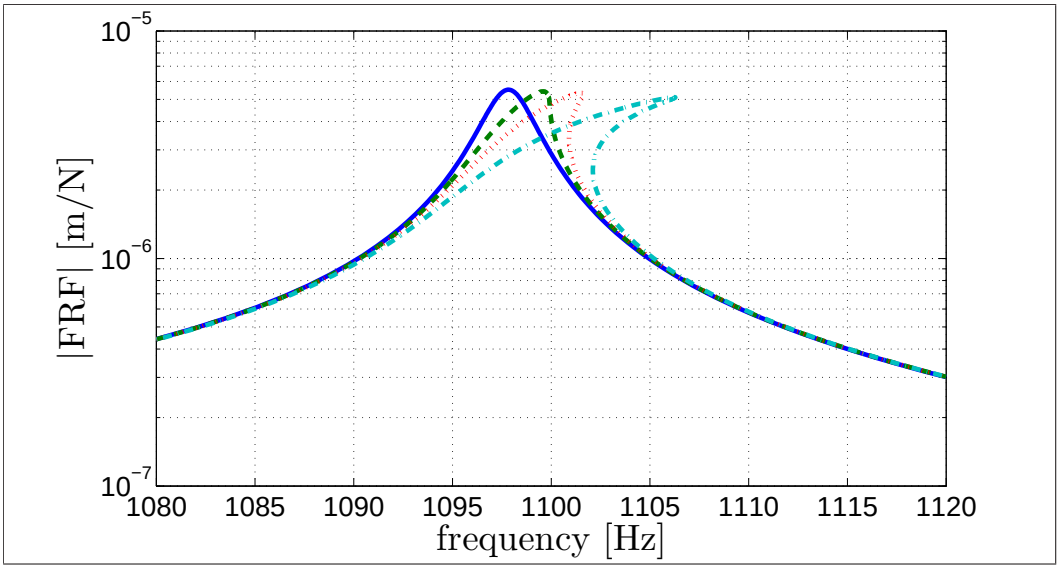

(b) Second mode

Figure 3.4. Zoomed views of the rigid body modes (log vs. linear). Solid: Low force. Dashed: F=70[N]. Dotted: F=100[N]. Dash-dotted: F=150[N]

3.4.2 Effects of Cutting Force Magnitude on Stability

Method of Altıntaş and Budak [18] is used for obtaining the stability lobes from the pseudo-FRFs calculated. For the stability analysis real parts of the FRFs are needed. The effect of cutting force magnitude on the real parts of first two modes can be seen in Figure 3.6.

Effect of using arc length continuation in Newton's method is shown in Figure 3.5. If ALC is not used with Newton's method, the jump from point A to point B in FRF curve corresponds to jumps in each lobe as shown in Figure 3.5.

The stability lobe diagram (SLD) of the linear system (under low cutting load) is obtained by trimming the stability lobes of the dominant modes with respect to each other. In Figure 3.7, SLDs before and after trimming are shown. As seen in Figure 3.7, the most flexible modes (first, second and fourth modes) affect the stability of the SHT system. Among these modes, the first mode has the most important effect on the SLD. So, the largest effect of cubic nonlinearity on the lobes related to the first mode, since the other lobes remains almost constant under the effect of the nonlinearity. The stability lobe related to first mode also shifts to the right as shown in Figure 3.8. Comparison of SLDs of the milling process is carried out in Figure 3.9.

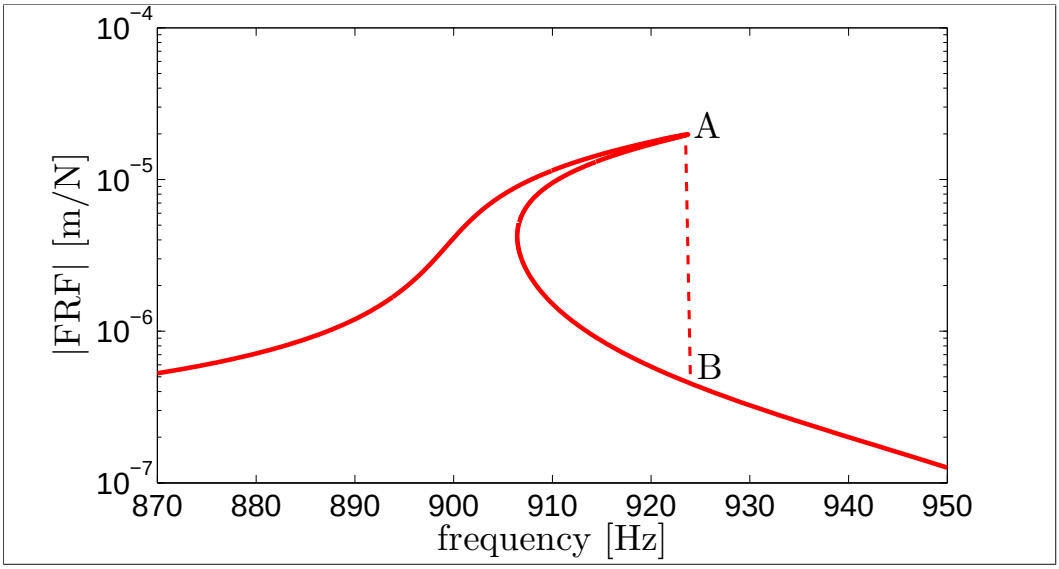

(a) Jump in FRF

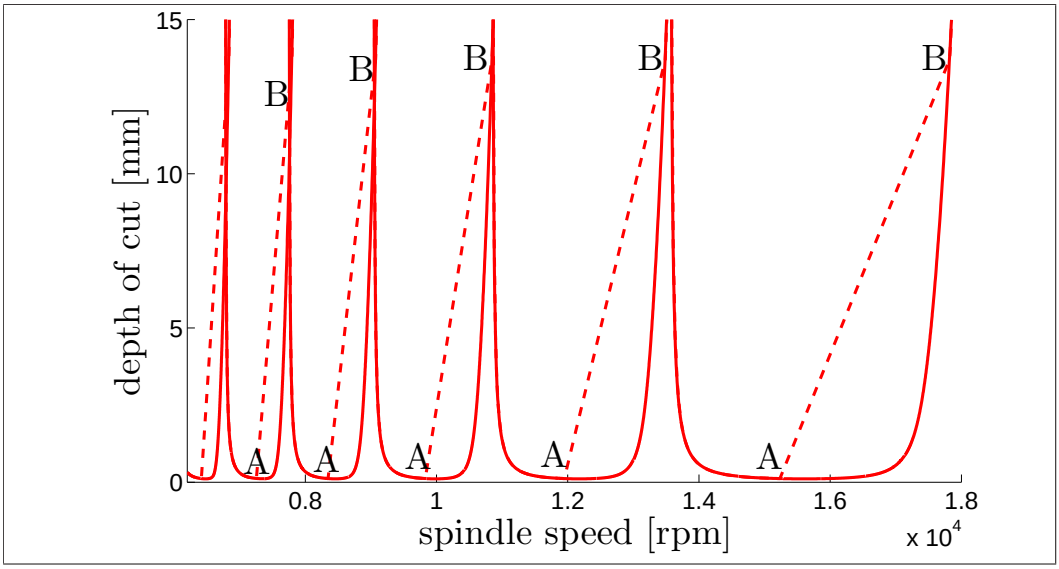

(b) Jump in SLD

Figure 3.5. Effect of ALC on the FRF and SLD of first mode for F=100[N]. Solid: Newton's method with ALC. Dashed: Newton's method without ALC (low-to-high sweep)

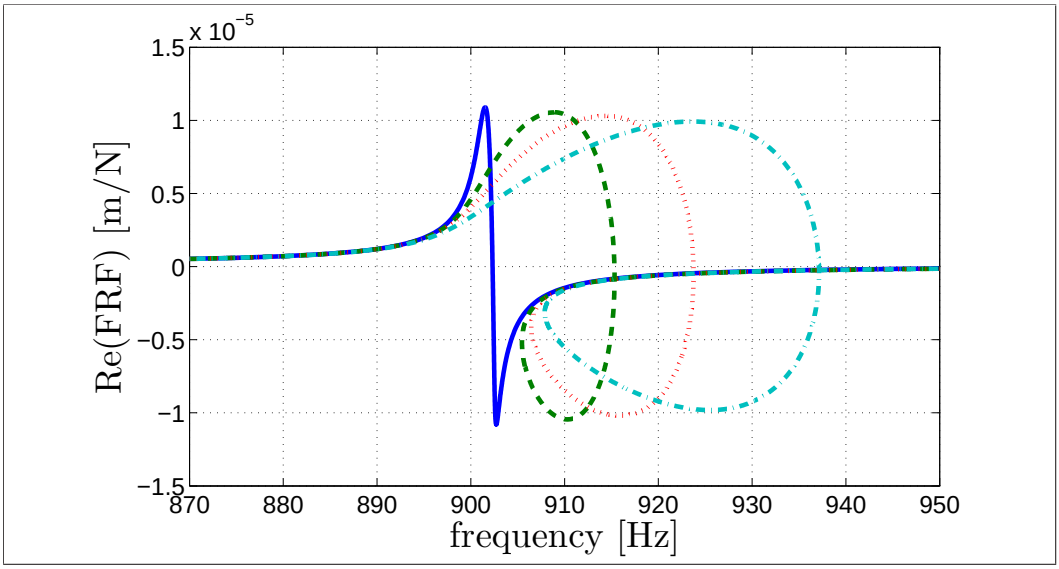

(a) First mode

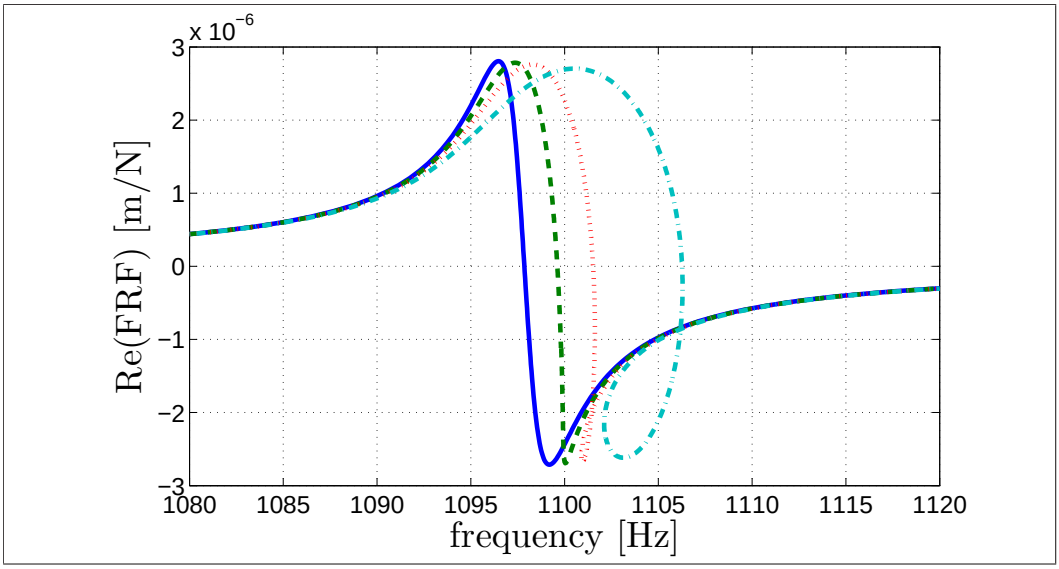

(b) Second mode

Figure 3.6. Zoomed views of the real parts of FRFs of rigid body modes (log vs. linear). Solid: Low force. Dashed: F=70[N]. Dotted: F=100[N]. Dash-dotted: F=150[N]

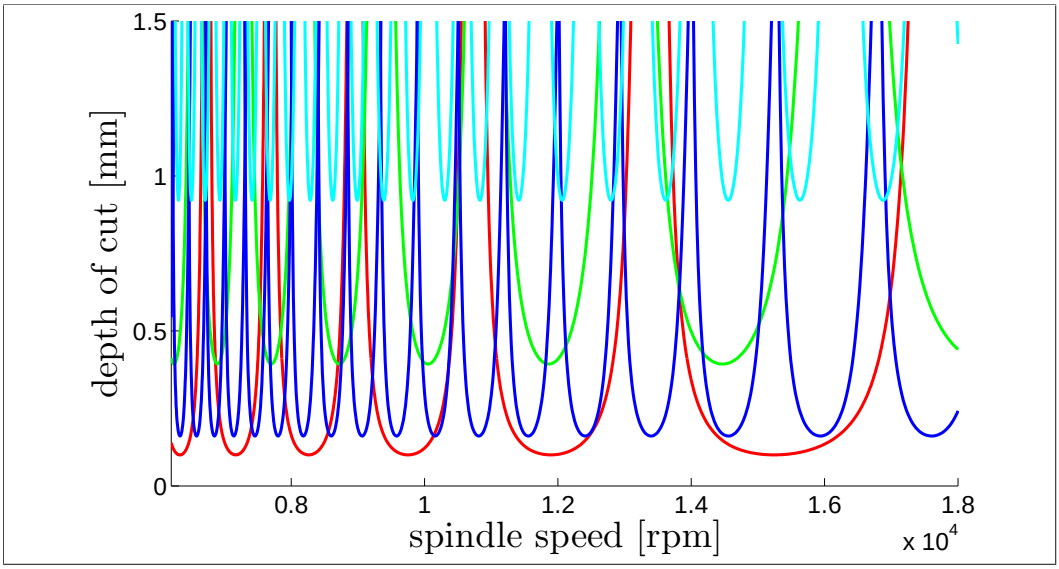

(a) Before trimming

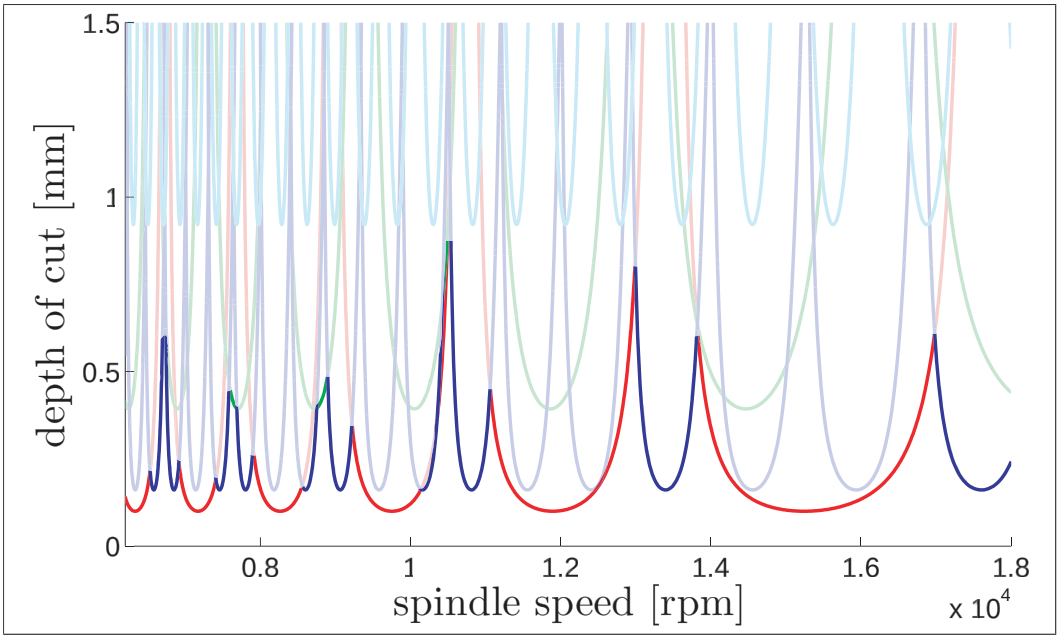

(b) After trimming

Figure 3.7. SLD of the linear SHT system. Red: First mode, Green: Second mode, Blue: Fourth mode, Cyan: Fifth mode

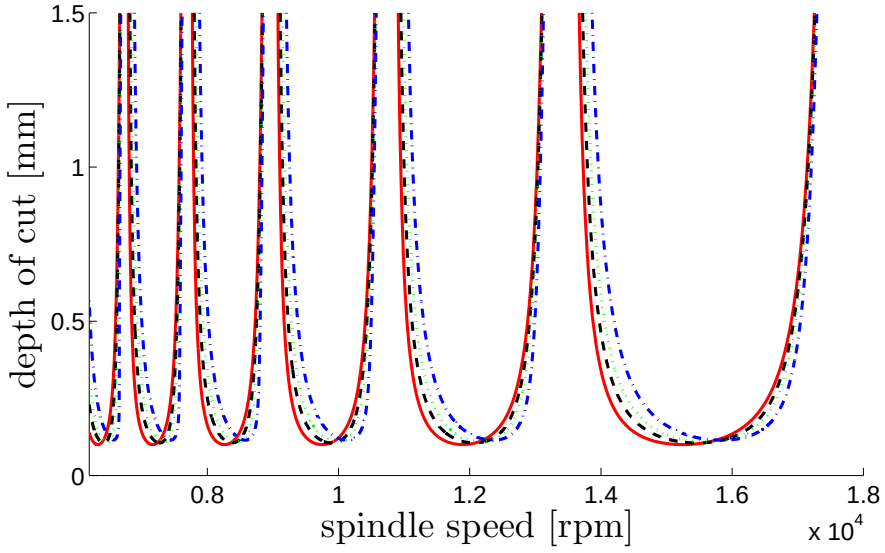

Figure 3.8. Effect of nonlinearity on the stability lobe related to the first mode. Solid: Low force. Dashed: F=70[N]. Dotted: F=100[N]. Dash-dotted: F=150[N]

3.5 Effects of Coefficient of Cubic Stiffness Nonlinearity

The coefficient of cubic stiffness nonlinearity of a bearing determines the sensitivity of its stiffness to displacement amplitude. For higher coefficient of nonlinearity, higher increase of stiffness is observed for an increase in displacement amplitude. Similar to the analysis done in Section 3.4, in this section, the coefficient of cubic nonlinearity is increased to observe its effects.

3.5.1 Effects of Coefficient of Nonlinearity on Response

The coefficient of nonlinearities are taken as $k_n = 1.0 \cdot 10^{14}[N/m^3]$, $k_n = 0.70 \cdot 10^{14}[N/m^3]$ and $k_n = 0.40 \cdot 10^{14}[N/m^3]$ for the front bearings, and $k_n =$

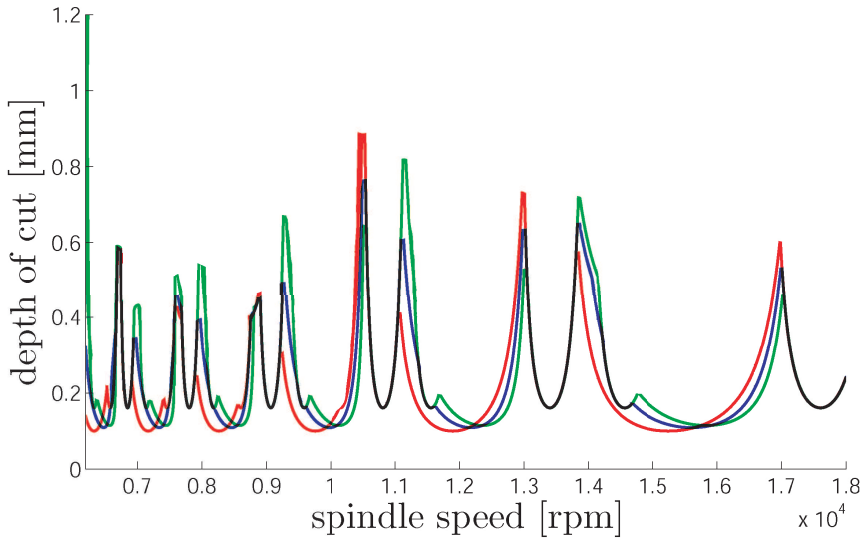

Figure 3.9. Comparison of SLDs. Red: Low force. Blue: F=100[N]. Green: F=150[N]

$0.86 \cdot 10^{14}[N/m^3]$, $k_n = 0.60 \cdot 10^{14}[N/m^3]$ and $k_n = 0.34 \cdot 10^{14}[N/m^3]$ for the rear bearing. The magnitude of cutting force is set constant as $F = 150[N]$ for all cases. Pseudo-FRFs for the two cases are compared in Figure 3.10. As the magnitude of the cutting force increases the first two modes of the system shift to the right because of the hardening effect of the cubic stiffness. For better view, first two modes are zoomed in Figure 3.11.

Similar to the analysis done in Section 3.4, the first mode of the system is more flexible than the second one. This causes the difference in the amount of shift of the peaks. The magnitude of response of the first mode is larger than that of the second one making the first mode more sensitive to the stiffness nonlinearity at the bearings. Therefore, the first mode is more sensitive to increase in the coefficient of cubic stiffness nonlinearity.

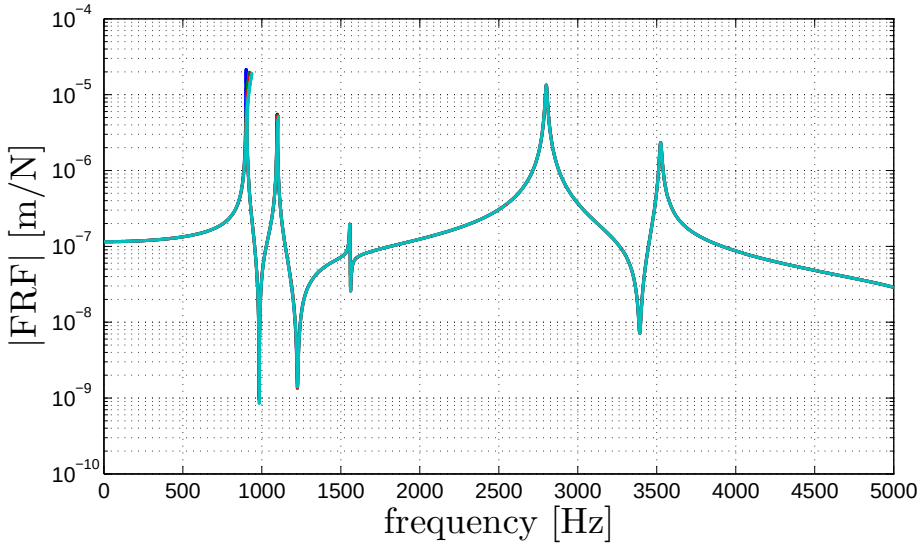

Figure 3.10. Tool tip pseudo-FRFs for different coefficients of nonlinearity (log vs. linear)

3.5.2 Effects of Coefficient of Nonlinearity on Stability

The effect of coefficient of nonlinearity on the real parts of first two modes can be seen in Figure 3.12. Comparison of SLDs of the milling process is carried out in Figure 3.13. The effect of increased coefficient of nonlinearity is same as the effect of increased magnitude of cutting force. The stability lobes related to the modes (rigid body modes), which are under the effect of nonlinearity, shift to the right because of the hardening effect. However, some stable zones do not shift to the right. This is because the lobes related to modes other than the rigid body modes that which do not change under the effect of nonlinearity.

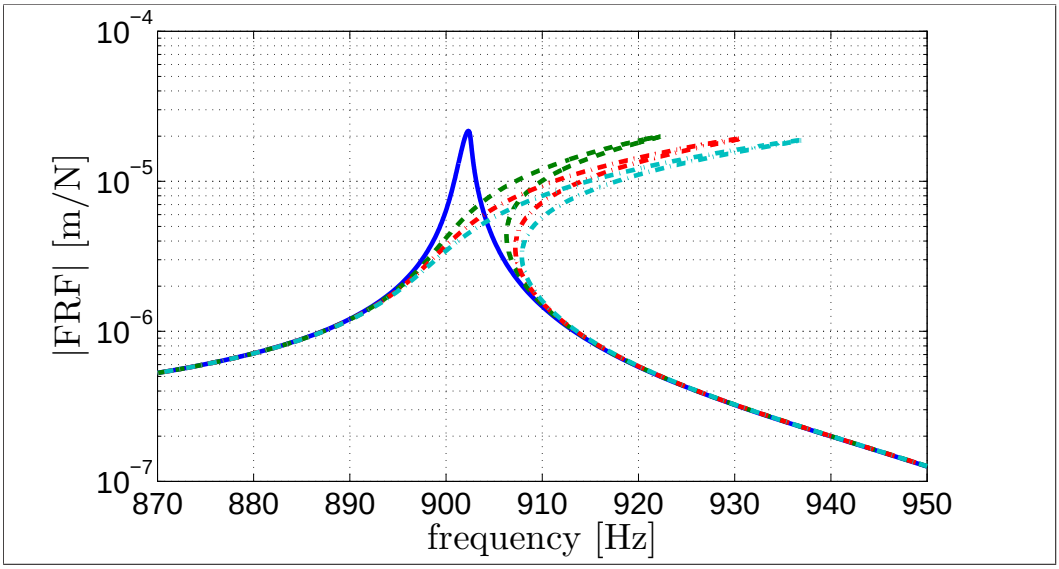

(a) First mode

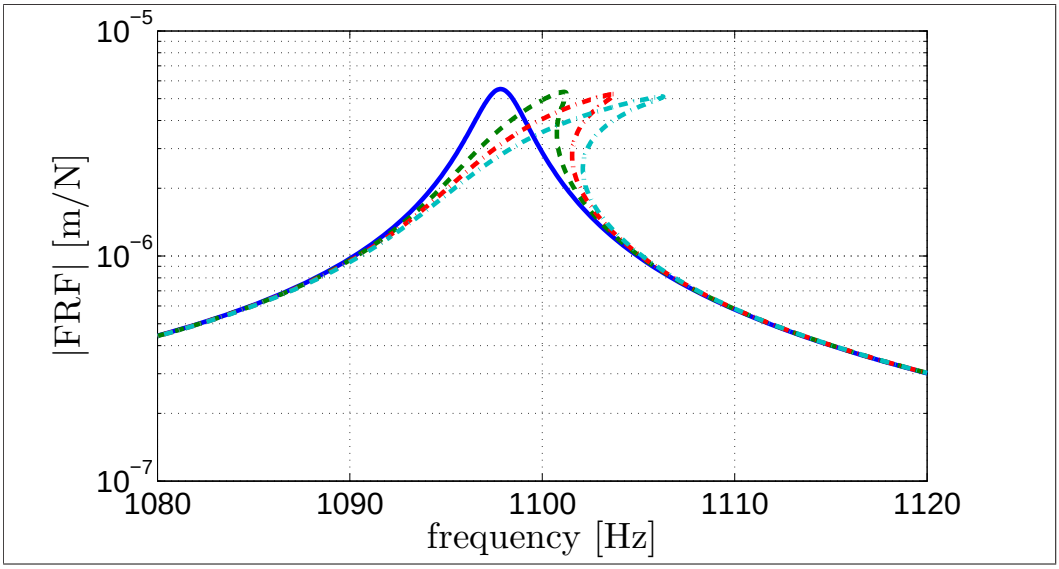

(b) Second mode

Figure 3.11. Zoomed views of the rigid body modes for $F = 150[N]$ (log vs. linear). Solid: Linear. Dashed: $k_n = \{0.40 \quad 0.34\}[N/m^3]$. Dotted: $k_n = \{0.70 \quad 0.60\}[N/m^3]$. Dash-dotted: $k_n = \{1.0 \quad 0.86\}[N/m^3]$

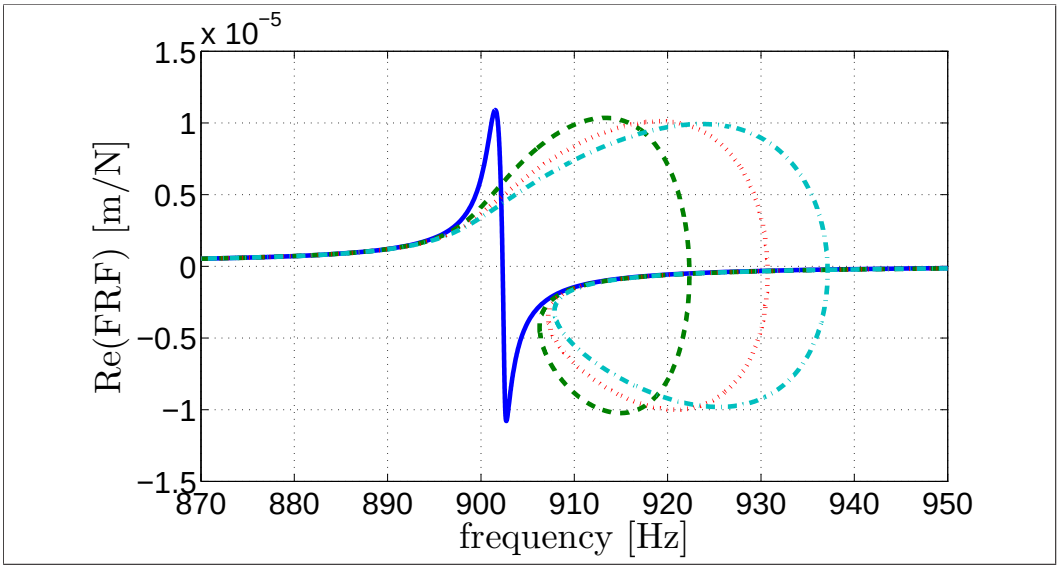

(a) First mode

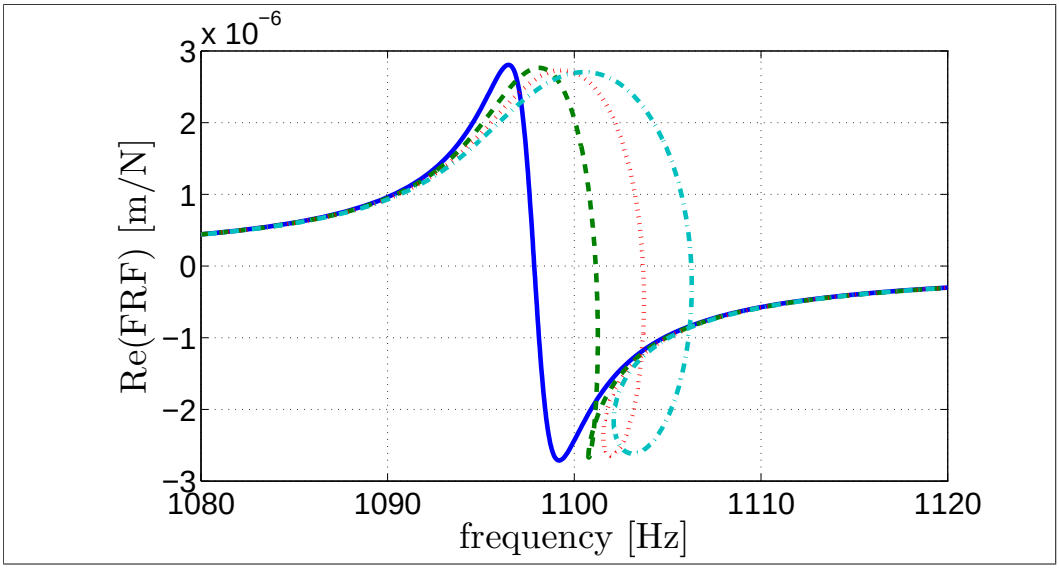

(b) Second mode

Figure 3.12. Zoomed views of the real parts of FRFs of rigid body modes for $F = 150[N]$ (log vs. linear). Solid: Linear. Dashed: $k_n = \{0.40 \quad 0.34\}[N/m^3]$. Dotted: $k_n = \{0.70 \quad 0.60\}[N/m^3]$. Dash-dotted: $k_n = \{1.0 \quad 0.86\}[N/m^3]$

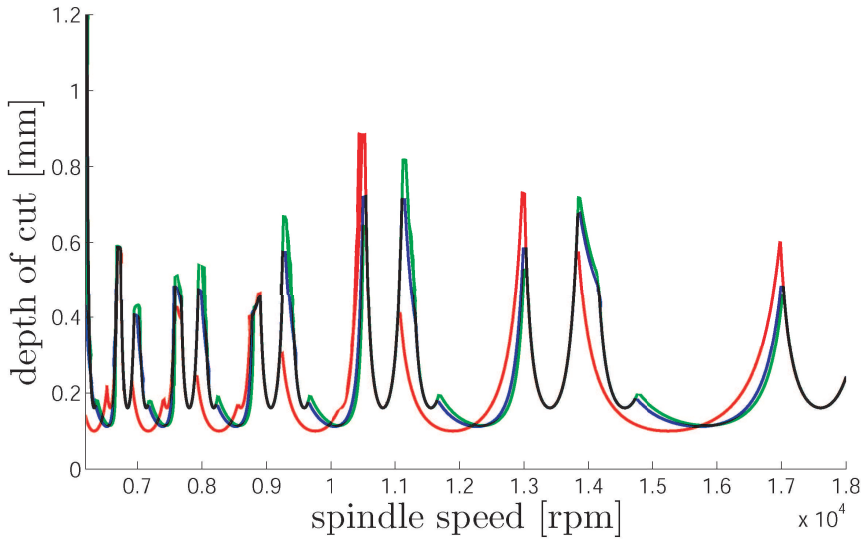

Figure 3.13. Comparison of SLDs $F = 150[N]$. Red: Linear. Blue: $k_n = \{0.70 \;\; 0.60\}[N/m^3]$. Green: $k_n = \{1.0 \;\; 0.86\}[N/m^3]$

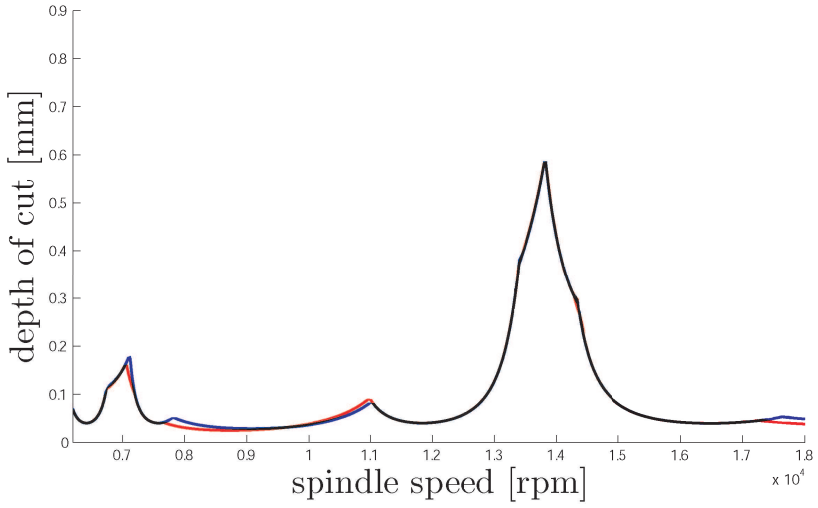

Figure 3.14. Change in SLD when highest nonlinearity is applied and the number of teeth on the cutter is four. Red: Linear. Blue: Nonlinear

3.6 Effects of Number of Teeth on the Cutter on Stability

The number of flutes on the cutter has a positive effect on chatter stability of the milling process. The magnitude of cutting force and the coefficient of bearing nonlinearity are taken $F = 150[N]$ and $k_n = \{1.0 \quad 0.86\}[N/m^3]$ in this section. When the number of flutes are increased from one to four in the equations of Altıntaş and Budak [18], the stability lobe diagram obtained from nonlinear analysis is almost the same as the diagram found from linear analysis. The comparison is shown in Figure 3.14.

CHAPTER 4

EXPERIMENTAL METHODS

In order to carry out an accurate stability analysis, frequency response function (or transfer function) of a system must be obtained accurately. Analytical modeling of the whole machine tool system of a milling machine is the most challenging part of conducting stability analysis of the milling process. Practically, analytical modeling of whole machine considering all effects (including effects of milling process) is hardly possible. Without modeling whole machine it is still possible to estimate chatter free cutting zones semi-analytically by identifying response, or frequency response function (FRF), of tool tip of spindle-toolholder-tool (SHT) experimentally.

Carrying out hammer test (tap test) at tool tip under static conditions is the most common method used in industry to obtain FRF for conducting chatter analysis. However, if static tap test is conducted, some important effects might be disregarded. Because of the nonlinearities of the structure, cutting forces and spindle speed during cutting might have an effect on the FRF of the structure. Under high speed conditions, for speeds above 15,000 rpm, gyroscopic effects of balls of bearings may have an effect on stiffness values of bearings. As a second effect, if high cutting forces are involved, stiffness of bearings might change resulting in altered FRF of structure. Speed and cutting force may introduce other effects such as altered bearing damping and additional damping at tool-workpiece contact during milling. Apparently, static tap test do not consider speed and force effects since it is carried out at 0 rpm spindle speed and low excitation force is applied by hammer.

A practical method to determine the dynamics of SHT is to conduct hammer

test while the spindle rotates. The FRF obtained by this way is usually called rotating FRF. Similarly, the FRF obtained by static tap test is called non-rotating FRF. By carrying out hammer test under dynamic conditions FRF of the structure can be estimated at different speeds and change of FRF depending on spindle speed can be seen. But, since tool tip is hit by hammer, there is an obligation of using a dummy tool. Possible changes might occur in natural frequencies and damping values related to the modes of cutting tool. So, replacing real cutter with a dummy tool might clear out some of its effects. Moreover, use of this method does not include the effects of milling.

In order to observe the effects on milling process on dynamics of the structure two types of experiments are done in this study. Experiments conducted in this study involve real cutting tests to include effects of milling in addition to nonlinearities of the structure. First study is to observe shifts in natural frequencies of the structure during milling. Cutting is done at different cutting speeds, then changes in dynamics of the structure are determined. Secondly, an experimental chatter test is explained to determine stability lobe diagram (SLD) at a certain speed experimentally. Then, a method to predict whole SLD of system using experimental data of the chatter test is introduced.

4.1 Run Up Test

Run up test is an experimental method to determine shifts in natural frequencies of the structure. Data collection is carried out while the SHT performs stable (chatter free) milling. Run-up test is widely used in rotor dynamics (explained by Swanson et al. [70]) to determine dependency of natural frequencies of the structure on rotational speed.

During milling, the structure is excited by the harmonics of the cutting force. For instance, if cutter has one tooth and spindle speed is 200Hz, cutting force excites the structure at 200Hz, 400Hz, 600Hz.... Usually, magnitude of first harmonic of cutting force is much larger than its higher harmonics. So,

generally, higher harmonics of cutting force can be neglected, and it is assumed to be composed of single harmonic. However, for highly intermittent cutting (low immersion cut), magnitudes of higher harmonics become considerably high, so higher harmonics of response of structure become relatively large as well. In this experiment, the workpiece is cut at low immersion to obtain response characteristics of the structure at a wider frequency band.

Figure 4.1 shows sketch of process during milling. In the experiment, the workpiece is cut by tool along x-direction at a constant y distance. During milling, the axial depth of cut is kept constant. The same cutting process with equal cutting time is conducted at each designed cutting speed. If the cutter takes all the material at the specified y, an incremental step is added to y distance and cutter performs another cut at new y distance along x-direction. Initial and final cutting speeds are 6,000 rpm and 20,000 rpm, respectively, and speed increment is set as 300 rpm. Thus, material is cut 48 times having the same cutting conditions except cutting speed (or feed per minute). Thus, frequency range that is swept is 100Hz-105Hz-. . .-295Hz-300Hz-333Hz.

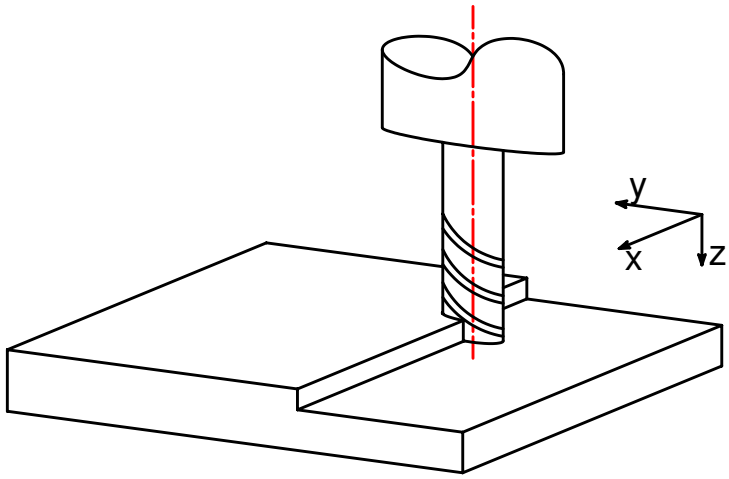

Figure 4.1. Sketch of the process during run up test

Table 4.1. Technical details of run up test

Material of the workpiece	Al7075-T6
Type of the cutter	single-insert carbide milling cutter
Cutter diameter	25 mm
Radial width of cut or tool engagement	5 mm
Axial depth of cut	5 mm
Maximum chip thickness	150 μm
Feed rate	188 $\mu m/rev$
Cutting time	2.5 s
Type of toolholder	HSK63A, Thermic (shrink-fit) toolholder
Name of Machine	Mori Seiki
Type of Spindle	Electro (motorized) spindle
Maximum speed of Spindle	20,000 rpm

The technical details are listed in Table 4.1. In order to observe the response of system at high frequencies, the cutting force need to have strong harmonics, i.e. the magnitudes of higher harmonics of cutting force should be comparable to magnitude of its first harmonic. This can be satisfied by selecting low tool engagement, hence, conducting intermittent cutting. However, the tool engagement should not be too low otherwise magnitude of cutting force becomes very low. To choose a sensible immersion, time domain simulation is carried out to estimate cutting force harmonics. For the selected engagement, the first six harmonics of cutting force are satisfactorily strong as shown in Figure 4.2. With six strong harmonics the frequency bandwidth of the experiment becomes 100Hz to 2000Hz ($333 \times 6 = 2000$).

4.1.1 Measurement Equipment

Acceleration sensors (accelerometers) are used to obtain the response of the structure during milling. Since the spindle housing is stationary, they are mounted on tip of the spindle housing. At static conditions, the tool tip FRF of

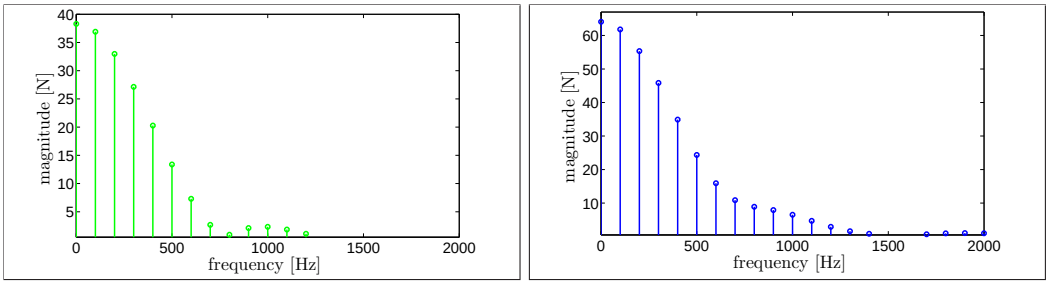

(a) in x-direction (b) in y-direction

Figure 4.2. Theoretical harmonics of cutting force at 6000 *rpm*

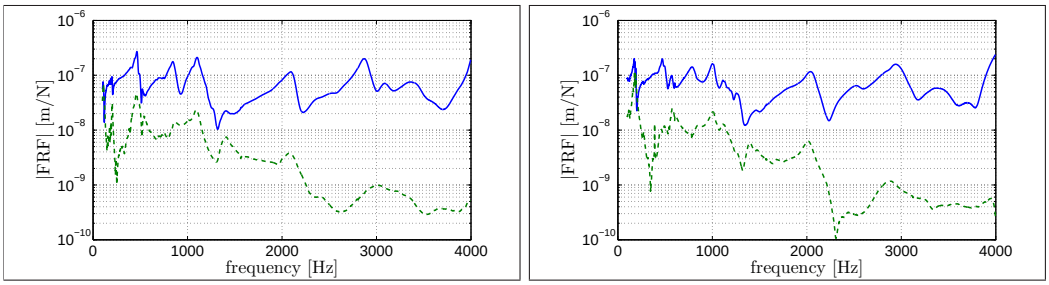

(a) x-direction (b) y-direction

Figure 4.3. Direct FRFs of the system in x and y directions. Solid line: Hit and measured at tool tip. Dashed line: Hit at tool tip and measured at housing tip

the system is obtained by hitting the tool tip and measuring tool tip response. As shown in Figure 4.3, the same vibration modes are observed when tool tip is hit and response at housing tip is measured. So, putting the accelerometers at housing tip is reasonable since that location does not coincide with any of the vibration modes (within the frequency range of interest). Accelerometers, generally, have no dominant modes which have adverse effects on measured data.

Another instrument that can be used for improving the experiment is force dynamometer. Force dynamometer is a device to collect force data during operation. The main disadvantage of using a force dynamometer is its frequency bandwidth. Unlike accelerometers, resonance frequencies of force dynamometers are close to frequency range of interest. For frequencies higher than 1000

Hz, the measured force values are not reliable because of having too much disturbance from the modes of the dynamometer itself. Thus, force dynamometer can measure force accurately up to 1000 Hz.

4.1.2 Use of Campbell Diagrams

Campbell diagrams or waterfall plots are tools for investigating shifts in natural frequencies of rotors during operation. For a rotor shaft with a large disk on it and fixed from two ends, unbalance on the disk creates forced vibration response of structure while rotor rotates at a certain speed. Firstly, time domain response of structure at a certain speed is measured, then Fourier transform (FT) is applied to the measured time data. Thus, magnitudes of harmonics of response data is obtained. Conducting same procedure at different speeds gives FTs of response data at different speeds (or frequencies of rotation). A 3D plot is formed with x, y and z axes being spindle speed, frequency of harmonics, and magnitude of harmonics, respectively. In other words, it is formed by putting FTs of responses side-by-side on the same graph. The formed 3D graph is called Campbell diagram or waterfall plot.

In this experiment, at each spindle speed forced vibration response (caused by cutting force) of tip of spindle housing is measured, and FT of the response is determined. 48 sets of FT analysis are put side-by-side and waterfall plot is obtained as shown in Figure 4.4.

The dashed lines of Figure 4.4 are drawn for determining shift in natural frequencies obtained by static tap test (hammer test). The constant slope solid lines in Figure 4.4 represent harmonics of response that are coherent to cutting force. For instance, the solid line which is closest to x-axis gives the change in first harmonic of response with increasing spindle speed. The first harmonic makes its first peak at natural frequency of first structural mode. Since the first six harmonics of cutting force are strongest, the first six harmonics of response have the strongest signals in Figure 4.4. Thus, it is only possible to make comments for frequencies up to 1500Hz.

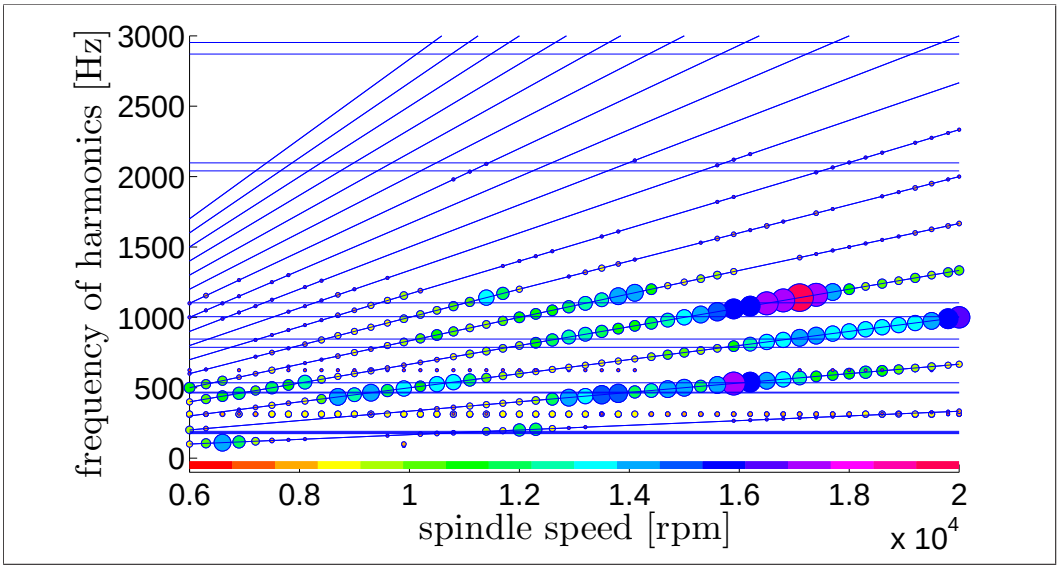

(a) in x-direction

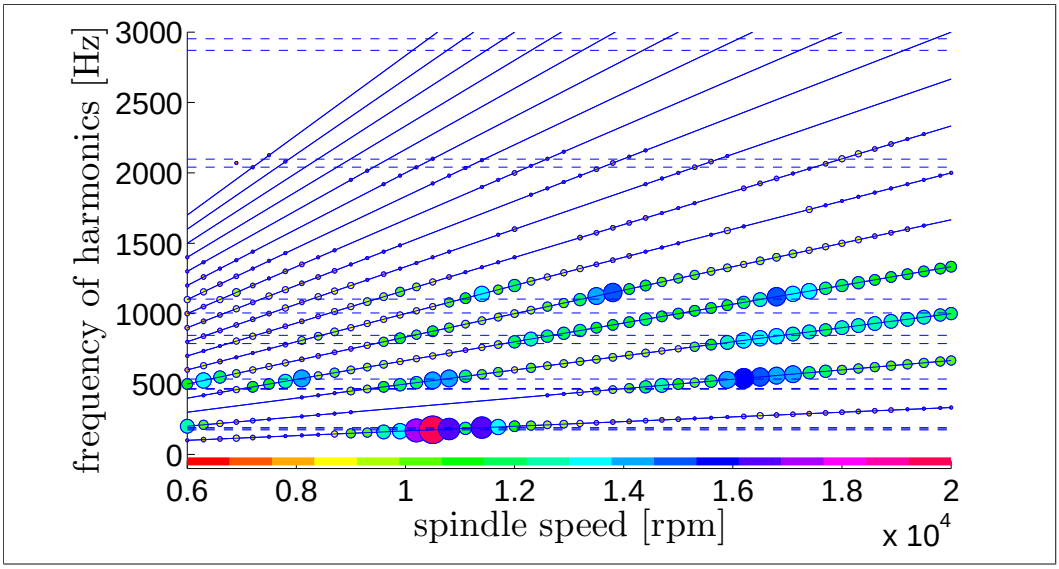

(b) in y-direction

Figure 4.4. Velocity response of housing tip in x and y directions. Horizontal dashed lines represent natural frequencies determined by static hammer test (Figure 4.3)

From Figure 4.4 it can be inferred that modes of the SHT system do not change significantly. In order to determine deviations from dashed lines more

Table 4.2. Technical details of slope cutting test

Material of the workpiece	Al7075-T6
Type of the cutter	Cylindrical end milling cutter
Cutter diameter	16 mm
Number of flutes on the cutter	4
Type of milling	Half immersion down milling
Maximum axial depth of cut	0.5 mm
Tool overhang length	116 mm
Type of toolholder	HSK63, Thermic (shrink-fit) toolholder
Name of machine tool	Danobat, Solaruze, SV6000
Type of spindle	Electro (motorized) spindle
Maximum speed of Spindle	18,000 rpm

clearly, cutting test can be performed with finer resolution of cutting speed increment.

4.2 Slope Cutting Test

Run up test is for determining shifts in natural frequencies of system. After observing changes in the stiffness of the modes, changes in stability of the milling process can be predicted. The stability of a milling process can directly be checked by cutting sloped materials. In this experiment, stability of an SHT system with long tool overhang is analyzed. FRF of the system has one dominant mode which is related to long overhang of cutting tool. Technical details of the process are listed in Table 4.2.

Before the experiment, the tap test is conducted to determine the natural frequency of the system. The tool tip FRF is shown in Figure 4.5. As seen in the figure, FRF of the system can be approximated as single-degree-of-freedom system. The dominant mode of the system is around 800Hz. The chatter frequency is close to natural frequency of the related mode. For this

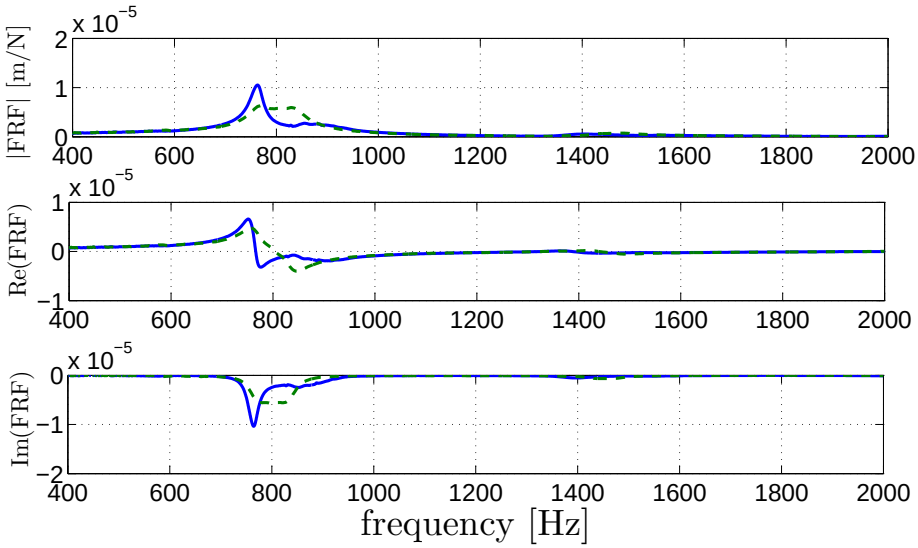

Figure 4.5. Tool tip FRF of the system. Solid: Point FRF in x-direction. Dashed: Point FRF in y-direction

system, flexibility of the dominant mode is very high such that chatter is always expected to occur at this mode. Hence, chatter frequency is supposed to be close to the natural frequency of the dominant mode, it is around 800Hz.

The schematic view of the experiment is shown in Figure 4.6. Cutting takes place along x-direction at constant y distance. The cutting speed is set constant while cutting at constant y distance. The axial depth of cut first increases up to mid point, then decreases until the end during milling at constant speed at constant y. At each spindle speed, the response of housing tip is measured. Similar to run up test a plot is formed by putting FTs of response acquired at each time step side-by-side (as shown in Figure 4.6). When the axial depth of cut exceeds a certain value, chatter occurs and values of response data become very large relative to the values of stable cutting (forced vibration response). While chatter occurs values of FT become very large not only at a single frequency. However, among the frequencies at which response is high, chatter frequency is sought around 800Hz, natural frequency of dominant mode of the system.

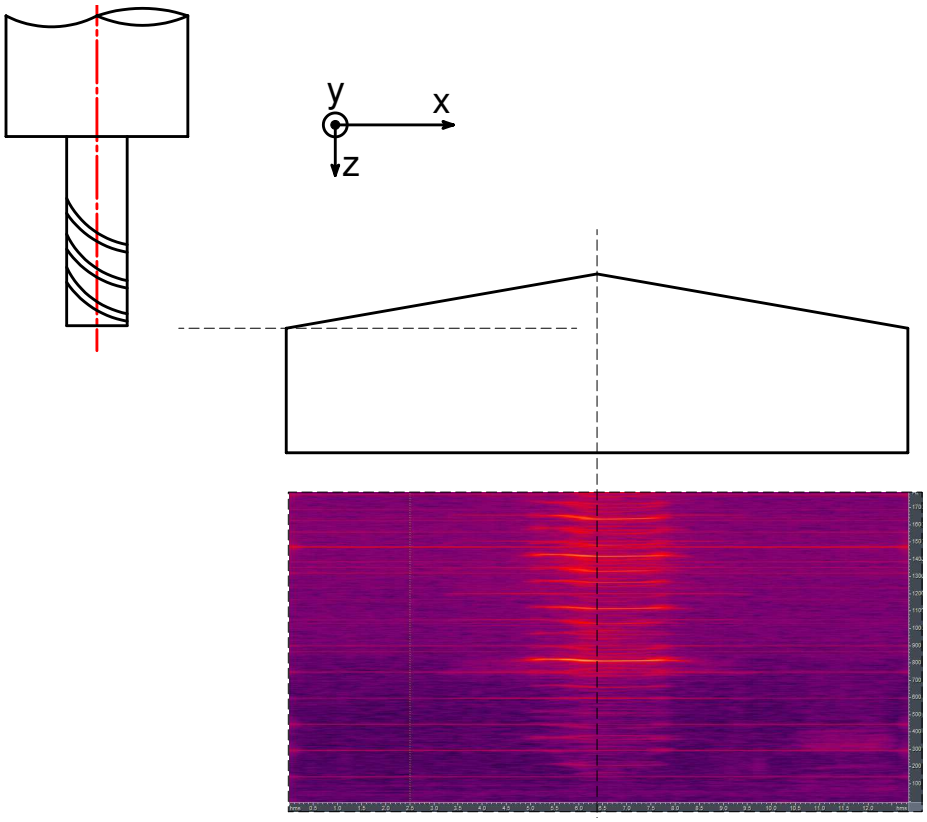

Figure 4.6. Schematic view of slope cutting test

In this study, the limiting depth of cut values, a_{lim}, obtained while the depth of cut increases (increasing slope) are listed in the results. The results obtained by slope cutting test is given in Table 4.3. The predicted a_{lim} values are determined by using FRF data (given in Figure 4.5) and the method of Altıntaş and Budak [18].

4.2.1 Inverse Analysis Using Experimental Data

Actual limiting depth of cut values at certain speeds are obtained via slope cutting test. For a system with single dominant mode, i.e. that can be approximated by an equivalent SDOF system, an inverse method to predict stability of the milling process using experimental data is introduced in this

Table 4.3. Results of slope cutting test

Data point	A	B	C	D	E	F	G
Spindle speed [rpm]	4200	4500	5200	6500	7500	9000	14000
Predicted a_{lim} **[mm]**	0.20	0.14	0.25	0.25	0.13	0.22	0.42
Measured a_{lim} **[mm]**	0.20	0.16	0.21	0.21	0.14	0.27	0.25
Chatter frequency [Hz]	783	791	819	769	783	806	790

section. The method is inverse analysis of method proposed by Altıntaş and Budak [18]. The purpose of the inverse method is to find parameters (mass, stiffness and damping) of equivalent SDOF system. Each lobe of SLD is analyzed separately. Inverse analysis is applied to each set of experimental data collected from each lobe, separately. In other words, for each lobe of SLD, a different set of system parameters are found. Inverse method can be considered as fitting curves (lobes) to experimental data.

The main assumption of the method is to consider the system to have cylindrical symmetry in its response. When Figure 4.5 is examined it is seen that only damping of the modes in x and y directions are slightly different, so, assuming cylindrical symmetry is reasonable. Then, transfer function matrix (tool tip FRF) identified at the cutter-workpiece contact zone becomes as in Equation 4.1.

$$\left[\Phi(i\omega)\right] = \begin{bmatrix} \Phi_{xx}(i\omega) & \Phi_{xy}(i\omega) \\ \Phi_{yx}(i\omega) & \Phi_{yy}(i\omega) \end{bmatrix} \tag{4.1}$$

where,

$\Phi_{xx}(i\omega)$: FRF obtained by exciting and measuring in x-direction

$\Phi_{yy}(i\omega)$: FRF obtained by exciting and measuring in y-direction

$\Phi_{xx}(i\omega) = \Phi_{yy}(i\omega) = \Phi$ - cylindrical symmetry

$\Phi_{xy}(i\omega) = \Phi_{yx}(i\omega) = 0$ - uncoupled modes

Frequency response function (FRF) of a SDOF system, Φ, is

$$\Phi = \frac{1}{m(\omega_n^2 - \omega^2 + i2\zeta\omega_n\omega_c)} \tag{4.2}$$

where,

$$\begin{aligned} m &: \text{modal mass} \\ \omega_n &: \text{natural frequency} \\ \zeta &: \text{damping ratio} \end{aligned}$$

So, eigenvalues become as

$$\Lambda = -\frac{1}{2a_0}\left(a_1 \pm \sqrt{a_1^2 - 4a_0}\right) \tag{4.3}$$

where,

$$\begin{aligned} a_0 &= \Phi^2(\alpha_{xx}\alpha_{yy} - \alpha_{xy}\alpha_{yx}) \\ a_1 &= \Phi(\alpha_{xx} + \alpha_{yy}) \end{aligned}$$

$$\Lambda = \underbrace{\alpha_{eq}}_{\alpha_R \pm i\alpha_I} \frac{1}{\Phi} \tag{4.4}$$

where, α_{eq} is the equivalent directional coefficient of the process and it is

$$\alpha_{eq} = -\frac{1}{2(\alpha_{xx}\alpha_{yy} - \alpha_{xy}\alpha_{yx})}\left[\alpha_{xx} + \alpha_{yy} \pm \sqrt{(\alpha_{xx} + \alpha_{yy})^2 - 4(\alpha_{xx}\alpha_{yy} - \alpha_{xy}\alpha_{yx})}\right] \tag{4.5}$$

Expressing Equation 4.4 in complex form gives,

$$\Lambda = \frac{\alpha_R \pm i\alpha_I}{G + iH} = \frac{(\alpha_R \pm i\alpha_I)(G - iH)}{G^2 + H^2} \tag{4.6}$$

First and second eigenvalues are written from Equation 4.6 as

$$\Lambda_1 = \frac{(\alpha_R - i\alpha_I)(G - iH)}{G^2 + H^2} = \frac{[(\alpha_R G - \alpha_I H) + i(-\alpha_R H - \alpha_I G)]}{G^2 + H^2} \tag{4.7a}$$

$$\Lambda_2 = \frac{(\alpha_R + i\alpha_I)(G - iH)}{G^2 + H^2} = \frac{[(\alpha_R G + \alpha_I H) + i(-\alpha_R H + \alpha_I G)]}{G^2 + H^2} \tag{4.7b}$$

where,

$$\begin{aligned}
\alpha_{eq} &: \text{equivalent directional coefficient} \\
\alpha_R &: \text{real part of } \alpha_{eq} \\
\alpha_I &: \text{imaginary part of } \alpha_{eq} \\
G &: \text{real part of FRF of SDOF system} \\
H &: \text{imaginary part of FRF of SDOF system} \\
G &= \frac{\omega_n^2 - \omega_c^2}{m\big((\omega_n^2 - \omega_c^2)^2 + 4(\zeta\omega_n\omega_c)^2\big)} \\
H &= -\frac{2\zeta\omega_n\omega_c}{m\big((\omega_n^2 - \omega_c^2)^2 + 4(\zeta\omega_n\omega_c)^2\big)}
\end{aligned}$$

κ is defined as

$$\kappa = \frac{\Lambda_I}{\Lambda_R} = \frac{-\alpha_R H \pm \alpha_I G}{\alpha_R G \pm \alpha_I H} = \frac{-2\zeta\omega_n\omega_c\alpha_R \mp (\omega_n^2 - \omega_c^2)\alpha_I}{-(\omega_n^2 - \omega_c^2)\alpha_R \pm 2\zeta\omega_n\omega_c\alpha_I} \tag{4.8}$$

Solving the equation gives,

$$C_1(\omega_n^2 - \omega_c^2) = C_2 2\zeta\omega_n\omega_c \tag{4.9}$$

where, C_1 and C_2 are constants,

$$\begin{aligned}
C_1 &= -\kappa\alpha_R \pm \alpha_I \\
C_2 &= -\alpha_R \mp \kappa\alpha_I
\end{aligned}$$

In Equation 4.9 κ is defined in terms of known variables as

$$\kappa = \frac{sin(\omega_c T)}{1 - cos(\omega_c T)} \tag{4.10}$$

where, T is tooth passing period of cutter ($\frac{\text{period of spindle rotation}}{\text{number of flutes on cutter}}$).

κ is a function of tooth passing period, T, and chatter frequency, ω_c. Equation 4.9 shows that ω_n and ζ depend on ω_c, T, α_R and α_I. In a typical chatter experiment ω_c, T, and a_{lim} can be determined. α_R and α_I are calculated quite accurately for milling processes, so, they are also known. Therefore, by conducting two chatter experiments (e.g. test of cutting slopes) in same lobe ω_n and ζ of system can be predicted. It is important to keep the engagement same during experiments, since directional coefficients depend directly on tool engagement. Thus, only cutting speed and depth of cut is changed (as done in test of cutting slopes).

The only remaining system parameter is modal mass, m. It is determined from the limiting depth of cut, a_{lim}, relation.

$$a_{lim} = -\frac{2\pi\Lambda_R}{NK_t}(1+\kappa^2) \tag{4.11}$$

where, Λ_R is real part of eigenvalue, N is number of flutes (teeth) on cutter, and K_t is tangential cutting coefficient.

The real part of eigenvalues is determined from Equation 4.7 as below

$$\Lambda_R = \frac{\alpha_R G \pm \alpha_I H}{G^2 + H^2} \tag{4.12}$$

In order to determine modal mass, it is extracted from G and H before putting into Equation 4.11. Λ'_R is defined as

$$\Lambda'_R = \frac{\Lambda_R}{m} = \frac{-(\omega_n^2 - \omega_c^2)\alpha_R \pm 2\zeta\omega_n\omega_c\alpha_I}{(\omega_n^2 - \omega_c^2)^2 + 4(\zeta\omega_n\omega_c)^2} \tag{4.13}$$

Inserting variables into Figure 4.11and rearranging the equation gives the expression for modal mass.

$$m = -\frac{NK_t}{2\pi}\frac{a_{lim}}{\Lambda'_R(1+\kappa^2)} \tag{4.14}$$

Modal mass depends on all experimental data. Both of the experiments give

close values of m, so Equation 4.14 is solved after determining ω_n and ζ from Equation 4.9.

4.2.2 An Application

The inverse method is applied to the results of slope cutting test (presented in Table 4.3). Analytical stability lobe diagram (SLD) of the system including chatter test results is presented in Figure 4.7.

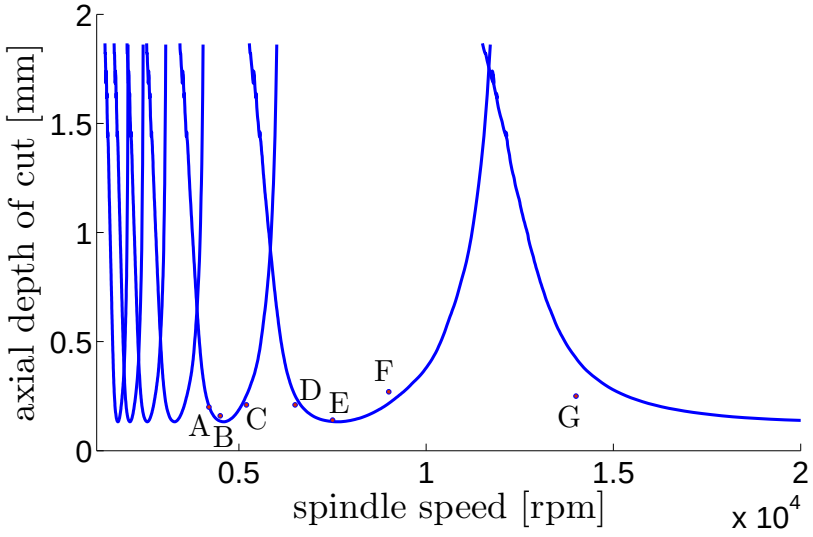

Figure 4.7. Analytical SLD computed based on [18] (solid curve) and slope cutting tests results (data points)

Experimental data points A, B and C are on the second lobe of the SLD. D, E and F are on first lobe of the SLD. G is on zeroth lobe. The data points at same lobes are analyzed separately using inverse method. Since the number of data points on zeroth lobe is less than two, point G could not be used in the analysis. The first and second lobes of Figure 4.7 are re-plotted with respect to the results of inverse method. The results of inverse chatter analysis using

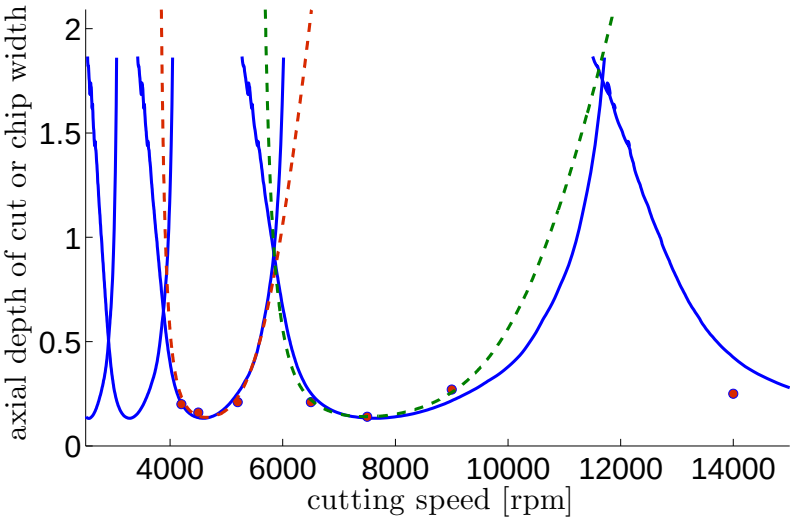

Figure 4.8. Comparison of analytical (solid curve) and re-plotted (dashed curve) SLDs

data in Table 4.3 are given in Table 4.4.

The obtained system parameters are used for re-plotting lobes of the SLD (shown in Figure 4.8). Modal mass values of SDOF systems representing both lobes are tried to kept almost constant during inverse analysis. Therefore, damping and stiffness values of SDOF system change for fitting stability lobes to experimental data. Parameters of the system are very sensitive to changes in chatter frequency values. The measured values of chatter frequency are

Table 4.4. Results of inverse chatter analysis using results of test of cutting slopes

Identified parameters of SDOF system	First lobe (using D, E and F)	Second lobe (using A, B and C)
Natural frequency [Hz]	778	792
Damping ratio	0.0265	0.0250
Modal mass [kg]	0.0766	0.0764
Modal stiffness [N/m]	$1.83 \cdot 10^6$	$1.89 \cdot 10^6$

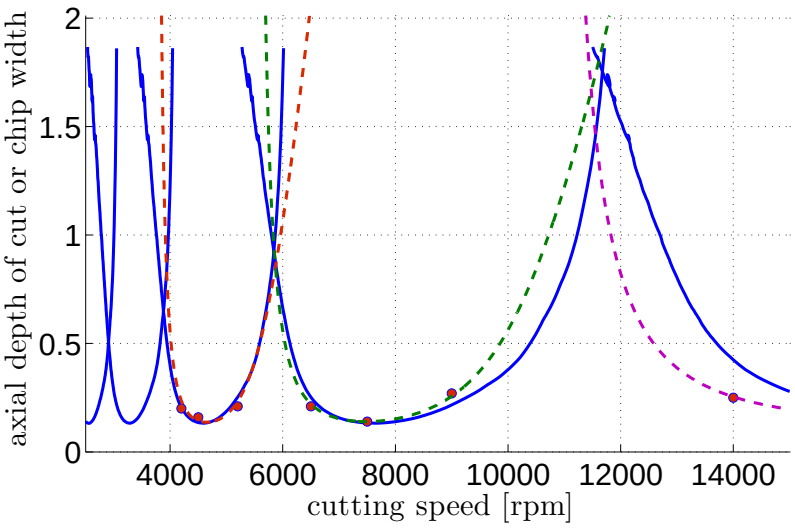

Figure 4.9. Comparison of analytical (solid curve) and re-plotted (dashed curve) SLDs including prediction for zeroth lobe

not as accurate as limiting depth of cut and cutting speed, and parameters found are not very sensitive to changes in limiting depth of cut and cutting speed. So, minor change is applied to chatter frequency values in order to get reasonable values for system parameters such as constant modal mass.

The reduction of stiffness from the second lobe to the first lobe is $0.06 \cdot 10^6 N/m$. If the same reduction is applied from first lobe to zeroth lobe, and the stiffness of zeroth lobe is taken as $1.77 \cdot 10^6 N/m$, and other parameters are taken same as parameters of the first lobe, the zeroth lobe fits the remaining data point as shown in Figure 4.9. However, if there were another data point on zeroth lobe, fit could be done more accurately.

From the two experimental study conducted in this chapter, it can be inferred that natural frequencies of spindles (SHT systems of the machines) do not change so much during operation. However, even small changes in dynamics of the SHT system have influence on chatter stability of the milling process. If changes in natural frequencies are considerable (as in rotor dynamics), they can be determined by conducting run up test. Since the error of measurement data of run up test is considerable, it can be hard to determine whether the

system characteristics change during milling. Slope cutting test directly determines chatter stability of the process. For systems with single dominant modes, inverse chatter analysis can be conducted to determine changes in system dynamics. For the machine tool used in the experiment, drop in natural frequency is observed for speeds above 10,000 *rpm*. Although there has not been significant changes observed in the FRFs for these machines used in cutting tests, it has been reported that the FRFs of the electro-spindles (motorized spindles) change significantly beyond 12,000 *rpm* due to real time preload adjustments of bearings.

CHAPTER 5

CONCLUSION

In this study, the effects of nonlinearity in the bearing supports of a typical motorized spindle-toolholder-tool (SHT) system on the chatter stability of the milling process are investigated. For this purpose, the analytical model of a SHT system suggested in an earlier study is developed further by including the nonlinear model of bearing supports. Changes in stability lobe diagram (SLD) due to nonlinear effects are studied. As nonlinearity, the nonlinear stiffness at bearings are considered. The changes in SLD due to the magnitude of the cutting force involved in the milling process, coefficient of nonlinearity of bearings, and number of flutes on the end milling cutter are considered. Furthermore, an experimental study is also conducted, and changes in dynamics of the SHT system during milling process are determined by carrying out cutting experiments on particular machines. Run up test involving chatter-free cutting and slope cutting test involving chatter are conducted to observe changes in dynamic parameters of the SHT system. Effects of the milling process are considered in addition to nonlinearities of the structure. Afterwards, an inverse chatter analysis is performed to analyze dynamics during milling using measured data.

5.1 Mathematical Model and Solution Method

The SHT system is modeled as Timoshenko beam elements coupled to each other. Frequency response function (FRF) matrix of each beam element is found using continuous beam model (CBM). CBM is an accurate method to

determine the response of a beam element of any length. FRF matrix of the SHT is found by coupling FRF matrices of Timoshenko beam elements to each other. In order to keep the points of bearing locations in the coupled FRF matrices, a modified FRF coupling method is applied. Thus, it is possible to keep the connection points in the coupled system formulation after coupling two elements.

The angular contact ball bearings are modeled as cubic stiffness elements composed of linear and nonlinear parts. Linear FRF of the SHT is obtained by coupling linear part of the stiffness with the previously obtained FRF matrix of the SHT system. The linear stiffnesses of bearings are coupled to the SHT at the points of bearing locations which were kept during the coupling of FRF matrices of the SHT system. The remaining nonlinear force vector representing nonlinear reaction forces of the bearings is put into response-dependent quasi-linear via describing function theory.

The equation of motion of the system is solved in frequency domain with numerical methods without path following, and jumps are observed in the frequency response function (FRF) of the SHT system when there is high nonlinearity. Therefore, a special numerical method, Newton's method with arc length continuation (ALC) method, is utilized in numerical solution of the equations. As a result, instead of observing discontinuities (jumps), turn points (turn-backs) are obtained in the frequency response curve (FRF) of the SHT. Since jumps in an FRF result in jumps in obtained SLD, it is observed that it is not possible to carry out stability analysis using FRFs having jumps. This difficulty is overcome by using Newton's method with ALC, with which the response around the frequencies at which jumps occur can easily be obtained. Thus, conducting stability analysis becomes possible using the FRFs with turn-backs.

Convergence of Newton's method with ALC method mainly depends on the selected error tolerance and nominal number of iterations. This brings difficulty while obtaining results for different cases. Another drawback of using Newton's method with ALC is that sometimes obtaining results might take

too long compared to using numerical methods without path following. Computation time naturally depends on how much the nonlinearity affects the response of the system. Higher nonlinearity causes sharper turns in the FRF, thus needs more solution steps at the turning points of the FRF.

5.2 Effect of Magnitude of the Cutting Force

The cutting force (cutting load) applied at tool tip of the SHT in transverse direction is assumed as a harmonic force with constant magnitude. Setting the coefficient of nonlinearity constant, increase in the magnitude of the force is investigated and it is observed that an increase in force increases displacements of the SHT system. Increase in the displacement at the bearing locations increases the effect of the nonlinearity defined. The cubic nonlinearity used in this thesis has a hardening effect on the structure. In other words, its stiffness increases with thane increased displacement. Since the bearings in the system have nonlinearity, the modes related to the bearings are affected by the increased cutting force. Modes of the SHT system related to the stiffness of bearings are rigid body modes of the SHT. Natural frequencies of the rigid body modes shift to the right with an increase in magnitude of cutting force. Since cubic nonlinearity is not dominant at low response level, only peaks of the rigid body modes shift to the right. This special condition of shifting is called snap-through.

The same snap-through behavior is seen in the SLD of the milling process. The lobes related to the rigid body modes shift to the right. The left sides of the lobes shifts more than the right sides. The lobes related to the modes other than rigid body modes do not shift to the right, they stay almost constant. Therefore, increase in the cutting force shifts the stable zones falling to the right of the lobes staying constant in the SLD to the right because of the hardening effect. Stable zones falling to the left of the unaffected lobes stay almost constant while getting little narrower. For the nonlinearity used in the case studies, 50% increase in cutting force magnitude causes the most affected

stable zone shift around 250 rpm to the right.

5.3 Effect of Coefficient of Nonlinearity of Bearing Stiffness

Similar conclusions made for increased cutting force can be made for increased coefficient of cubic nonlinearity. Increasing cutting force brings about increased displacements at the bearing locations. Similarly, increasing coefficient of nonlinearity while keeping cutting force constant increases the sensitivity of the displacement amplitude-dependent stiffness to increased response. Higher coefficient means the nonlinearity is more dominant at lower response levels. 50% increase in coefficient of nonlinearity of bearing stiffness causes the most affected stable zones shift about 125 rpm to the right.

5.4 Effect of Number of Flutes on the Cutter

The number of flutes (or number of teeth) has a different effect on the stability of the process. Increased number of teeth on the cutter decreases the effect of nonlinearity on the SLD. Increased number of flutes increases the number of lobes needed to consider for the range of interest (e.g. between 5,000 Hz and 20,000 Hz). The effect of shift in the FRF of the SHT is lower at higher lobes. At higher lobes frequency of rotation of spindle is much lower than frequency of vibration waves imprinted on the cut arc. Thus, if the lobe number is higher at the same spindle speed the effect of change in FRF is lower because of the higher difference between frequency of excitation and frequency of rotation. Quadrupling number of flutes decreases the shift in the lobes corresponding to rigid body modes. Almost no shift occurs in SLD after increasing number of flutes from one to four, even when highest nonlinearity used is applied.

Physical meaning of lobe number on a SLD is that it determines phase differ-

ence between waves on left and generated surfaces while system vibrates at chatter frequency (cutting conditions are selected just on stability lobe curve). Higher the phase difference, higher the tooth passing period and higher the lobe number at fixed chatter frequency. Therefore, increase of lobe number (tooth passing period) results in decrease of spindle speed. At higher lobe numbers (at left side of SLD) tooth passing frequency is higher, thus spindle speed is lower during chatter. For instance, if a possible shift in natural frequency of a system shifts tooth passing period at first lobe by T_1, it will shift tooth passing period of second lobe about $2 \cdot T_1$. Shift in tooth passing period is higher on second lobe than on first lobe. Therefore, shift in frequency of second lobe is lower than of first lobe.

For a fixed interested spindle speed range on SLD, say 10,000-15,000 rpm, corresponding lobe number in the interested range is higher for higher number of flutes on cutter (for higher chatter frequency). Higher lobe is affected less by a frequency shift in the first lobe. Therefore, for higher number of flutes, SLD is expected to be affected less in the spindle speed range of interest.

5.5 Assessment of Experimental Study

Two experimental methods, run up and slope cutting tests, are investigated in this study. Both of the experiments involve cutting, so, the test results include the effects of the milling process. Some electro-spindles used in the industry have preload mechanism changing during milling process depending on the conditions of cutting. For such electro-spindles change in the SLDs can be considerable due to real time preload adjustment of bearings. For the spindles of the machines tested there has not been a significant change in natural frequencies. Results of run up test are almost confirmed with results of conducted FRF measurements. Changes in dynamics of the system is so small that errors involving in run up test makes it hard to make comments. Results of cutting slopes test is clearer as the SLD of the system is obtained directly. For systems having only one dominant modes (e.g. SHT with long

tool overhang) inverse chatter analysis is applied to obtain modal parameters representing the system. It is observed that even 14 Hz change in natural frequency of the system may lead to 500 rpm shift of SLD to the left (for speeds above 10,000 rpm). This shift might be because of the speed-dependent characteristics of ball bearings or real time preload adjustment of ball bearings.

5.6 Suggestions for Future Studies

The bearing model used in this study has one degree of freedom. It is considered to have hardening effect on the structure. However, in some cases because of the bending moment applied on the bearings, they might show softening effect (decreased stiffness). Bearing models used in literature can be implemented into this study to have more realistic results. However, the solution algorithm should be modified to be used in order to solve equations of motion in frequency domain.

The solution method used in this thesis can be improved to be faster and more stable. This can be done by forcing the numerical continuation method to converge at each step by using more effective algorithm such as assigning a predictor for the direction of the solution path. Furthermore, numerical path following can only be applied at the frequency ranges where turn-backs occur in the solution curve. Thus, computation time can be decreased significantly.

The inverse chatter analysis used may be modified for predicting stability of systems involving two dominant modes instead of one. An optimization algorithm can be implemented for fitting best curve to experimental data and obtaining system parameters accordingly.

REFERENCES

[1] Y. Altıntaş. *Manufacturing Automation*. Cambridge University Press, 2000.

[2] F.W. Taylor. On the art of cutting metals. *Transactions of ASME*, 28: 31–350, 1907.

[3] R.N. Arnold. The mechanism of tool vibration in the cutting of steel. *Proceedings of the Institution of Mechanical Engineers*, 154(4):261–276, 1946.

[4] J. Tlusty and M. Polacek. The stability of machine tools against self-excited vibrations in machining. In *Proceedings of the International Research in Production Engineering*, Pittsburgh, USA, 1963. ASME New York.

[5] S.A. Tobias and W. Fishwick. Theory of regenerative machine tool chatter. *The Engineer*, 205, 1958.

[6] S.A. Tobias and W. Fishwick. The chatter of lathe tools under orthogonal cutting conditions. *Transactions of ASME*, 80:1079–1088, 1958.

[7] H.E. Merritt. Theory of self-excited machine tool chatter. *Transactions of ASME - Journal of Engineering for Industry*, 87:447–454, 1965.

[8] F. Koenigsberger and J. Tlusty. *Machine Tool Structures*. Pergamon Press, 1970.

[9] H. Opitz and F. Bernardi. Investigation and calculation of the chatter behavior of lathes and milling machines. *Annals of the CIRP*, 18(1): 335–344, 1970.

[10] R. Sridhar, R.E. Hohn, and G.W. Long. A stability algorithm for the general milling process. *Transactions of ASME - Journal of Engineering for Industry*, 90(2):330–334, 1968.

[11] J. Tlusty and F. Ismail. Basic nonlinearity in machining chatter. *Annals of the CIRP*, 30:21–25, 1981.

[12] J. Tlusty. Dynamics of high speed milling. *Transactions of ASME - Journal of Engineering for Industry*, 108(2):59–67, 1986.

[13] Y. Altıntaş and A. Spence. End milling force algorithms for CAD systems. *Annals of the CIRP*, 40(1):31–34, 1991.

[14] Y. Altıntaş, M. Eynian, and H. Onozuka. Identification of dynamic cutting force coefficients and chatter stability with process damping. *Annals of the CIRP*, 57(1):371–374, 2008.

[15] E. Budak and L.T. Tunc. A new method for identification and modeling of process damping in machining. In *1st CIRP International Conference on Machine Interactions*, Hannover, Germany, September 2008.

[16] Y. Altıntaş and M. Weck. Chatter stability of metal cutting and grinding. *Annals of the CIRP*, 53(2):619–642, 2004.

[17] I. Minis and R. Yanushevsky. A new theoretical approach for the prediction of machine-tool chatter in milling. *Transactions of ASME - Journal of Engineering for Industry*, 115(1):1–8, February 1993.

[18] Y. Altıntaş and E. Budak. Analytical prediction of stability lobes in milling. *Annals of the CIRP*, 44(1):357–362, 1995.

[19] S.A. Jensen and Y.C. Shin. Stability analysis in face milling operations, part 1: Theory of stability lobe prediction. *Transactions of ASME - Journal of Manufacturing Science and Engineering*, 121(4):600–605, 1999.

[20] Y. Altıntaş. Analytical prediction of three dimensional chatter stability in milling. *JSME International Journal Series C Mechanical Systems, Machine Elements and Manufacturing*, 44(3):717–723, 2001.

[21] M.A. Davies, J.R. Pratt, B. Dutterer, and T.J. Burns. Stability prediction for low radial immersion milling. *Transactions of ASME - Journal of Manufacturing Science and Engineering*, 124(2):217–225, May 2002.

[22] S.D. Merdol and Y. Altıntaş. Multi frequency solution of chatter stability for low immersion milling. *Transactions of ASME - Journal of Manufacturing Science and Engineering*, 126(3):459–466, August 2004.

[23] P. Bayly, J.E. Halley, B.P. Mann, and M.A . Davies. Stability of interrupted cutting by temporal finite element analysis. *Transactions of ASME - Journal of Manufacturing Science and Engineering*, 125(2):220–225, 2003.

[24] T. Insperger and G. Stépán. Stability of the milling process. *Periodica Polytechnica - Mechanical Engineering*, 44(1):47–57, 2000.

[25] T. Insperger and G. Stépán. Updated semi-discretization method for periodic delay-differential equations with discrete delay. *International journal for numerical methods in engineering*, 61(1):117–141, 2004.

[26] C. Brecher and M. Esser. Stability prediction - advances and current restrictions. In *6th International Conference on High Speed Machining*, San Sebastian, Spain, March 2007.

[27] C.-H. Cheng, T.L. Scmitz, and G.S. Duncan. Rotating tool point response prediction using RCSA. *International Journal of Manufacturing Science and Technology*, 11:433–446, 2007.

[28] C. Brecher, M. Esser, and S. Witt. Erfolge und problemstellungen der stabilitätssimulation. 2008.

[29] M. Rantatalo, J.-O. Aidanpää, B.Göransson, and P. Norman. Milling machine spindle analysis using FEM and non-contact spindle excitation and response measurement. *International Journal of Machine Tools and Manufacture*, 47:1034–1045, 2007.

[30] C. Brecher and M. Esser. The consideration of dynamic cutting forces in the stability simulation of hpc-milling processes. In *1st CIRP International Conference on Machine Interactions*, Hannover, Germany, September 2008.

[31] G. Quintana, J. Ciurana, and D. Teixidor. A new experimental methodology for identification of stability lobes diagram in milling operations. *International Journal of Machine Tools and Manufacture*, 48:1637–1645, 2008.

[32] J.P. Kruth, A.M. Liu, P. Vanherck, and B. Lauwers. A strategy for selection of optimal cutting parameter in high-speed milling to avoid chatter vibration. *International Journal of Production Engineering and Computers*, 4(5):35–42, 2002.

[33] N. Suzuki, Y. Kurata, R. Hino, and E. Shamoto. Identification of transfer function of mechanical structure by inverse analysis of regenerative chatter vibration in end milling. In *3rd CIRP International Conference on High Performance Cutting*. CIRP, May 2008.

[34] Y. Cao and Y. Altıntaş. A general method for the modeling of spindle-bearing systems. *Journal of Mechanical Design*, 126:1089–1104, 2004.

[35] *High Precision Ball Bearings catalogue*. GMN.

[36] M. Namazi. Mechanics and dynamics of the toolholder-spindle interface. *International Journal of Machine Tools and Manufacture*, 47:1333–1341, 2007.

[37] Y. Cao. *Modeling of High-Speed Machine Tool-Spindle Systems*. PhD thesis, The University of British Columbia, 2006.

[38] T.L. Schmitz and G.S. Duncan. Three-component receptance coupling substructure analysis for tool point dynamics prediction. *Transactions of ASME - Journal of Manufacturing Science and Engineering*, 127:781–790, November 2005.

[39] E. Budak, A. Ertürk, and H.N. Özgüven. A modeling approach for analysis and improvement of spindle-holder-tool assembly dynamics. *Annals of the CIRP*, 55(1):369–372, 2006.

[40] O. Özşahin, A. Ertürk, H.N. Özgüven, and E. Budak. A closed-form approach for identification of dynamical contact parameters in spindle-holder-tool assemblies. *International Journal of Machine Tools and Manufacture*, 49:25–35, 2008.

[41] C.-H. Cheng. *Improved Prediction of Spindle-Holder-Tool Frequency Response Functions*. PhD thesis, University of Florida, 2007.

[42] O. Özşahin, H.N. Özgüven, and E. Budak. Estimation of dynamic contact parameters for machine tool spindle-holder-tool assemblies using artificial neural networks. In *3rd International Conference on Manufacturing Engineering (ICMEN)*, Chalkidiki, Greece, November 2008.

[43] S.M. Han, H. Benaroya, and T. Wei. Dynamics of transversely vibrating beams using four engineering theories. *Journal of Sound and Vibration*, 225(5):935–988, 1999.

[44] A. Ertürk. Dynamic modeling of spindle-tool assemblies in machining centers. Master's thesis, Middle East Technical University, 2006.

[45] L. Meirovitch. *Fundamentals of Vibrations*. McGraw-Hill, 2001.

[46] T.L. Schmitz and R. Donaldson. Predicting high-speed machining dynamics by substructure analysis. *Annals of the CIRP*, 49(1):303–308, 2000.

[47] D.J. Ewins. *Modal Testing: Theory and Practice*. Research Studies Press Ltd., England, 1985.

[48] J. Dario Aristizabal-Ochoa. Timoshenko beam-column with generalized end conditions and nonclassical modes of vibration of shear beams. *Journal of Engineering Mechanics*, 130(10):1151–1159, 2004.

[49] A.B. Jones. A general theory for elastically constrained ball and radial roller bearings under arbitrary load and speed conditions. *ASME Journal of Basic Engineering*, pages 309–320, June 1960.

[50] B. Bossmanns and J.F. Tu. A thermal model for high speed motorized spindles. *International Journal of Machine Tools and Manufacture*, 39: 1345–1366, 1999.

[51] X. Min, J. Shuyun, and C. Ying. An improved thermal model for machine tool bearings. *International Journal of Machine Tools and Manufacture*, 47:53–62, 2007.

[52] Y.C. Shin. Bearing nonlinearity and stability analysis in high speed machining. *Transactions of ASME - Journal of Engineering for Industry*, 114:23–30, February 1992.

[53] T.L. Schmitz, J. Ziegert, and C. Stanislaus. A method for predicting chatter stability for systems with speed-dependent spindle dynamics. In *Transactions of NAMRI/SME*, volume 32, 2004.

[54] B.R. Jorgensen and Y.C. Shin. Dynamics of spindle-bearing systems at high speeds including cutting load effects. *Transactions of ASME - Journal of Manufacturing Science and Engineering*, 120:387–394, May 1998.

[55] D.P. Fleming and J.V. Poplawski. Unbalance response prediction for rotors on ball bearings using speed- and load-dependent nonlinear bearing stiffness. *International Journal of Rotating Machinery*, 1:53–59, 2005.

[56] J.V. Ferreira. *Dynamic Response Analysis of Structures with Nonlinear Components*. PhD thesis, University of London, 1998.

[57] N.E. Gürkan. Nonlinear mathematical modelling of gear rotor bearing systems including bearing clearance. Master's thesis, Middle East Technical University, 2005.

[58] G. Orbay. Nonlinear vibration of mistuned bladed disk assemblies. Master's thesis, Middle East Technical University, 2008.

[59] J.V. Ferreira and A.L. Serpa. Application of the arc-length method in nonlinear frequency response. *Journal of Sound and Vibration*, 284:133–149, 2005.

[60] H.D. Nelson and J.M. McVaugh. The dynamics of rotor-bearing systems using finite elements. *Transactions of ASME - Journal of Engineering for Industry*, 98:593–600, 1976.

[61] H.D. Nelson. A finite rotating shaft element using Timoshenko beam theory. *ASME Journal of Mechanical Design*, 102(4):793–803, 1980.

[62] M.R. Movahhedy and P. Mosaddegh. Prediction of chatter in high speed milling including gyroscopic effects. *International Journal of Machine Tools and Manufacture*, 46:996–1001, 2006.

[63] G.R. Cowper. The shear coefficient in Timoshenko beam theory. *ASME Journal of Applied Mechanics*, 33:335–340, 1966.

[64] W. Liu. *Structural dynamic analysis and testing of coupled structures*. PhD thesis, University of London, 2000.

[65] E. Ciğeroğlu, W. Lu, and C.-H. Menq. One-dimensional dynamic microslip friction model. *Journal of Sound and Vibration*, 292:881–898, 2006.

[66] Ö. Tanrıkulu, B. Kuran, H.N. Özgüven, and M. İmregün. Forced harmonic response analysis of non-linear structures using describing functions. *AIAA Journal*, 31:1313–1320, 1993.

[67] A. Gelb, E. Wallace, and V. Velde. *Multiple-input describing functions and nonlinear system design*. McGraw-Hill, New York, 1968.

[68] H.N. Özgüven. A new method for harmonic response of non-proportionally damped structures using undamped modal data. *Journal of Sound and Vibration*, 117:313–328, 1987.

[69] M.A. Crisfield. *Non-linear finite element analysis of solids and structures*. Wiley, New York, 1991.

[70] E. Swanson, C.D. Powell, and S. Weissman. A practical review of rotating machinery critical speeds and modes. *Sound and Vibration*, 39(5):10–17, 2005.